

**DESIGN AND EVALUATION OF A DISTRIBUTED OPTICAL FIBER SENSOR
FOR HAZARD DETECTION IN MINING**

NYARANGI WILFRED KIBET

**A Research Thesis Submitted to the Board of Graduate Studies in Partial
Fulfillment of the Requirements for the Conferment of the degree of Masters of
Science in Physics of the University of Kabianga.**

UNIVERSITY OF KABIANGA

OCTOBER, 2024

DECLARATION AND APPROVAL

This thesis is my own original work and has not been presented for the conferment of a degree or award of a diploma in this or any other institution.

Signature.....Date.....

Nyarangi Wilfred Kibet

PGC/PHY/0003/2021

APPROVAL

This thesis has been presented for with our approval as university supervisors.

Signature.....Date.....

Dr. Enoch K. Rotich Kipnoo

Department of Mathematics, Actuarial and Physical Sciences. (MAPS)

University of Kabianga.

Signature.....Date.....

Dr. Fred Wekesa Masinde

Department of Mathematics, Actuarial and Physical Sciences. (MAPS)

University of Kabianga.

COPYRIGHT

All rights reserved. No part of this thesis may be reproduced in any form by any means, electronic or mechanical including photocopying, recording or by any information storage and retrieval system, without the permission of the author or University of Kabianga.

© Nyarangi Wilfred Kibet, 2024

ABSTRACT

Mining of precious metals and construction rocks has grown tremendously in Kenya and across the globe. It is a significant source of employment for Kenyans, playing a key role in reducing poverty and dependency rates. Although it acts as a source of livelihood to many, it poses high risks including deaths owing to mine collapse, inhalation of poisonous gases and rock bursts among others. This study aims at developing a fiber optical sensor (FOS) for strain, stress and tensional force measurement. This was achieved by experimental work. A laboratory test-bed was built where by the Fiber Under Test was subjected to strain/stress/tension as power and polarization were monitored. The transmission performance of a distributed feedback (DFB), wave division multiplexing (WDM) and Mach-Zehnder modulator (MZM) laser sources over various fiber links was investigated to enhance maximum coverage of the risk potential area. A 10 Gbps pseudo random bit stream (PBRS) error free transmission of 75 km was achieved on an MZM source while the DFB and WDM source managed to transmit up to 50 km. The effect of mechanical disturbance/stress on power and states of polarization (SOPs) of a signal transmitted through an optical fiber was investigated both in a linear and coiled fiber orientation. Four fiber types namely; G652 Corning, G655 Corning, G655 OFS and PMF Corning were considered. Power fluctuations and SOPs were monitored using the power meter and polarization analyzer respectively when a fiber section was subjected to mechanical stress. It was noted that as loading was done gradually there was a significant decrease in power. The power loss was established after loading the fibers with 18 kg at different times so as to establish their sensitivities kg^{-1} . The achieved states of polarization were analyzed offline by digital signal processing (DSP) so as to establish the SOP speeds. This was enabled by the use of MATLAB software. The optimal laser-fiber combination for the design was MZM and G655 OFS, with a strain sensitivity of 0.024 dB/kg and SOP speed of 7.29 $^{\circ}/\text{s}$. To trigger the alarm, the threshold values were set for the designed sensor. The thresholds for power change and polarization fluctuation were set at 0.2 dB and 100 $^{\circ}$ respectively. It is through this automation that the designed FOS is expected to give an early alert of the change in soil profile of mines, enabling communication between the miners and the monitors. This will facilitate appropriate emergency response and safety of miners.

DEDICATION

I wish to dedicate this work to my entire family and friends.

ACKNOWLEDGEMENT

First and foremost, I thank our Mighty Lord for life, wisdom, care, guidance and protection that He has bestowed in me for the entire period as a postgraduate student at the University of Kabianga.

My heartfelt gratitude goes to my supervisors, Dr. E.K. Rotich Kipnoo and Dr. F.W Masinde during the entire process of research work. Their input and insight in my work has been very valuable throughout the process. For sure, through them I have gained a lot.

My sincere appreciation is directed to the University of Kabianga, School of Science and Technology and the Department of Mathematics, Actuarial and Physical Sciences (MAPS) for offering me the opportunity to partake my postgraduate studies at such a prestigious institution of higher learning.

Special thanks to Centre for Broadband Communication (CBC), Nelson Mandela University (NMU) and the African Laser Centre (ALC) through a collaboration with the University of Kabianga for facilitating the research work through a grant.

I wish to appreciate the endless efforts made by my family, for their prayers, financial support and the encouragements they have always offered to me during my course work and now research work.

To my course mate Faith, I am much thankful for the knowledge and advice we've shared throughout our period as postgraduate students at the University of Kabianga.

May the Almighty God bless you all.

TABLE OF CONTENTS

DECLARATION AND APPROVAL..... i

COPYRIGHT ii

ABSTRACT..... iii

DEDICATION..... iv

ACKNOWLEDGEMENT..... v

TABLE OF CONTENTS vi

LIST OF FIGURES ix

ABBREVIATIONS AND ACRONYMS..... xv

LIST OF SYMBOLS xvii

OPERATIONAL DEFINITION OF TERMS..... xviii

CHAPTER ONE 1

INTRODUCTION..... 1

 1.1 Overview 1

 1.2 Background of the Study..... 1

 1.3 Statement of the Research Problem 3

 1.4 Objective of the Study 4

 1.4.1 General objective 4

 1.4.2 Specific objectives 4

 1.5 Research Questions 4

 1.6 Justification of the Study..... 5

 1.7 Significance of the Study 6

CHAPTER TWO 8

LITERATURE REVIEW 8

 2.1 Introduction 8

 2.2 Review of related literature 8

 2.3 Theoretical framework 14

 2.3.1 Optical Fiber System 15

 2.3.2 Fiber Types 16

 2.3.2.1 Single Mode Fiber (SMF)..... 16

 2.3.2.2 Multimode Fibers..... 17

2.3.3 Fiber Optic Sensor	17
2.3.3.1 Fiber-Optic Sensor types.....	19
2.3.4 Fiber Optic Sensors Applications	25
2.3.5 Optical Time-Domain Reflectometer (OTDR).....	26
2.3.5.1 OTDR working principles.....	26
2.3.5.2 Optical Frequency Domain Reflectometry (OFDR).....	30
2.3.6 Fiber Bragg Grating Sensor	30
2.3.7 Polarization in fibers.....	32
2.4 Identification of Knowledge gap.....	33
CHAPTER THREE	34
METHODOLOGY	34
3.1 Introduction	34
3.2 Materials.....	34
3.3 Research Design.....	34
3.4 Location.....	38
CHAPTER FOUR.....	39
RESULTS AND DISCUSSIONS	39
4.1 Introduction	39
4.2 Power and States of Polarization (SOP) Fluctuation	39
4.2.1 Linear fiber orientation.....	40
4.2.1.1 Performance of different laser sources during loading on various fiber types	40
4.2.1.2 Performance of the signal during the mass unloading for different laser sources.....	50
4.2.1.3 Investigation of SOP and Power fluctuation on various fiber types during loading.....	54
4.2.1.4 Investigation of SOP and Power fluctuation on various fiber types during unloading.....	57
4.2.2 Coiled Fiber Orientation.....	60
4.2.2.1 Investigation of SOP and Power fluctuation of fiber types during loading.....	62
4.2.2.2 Investigation of SOP and Power fluctuation of fiber types during unloading	70

4.2.2.3 Performance of different laser sources during loading	74
4.2.2.4 Evaluation of laser sources during unloading on different fiber types	78
4.3 Transmission of the designed link.....	81
CHAPTER FIVE	84
SUMMARY, CONCLUSIONS AND RECOMMENDATIONS	84
5.1 Introduction	84
5.2 Summary	84
5.3 Conclusions	85
5.4 Recommendations	87
REFERENCES.....	89
APPENDICES	95
Appendix I: Power fluctuations for various fiber types in a coiled orientation	95
Appendix II: Fiber spools.....	98
Appendix III: Stokes' parameter changes for MZM on G655 OFS.....	99
Appendix IV: Data collection	100
Appendix V: Program for turning on an alarm	101
Appendix VI: List of publications.....	104
Appendix VII: Clearance by Board of Graduate Studies	105
Appendix VIII: Research permit	106

LIST OF FIGURES

Figure 1.1: Illustration of fiber optic sensor installed in a mine	3
Figure 2.1: Different types of sensors.....	14
Figure 2.2: The working principle of sensors	15
Figure 2.3: The structure of an optical fiber (OF)	15
Figure 2.4: Diagrammatic representation of fiber-optic sensor	18
Figure 2.5: Intrinsic fiber optic sensor	19
Figure 2.6: Extrinsic fiber optic sensor.....	20
Figure 2.7: Intensity based fiber optic sensor	21
Figure 2.8: Fiber optic sensor based on polarization	22
Figure 2.9: Fiber optic sensor based on phase: a) Mach Zehnder b) Michelson	23
Figure 2.10: Illustration of the chemical sensor.....	25
Figure 2.11: OTDR working principle	27
Figure 2.12: Information in the OTDR trace	28
Figure 2.13: Illustration of Rayleigh scattering and backscattering	28
Figure 2.14: Illustration of Fresnel reflection	29
Figure 2.15: Fiber Bragg grating	31
Figure 3.1 (a): Schematic representation for investigating transmission over various fiber lengths.....	35
Figure 3.1 (b): A picture of experimental setup in investigating transmission over various fiber lengths.	35
Figure 3.2 (a): schematic representation of the proposed fiber optic sensor design.....	36
Figure 3.2 (b): A picture of a laboratory setup of the proposed fiber sensor design	37

Figure 4.1 (a): Power fluctuation of light from each of the three laser sources; DFB, MZM and WDM sources injected on a G652 Corning fiber.....	40
Figure 4.1 (b): Power fluctuation of light from each of the three laser sources; DFB, MZM and WDM sources injected on a G652 Corning fiber (y-axis scale enlarged)	41
Figure 4.1 (c): Poincare' sphere representation of SOP for DFB source injected on a G652 Corning fiber.....	42
Figure 4.1 (d): A graph of SOP change with respect to time for DFB source injected on a G652 Corning fiber.....	42
Figure 4.2 (a): Power fluctuation of light from each of the three laser sources; DFB, MZM and WDM sources injected on a G655 Corning fiber during loading.	43
Figure 4.2 (b): Power fluctuation of light from each of the three laser sources; DFB, MZM and WDM sources injected on a G655 Corning fiber (enlarged y-axis scale)	44
Figure 4.2 (c): Poincare' sphere representation of SOP change for a signal from WDM source propagating through a G655 Corning fiber during loading	44
Figure 4.2 (d): A graph of SOP change with respect to time for the WDM source employed on a G655 Corning fiber	45
Figure 4.3 (a): Power fluctuation of light from each of the three laser sources; DFB, MZM and WDM sources injected on a G655 OFS fiber	46
Figure 4.3 (b): Poincare' sphere representation of a signal from a WDM source propagation through a G655 OFS.....	47
Figure 4.3 (c): A graph of SOP change with respect to time for the WDM source employed on a G655 OFS fiber.....	47

Figure 4.4 (a): Power fluctuation of light from each of the three laser sources; DFB, MZM and WDM sources injected on a PMF Corning fiber.....	48
Figure 4.4 (b): Poincare' sphere representation of a signal from an MZM source propagation through a PMF Corning.....	49
Figure 4.4 (c): A graph of SOP change with respect to time for the MZM source employed on a PMF Corning fiber	50
Figure 4.5: Power fluctuation of light from each of the three laser sources; DFB, MZM and WDM sources injected on a G652 Corning fiber	51
Figure 4.6: Power fluctuation of light from each of the three laser sources; DFB, MZM and WDM sources injected on a G655 Corning fiber	52
Figure 4.7: Power fluctuation of light from each of the three laser sources; DFB, MZM and WDM sources injected on a G655 OFS fiber	53
Figure 4.8: Power fluctuation of light from each of the three laser sources; DFB, MZM and WDM sources injected on a PMF Corning fiber	53
Figure 4.9: Performance of the four fiber types when coupled with a DFB laser	55
Figure 4.10: Performance of the four fiber types when coupled with an MZM laser source	56
Figure 4.11: Performance of the four fiber types when coupled with a WDM laser source	57
Figure 4.12: Performance of the four fiber types when coupled with a DFB laser source	58
Figure 4.13: Performance of the four fiber types when coupled with an MZM laser source	59

Figure 4.14: Performance of the four fiber types when coupled with a WDM laser source	60
Figure 4.15: A picture of a coiled fiber section in the laboratory	61
Figure 4.16 (a): Performance of the four fiber types when coupled with a DFB laser source	63
Figure 4.16 (b): Poincare' representation of SOP change for light from a DFB source propagating through a G652 Corning fiber	64
Figure 4.16 (c): A graph of SOP change with respect to time for light from a DFB source propagating through a G652 Corning fiber	64
Figure 4.17 (a): Performance of the four fiber types when coupled with an MZM laser source	65
Figure 4.17 (b): Poincare' representation of SOP change for light from an MZM source propagating through a G655 OFS fiber	66
Figure 4.17 (c): A graph of SOP change with respect to time for light from an MZM source propagating through a G655 OFS fiber	67
Figure 4.18 (a): Performance of the four fiber types when coupled with a WDM laser source	68
Figure 4.18 (b): Poincare' representation of SOP change for light from a WDM source propagating through a PMF Corning fiber	69
Figure 4.18 (c): A graph of SOP change with respect to time for light from a WDM source propagating through a PMF Corning fiber	69
Figure 4.19 (a): Performance of the four fiber types when coupled with a DFB laser source	70

Figure 4.19 (b): Poincare' sphere representation of SOP change for light from a DFB source coupled with a G652 Corning fiber.....	71
Figure 4.19 (c): A graph SOP change with respect to time of light from a DFB source coupled with a G652 Corning fiber	72
Figure 4.20: Performance of the four fiber types when coupled with an MZM laser source	72
Figure 4.21: Performance of the four fiber types when coupled with a WDM laser source	73
Figure 4.22: Power fluctuation of light from each of the three laser sources; DFB, MZM and WDM sources injected on a G652 Corning fiber	75
Figure 4.23: Power fluctuation of light from each of the three laser sources; DFB, MZM and WDM sources injected on a G655 Corning fiber	75
Figure 4.24: Power fluctuation of light from each of the three laser sources; DFB, MZM and WDM sources injected on a G655 OFS fiber	76
Figure 4.25: Power fluctuation of light from each of the three laser sources; DFB, MZM and WDM sources injected on a PMF Corning fiber	77
Figure 4.26: Power fluctuation of light from each of the three laser sources; DFB, MZM and WDM sources injected on a G652 Corning fiber	78
Figure 4.27: Power fluctuation of light from each of the three laser sources; DFB, MZM and WDM sources injected on a G655 Corning fiber	79
Figure 4.28: Power fluctuation of light from each of the three laser sources; DFB, MZM and WDM sources injected on a G655 OFS fiber	80

Figure 4.29: Power fluctuation of light from each of the three laser sources; DFB, MZM and WDM sources injected on a PMF Corning fiber	81
Figure 4.30: Transmission performance of a DFB laser source	82
Figure 4.31: Transmission performance of a WDM laser source	83
Figure 4.32: Transmission performance of an MZM laser source.....	83

ABBREVIATIONS AND ACRONYMS

AIC	Akaike Information Criterion
AM(s)	Artisanal Miner(s)
ASM	Artisanal and Small-scale Mining
BOTDA	Brillouin Optical Time-Domain Analysis
BOTDR	Brillouin Optical Time Domain Reflectometry
BER	Bit Error Rate
BERT	Bit Error Rate Tester
CH ₄	Methane
CO	Carbon (ii) Oxide
CO ₂	Carbon (iv) Oxide
CPU	Central Processing Unit
CW	Continuous Wave
DD	Direct Detection
DOFS	Distributed Optical Fiber Sensor
DSO	Digital Signal Oscilloscope
DSP	Digital Signal Processing
FBG	Fiber Bragg Grating
FBGs	Fiber Bragg Gratings
FOS	Fiber Optic Sensor
FOSs	Fiber Optic Sensors
FUT	Fiber Under Test
Gbps	Gigabytes per second

LAN	Local Area Network
LASER	Light Amplification by the Stimulated Emission of Radiation
LED	Light Emitting Diode
LO	Local Oscillator
MENR	Ministry of Environment and Natural Resources
MOM	Ministry of Mining
NLC	National Land Commission
OF	Optical Fiber
OFS	Optical Fiber Sensor
OFDR	Optical Frequency-Domain Reflectometry
OSA	Optical-Spectrum Analyzer
OTDR	Optical Time-Domain Reflectometer
PPG	Programmable Pattern Generator
PD	Photodetector
SOP	State of Polarization
TIR	Total Internal Reflection
UAV	Unmanned Aerial Vehicle
UNDP	United Nations Development Programme
VOA	Variable Optical Attenuator
WHO	World Health Organization

LIST OF SYMBOLS

K_ε	The physical elongation of the grating pitch and strain-optic coefficient of the fiber.
K_T	The thermal expansion coefficient and the thermal-optic coefficient of the fiber.
n_{eff}	The effective refractive index of the fiber core
T	Temperature Changes
λ_B	Resonance (or Bragg) wavelength
Λ	The periodicity (pitch) of the grating
ε	Applied strain

OPERATIONAL DEFINITION OF TERMS

Distributed Optical Fiber Sensor: A sensing technology using fiber optics to detect physical changes (e.g., strain, temperature) along the length of the fiber. In this technique, a fiber can be utilized both as a transmission medium as well as a sensing element since sensing is done continuously along the fiber.

Hazard detection: The process of identifying potential risks or safety threatening conditions in a mining environment, such as sudden collapse of mine support elements, or gas leakages.

Design: Is the systematic planning and creation of the sensor system. This includes its configuration, materials, and technologies employed to optimize its effectiveness in a mining setup.

Evaluation: Assessment of the sensor's performance, reliability, and accuracy in detecting hazards, often involving testing under simulated conditions.

Mining: An act of extracting valuable minerals from the earth, which poses unique hazards that calls for monitoring.

CHAPTER ONE

INTRODUCTION

1.1 Overview

The present chapter provides an overview of the research background, statement of the problem, general and specific objectives, research questions, justification and significance of the study

1.2 Background of the Study

The craze for mine prospecting in Kenya has driven villagers relent on farming practices and lease out their land to hordes of artisanal miners (AMs) and for quarrying activities. The painstaking job needs patience and can take a couple of weeks or months before miners' stumble on a few milligrams of the precious metals and earth minerals. There are several people who depend on mining for a living. Much of the land owned by various families has been converted into mining sites, with mines that are up to 150 fts deep - potential death traps for miners who enter them to get soils containing rocks that are crushed and sized for traces of these minerals.

Mine safety hazards such as great strata pressure, increased heat and gas contents increases significantly with greater mine depths (Liu *et al.*, 2018). The AMs descend into the tunnels using a container fastened to a cable connected to a rudimentary manual pulley (Amadala, 2021, May 13). As the miners descend into the dark pit, they are aware of a possible mine collapse that can bury them alive. Many of them have lost lives in these mines. They employ wooden planks to compact the soils so as to enhance safety. This is not a sure way of enhancing safety in mines.

There is need to develop a safety monitoring system so as to anticipate mine accidents through multi-parameter sensing which enables real-time disaster communication (Reddy *et al.*, 2016). Various mine risks can be monitored and analyzed effectively in real time by applying Fiber-Optic Sensors (FOS). A FOS integrated safety monitoring system has an ability to detect a disaster, giving an earlier warning basing on various parameters (United States Mine Rescue Association, 2022) as shown in Figure 1.1. The introduction of the FOS monitors will enhance safety in mines. Advantages of FOS early warning in mines are as follows; they are intrinsically safe in hazardous environments because the sensor head is electrically inactive, it is multifunctional in that it may detect various gases at once and can act as an intelligent decision-maker; in that it can foresee a disaster and give an alert earlier (Liu *et al.*, 2009).

At present, fibers-optic lines are on the lead and most reliable in data transmission with high speed and large volume (Buimistryuk, 2013). Conversations can be transmitted over a very wide area using a single optical fiber (OF). The tiny glass of an OF is stronger than a steel wire of similar diameter. Because of its small diameter it can be bent easily. It can break on bending if it surpasses a particular critical value. Some light leaves the cladding and get lost during the bending of the OF (Buimistryuk, 2013, Buimistryuk 2005). At the moment, distributed monitoring of the surrounding rock deformation and destruction during mining process needs further development to perform high-accuracy and real-time monitoring (Zhu *et al.*, 2010). This study proposes a design of a Distributed Optical Fiber Sensor (DOFS) for hazard detection in mining.

The optical fiber (OF) has been described by many scientific works. Although several studies and experiments aiming the development of various sensors have been

conducted globally, there has been no wide application of FOS in the field mining. Through this, it makes it critical to develop alternative ways to monitor the different parameters jeopardizing mine working by FOS to get rid of mechanical and electrical methods.

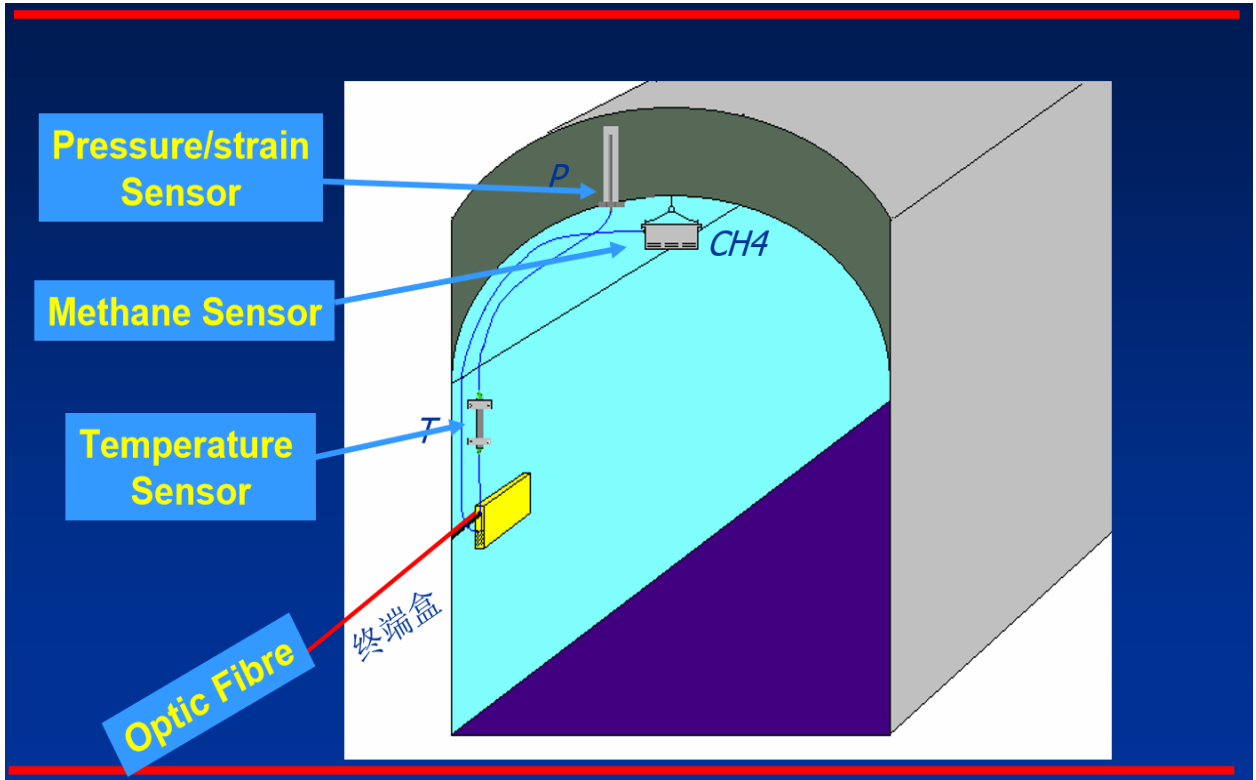


Figure 1.1: Illustration of fiber optic sensor installed in a mine (United States Mine Rescue Association, 2022)

1.3 Statement of the Research Problem

The number of deeper mining operations has increased globally as a result of depletion of shallow reserves and continuous economic growth which has resulted to higher stresses, heat and increased gas contents that have made safety and productivity in the mines more difficult. The present monitoring methods which involve use of wooden planks to make the soil compact and provide safety to miners are unreliable, inaccurate and expensive to operate and invest in. Any significant increases in productivity and safety necessitate a dependable real-time monitoring system that offers more thorough data about

multiple processes. There is limited data in the literature on developing a comprehensive mine disaster management system based on fiber optic sensor network, capable of early warning (real-time monitoring system) and control of mining hazard. A major safety hazard of underground miners is posed by the sudden destruction of the mine supports, which causes the collapse of the mine workings. Optical fiber sensor for monitoring pressure changes in mine supporting elements will expand the share of mining automation hence a reduction in the share of manual labor; abolishing errors due to measurement linked with the human factor.

1.4 Objective of the Study

1.4.1 General objective

The main objective of the study is to design and evaluate a distributed optical fiber sensor for hazard detection in mining.

1.4.2 Specific objectives

- (i) To design a distributed optical fiber sensor capable of transmitting 10 Gbps signal over a distance of 50 km.
- (ii) To determine the effect of mechanical disturbance/stress on the signal power transmitted through an optical fiber.
- (iii) To investigate the effect of mechanical disturbance/stress on the states of polarization of signal transmitted through an optical fiber.

1.5 Research Questions

- (i) Can light from a laser source propagate through optical fiber over a distance of 50 km?

(ii) What is the effect of mechanical stress on states of polarization of a signal transmitted through an optical fiber?

(iii) What is the effect of mechanical stress on power of a signal transmitted through an optical fiber?

1.6 Justification of the Study

Mining of precious metals and construction rocks (quarrying) is a key industry and one of the biggest contributors to the global economy. Artisanal Mining (AM) is a significant source of livelihood for people in areas it is practiced. Artisanal and Small-scale Mining (ASM) activities have risen tremendously across the country making it a relevant employer for many Kenyans hence reduction in poverty and rural development. It has been reported that 40.5 million people were involved directly in ASM in 2017 which was a rise from 30 million in 2014, 13 million in 1999 and 6 million in 1993 which is a comparison with only 7 million persons who work in mine industries (Fritz *et al.*, 2018).

Quarrying on the other hand is very advantageous in that, with a rapid growth in the middle class and construction industry, there is and will be a demand on housing triggering the construction business to another scale. The national and various county governments have embarked on doing various road networks across the country in which most of the materials used are quarry products. It is also becoming a major source of employment to many across the country because of the increasing demand for the quarrying products, such as building stones, marram and cement blending materials such as limestone. Quarrying also provides income to local councils through taxation.

Although mining acts as a major employer, it poses high risk of deaths where mines and quarry pits collapse and bury many artisanal miners alive. Some are rescued with

injuries, others in critical condition while others succumb on the spot. To mitigate all these dangers, research is needed to improve the working environment of ASM; reducing risks in the mining sites. This will be achieved by use of a distributed optical fiber sensor (DOFS) because of their long-distance monitoring, resistance to harsh environmental conditions and distributed sensing. Optical fibers have an ability of transmitting signals over long distances (up to kilometers), making it ideal for large mining. Unlike point sensors, DOFS can monitor conditions along the entire length of the fiber, providing real-time data on critical parameters such as strain hence early hazard detection.

This research on safety of miners will aid various county governments that undertake the mining and quarrying activities, the national government of Kenya and other related bodies like WHO, NLC, MOM and MENR in improving the working conditions of ASM in all the mining areas across the country. Through this there will be a rapid economic growth in these counties and Kenya at large since mining of precious metals and quarrying will be secure activities in which one can engage without any fear hence this can reduce poverty and dependence rates. This will enhance the growth of mining industry in Kenya. This will as well enable the government of Kenya in achieving most of its big four agendas that is, affordable housing, manufacturing and job creation.

1.7 Significance of the Study

The research findings obtained from this study are of great importance in that it will expand on existing knowledge on fiber optic applications for safety in mining locations. Implementation of this fiber optic sensor in mines increases the employment of digital technologies in mining. Given that mitigating the effects of destruction is connected with large material costs, timely alert of a mine collapse threat would both raise the degree of

safety in mining operations and lower the cost of maintaining mine workings. The information derived from this study may potentially help in formulating and integrating policies concerning a comprehensive mine disaster management system based on fiber optic sensor network.

CHAPTER TWO

LITERATURE REVIEW

2.1 Introduction

This chapter provides information on some of the reported fiber optic sensors. It also gives a description on the working principle of sensors, optical fiber system, various types of fibers and polarization concept.

2.2 Review of related literature

In this particular section we focus on the various experiments and scientific studies conducted on various FOSs. Our interest lies on how various FOSs can be interrogated to measure various parameter the main one being strain/stress.

Development of FOSs to monitor pressure changes on the elements of mine anchors has been presented by (Yugay *et al.*, 2022). This model realizes a rise in new technologies in the mining sector. They presented a laboratory test-bench simulating a functional mine and anchor elements installed with FOSs that are connected to an automatic measuring unit. There was a spot of light incident on a television matrix positioned at the other end of an OF which was processed by the hardware and software complex developed. It is through this hardware-software design that the rate of changes in the derivative of the light wave intensity in time were controlled, and furthermore the changes in the spot's shape and the change of pixels from white to black. It was noted that with when the OF was subjected to more pressure, the white pixels increased in number also. Visual processing results were transformed into numerical data which were used in decision making about a parameter

under consideration. FOS depicted a very high linearity hence its ability to control pressure changes on mine supporting elements with a very high accuracy.

A state-of-the-art review of DOFS applications for monitoring and assessing the deformation behavior of a typical tunnel infrastructure has been presented (Zhang *et al.*, 2024). Both Brillouin and Rayleigh scattering based DOFS were taken into contribution. This study focused on four aspects of monitoring that is proper selection of the sensing fiber, selection for the specific application, design of the effective sensor layout and establishment of a robust field sensor instrumentation.

A polarization-based fiber optic sensor has been proposed (Kipnoo *et al.*, 2020). In this study a fiber is used as a sensing element. This sensor depends on linear optics for application in earth mass movements due to environmental factors. Power and SOP fluctuations were monitored on a fiber subjected to laboratory strain. An SOP speed of 0.83 $^{\circ}/s$ was achieved. This was enabled by DSP. A sensitivity of 0.075 kg^{-1} was realized.

A study aimed at creating safer mine working conditions based on early detection models for accidents has been reported (Komane & Mathonsi, 2019). It consisted of a wireless sensor network made up of multiple sensors, the processing and a unit for tracking so as to locate miners in real time. A wireless sensor network, redundancy system, ZigBee technology and real time tracking have been adopted in this particular model. They tried to close the gap of sensor models being physical damaged when mounted on mine walls due to deformations underground. Due to this, the sensor model was attached directly to the miner's t-shirt. They focused on a redundancy system that ensures there is a backup at the monitoring office. The t-shirt is comprised of a tracking device, a processor and variety of sensors. The ZigBee unit makes up the communication model making it possible to reach

dark regions in which sensors can't be fixed and also enhances communication with the sink node situated on the mines. The monitoring center is responsible for analyzing, interpreting and displaying data collected from the mines. This model is capable of communicating directly to the monitor in-case of a breakdown between it and the sink-node because of the ZigBee that enhances reliable communication. This is possible because of the redundancy technology.

Based on geotechnical monitoring, various uses of Brillouin Optical Time-Domain Analysis (BOTDA) have been presented (Zeni *et al.*, 2015). In particular, he presented how detection of soil slope movements can be detected earlier by these sensors. This was achieved by directly embedding appropriate fiber cables underground. A smart foundation anchor was designed and achieved on which masses were loaded. It was observed that strain decreases linearly from the shallow region and vanished at the deepest end of the cable; this was an indication that the entire cable length was responsible for transmission of the pullout force into the soil. Innovative inclinometers and anchors can be achieved through the application of this technology. One of the shortcomings of the proposed technology in geotechnical monitoring is that it lacked appropriate algorithm for sensing cables installation in large areas. A hitch in interpreting data and accurate designing of ground/sensor interaction was also experienced.

A highlight on recent research and development based on structural health monitoring involving civil engineering systems have been reported (Li *et al.*, 2004). A review on health monitoring optical sensor for different civil engineering structures such as buildings and bridges among others.

It is through the monitored modulation of light within a loaded fiber that an intensity-based sensor operates (Kuang *et al.*, 2003). They conducted a number of three- and four-point bend tests on a variety of structures. From the three-point bend tests done on samples collected from small concrete structures, the crack propagation at the peak load was followed by a significant drop in the sensor response in each of the six specimen. The rate of light attenuation was not significant prior to peak load compared to the sensor response after that critical point. The second specimen depicted a higher signal attenuation rate than other specimen hence a higher sensitivity. The rise in sensitivity is a clear indication that the OF can be adopted in monitoring pre-crack vertical deflections in the process of loading. In this study, it was observed that there was a change in the response of the sensor before and after crack initiation of the highest load (i.e for a prior crack initiation, there was a slight loss of light and a sudden rise in light attenuation rate at the point of peak load). At the crack site, the plastic OF underwent some necking suggesting the presence of stress crazing. The sensor also displayed a potential to show an after-crack vertical deflection due to a greater linearity in optical signal after peak load. On conducting the four-point bend tests, similar results were obtained. After a keen observation, it was noted that the cracked part also depicted an availability of stress whitening suspected to be as a result of material crazing. The results demonstrated that OF can be used in identifying hair-like cracks and maximum failure cracks as well as monitoring crack progression up to maximum failure in civil engineering structures. Apart from detecting the crack origin, there was a good agreement dilate between the output of the sensor and progression of the crack when loading.

Mekhtiyev et al.,(2021) focused on designing a monitoring system for rock deformation and displacement that leads quarry sites to collapsing. This system adopts point-to-point FOSs. A laboratory sensor was developed concerning the point FOS built basing on the two-arm Mach-Zender interferometer utilizing a single mode OF for monitoring displacements with a changed sensitivity and a reduction of temperature intereference which leads to zero drift. The laboratory sample showed a fairly high linearity and can be adopted in controlling the mass strain once the design has been refined appropriately.

Some results of an innovative analysis method based on the intergration of DOFS, digital photogrammetry through Unmanned Aerial Vehicle (UAV), topographic and geotechnical monitoring systems have been shown (Lanciano & Salvini, 2020). Strain and temperature values were acquired from DOFS measurements and verified with displacement data from topographic and geotechnical instruments.

An introduction of some basic concepts about optical fiber sensing, particularly focusing on two different types of sensors, i.e. Fiber-Bragg gratings and distributed FOSs is given (Schenato, 2014). They are unideniably the most mature fiber optic sensors and have become very popular. Based on their unique feature (i.e. it can map the physical field of a mesurand along an OF distributively), distributed FOSs represent the most preferable sensors in geophysics monitoring.

Conventional monitoring techniques demands a lot of strenuous manual work and limits themselves to stress and strain detection within the shallow layers of rocks only (Tang & Cheng, 2018). The strain and deformations that occurred in front excavation face were not detected because the instruments used in monitoring were located behind the

excavation face. An innovative monitoring system based on Brillouin Optical Time Domain Reflectometry (BOTDR) for rock deformation was developed so as to mitigate these limitations. Compared to conventional monitors, this model gave a reliable, accurate and real-time measure for roadway surrounding rock deformation control over a large extension. The behaviors of the surrounding rock deformation were studied easily because the Optical Fiber Sensors (OFSs) were positioned in boreholes located ahead of the excavation face; this also enhanced the protection of the sensors. In relation to conventional monitors, OFs employed in BOTDR-based monitoring system can serve as sensors as well as signal propagating media. A single OF has the capability of strain detection over a wide region of the surrounding rocks. By addition or reduction of OFs, the area under monitorization is controlled. The BOTDR-based monitoring system was employed in studying the disturbances and damages behaviours of rocks under the TBM excavation. It was found out that this system has a capacity to measure $\pm 15000 \mu\epsilon$ with an accuracy of $\pm 15 \mu\epsilon$. Contrary, the mechanical monitors have an ability of measuring $200 \mu\epsilon$ (strain). This is a clear indication that the BOTDR-based monitoring system has a greater accuracy compared to conventional monitoring devices.

An all FOS-based comprehensive mine hazard detection system was developed (Liu *et al.*, 2009). It comprised of various sensors installed in underground coal mine for measuring various parameters such as strain, temperature, methane, seismic and temperature. The sensors were placed at distances between 5 and 6 km from the monitoring centre. It exhibited a very great advantage over conventional methods of mine monitoring. To be specific, fibre optic methane sensors did not require a regular calibration as employed by conventional electro-chemical methane sensors.

It is clear that from the above literature, FOS(s) are more efficient in monitoring various parameters of a mine working compared to conventional (mechanical and electrical) methods. Most of these techniques used have depicted a high degree of linearity and had a capacity to controll the change in soil profile on mine support elements with a very high accuracy.

2.3 Theoretical framework

A sensor is an input device that gives an output in regard to a particular physical quantity (input). The use of sensors across the globe is becoming rapid and almost a day-to-day encounter. Figure 2.1 gives various sensors for application in our day to day lives. These sensors perform different automation tasks such as lights turning on after detecting presence of a body, adjusting car and room temperatures among many others. It is because of these sensors that we are able to realize these automations and many others.

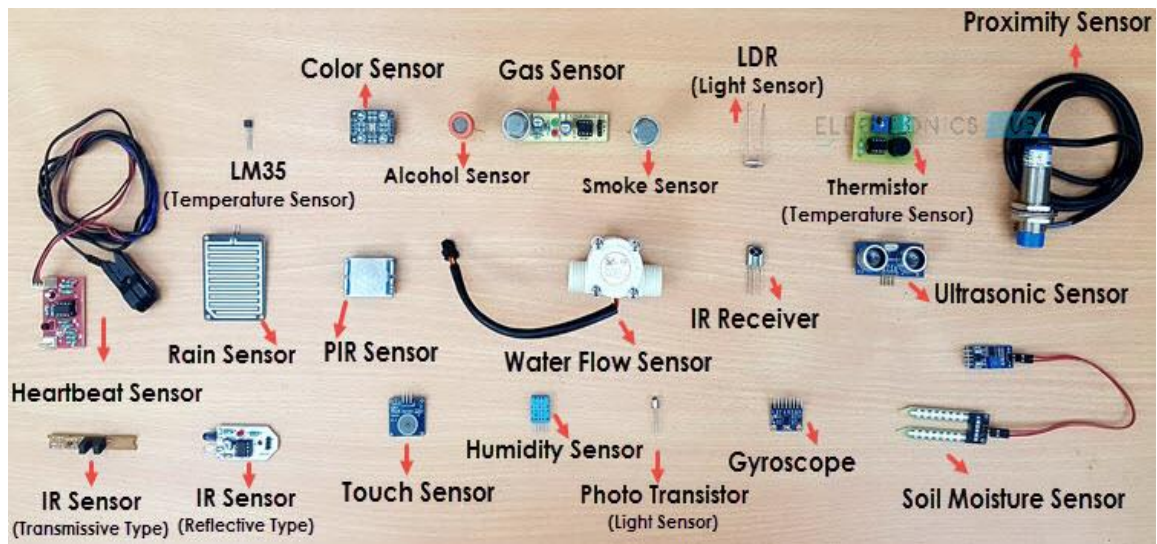


Figure 2.1: Different types of sensors (Elprocus, 2022)

Figure 2.2 illustrates a block diagram of sensor operation. It consists of sensors (input), computer (processing unit) and the output. The sensors provide the desired information (input) to the computer. The computer then collects all the data from various

sensors and then processes them by comparing them with pre-designed values. The computer is then responsible for providing a signal to the output. It is through the integration of the elements/components shown in Figure 2.2 below that an automated system is built.

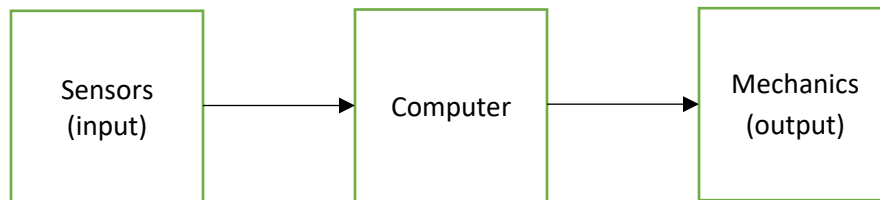


Figure 2.2: The working principle of sensors

2.3.1 Optical Fiber System

Optical fiber (OF) is a very tiny strand of glass or plastic that transmits data from one point to another in form of light by a phenomenon known as total internal reflection (TIR). It comprises of the core, cladding and sheath as shown in Figure 2.3. The core is the innermost part of the OF. It is then followed by the cladding and later on the sheath.

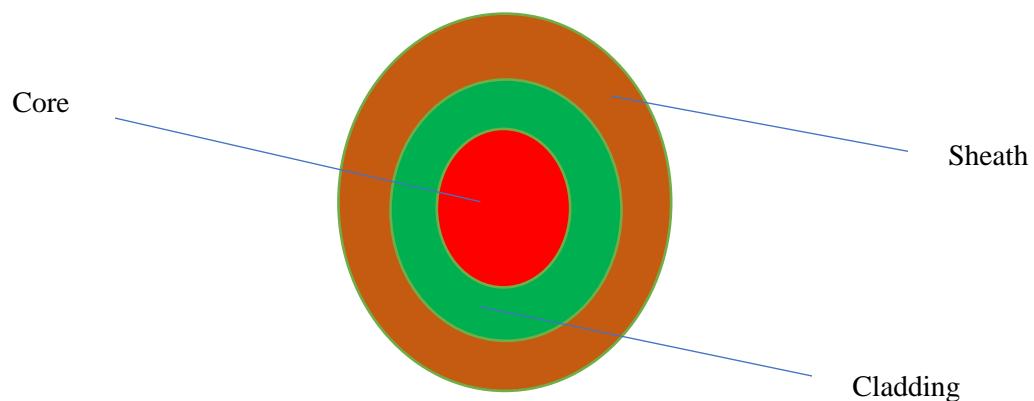


Figure 2.3: The structure of an optical fiber (OF)

The refractive index of the core is greater than that of the cladding. It is because of the core-cladding interface (difference in refractive indices) that light traps inside the core

due to TIR. To safeguard the OF from damage and moistures, it is covered by a protective layer known as the sheath (Fenta *et al.*, 2021).

2.3.2 Fiber Types

A fiber can either be single mode or multimode. The multimode fibers are categorized into; multimode graded index, and multimode step-index. The behavior in which light propagates through a fiber characterizes it.

2.3.2.1 Single Mode Fiber (SMF)

For a SMF it's only the fundamental zero-order mode that is transmitted. No reflections are encountered at the core-cladding in this fiber because light travels straight as a single strand. It is characterized by the cutoff wavelength value, dependent on core diameter, Numerical Aperture (NA), and operational wavelength. It is below this wavelength that higher-order modes may be transmitted hence change in the properties of the fiber. Modal dispersion is got rid of because SMF propagates the fundamental order alone. This type has got a higher bandwidth compared to a multimode fiber making it suitable for long distance communication. The diameter of the core, numerical aperture and light wavelength dictates the real number of modes that can be transmitted through a fiber. They have a diameter of about 8 -9 μm . The normalized frequency parameter or V number combines all these features by the equation:

$$V = \frac{2\pi}{a} \sqrt{n_1^2 - n_2^2} = \frac{2\pi}{\lambda} \text{NA} \quad (2.1)$$

Where core radius is given by a , wavelength of the transmitted light is λ , and the refractive indices of the core and cladding are given by n_1 and n_2 .

A SMF operates under a condition:

$$V \leq V_{\text{cutoff}} = 2.405 \quad (2.2)$$

The cut off wavelength below which two or more modes can be transmitted through a fiber is given by:

$$\lambda \geq \lambda_{\text{cutoff}} = 2.6 \text{ aNA} \quad (2.3)$$

When choosing a fiber, you consider the one with a lower cutoff wavelength compared to the desired operational wavelength.

For distributed sensing applications, SMF are preferred over the multimode fibers because they tend to maintain the optical signal intensity along the fiber (Zhang *et al.*, 2024).

2.3.2.2 Multimode Fibers

They have very large core diameters compared to SMFs hence resulting to the propagation of higher-order modes. The alignment of optical sources and connection is easily achieved because of the larger core diameter (Güemes, 2014). Their diameter is about 50 μm . They are applicable in light guiding applications such as in medicine or in Local Area Network (LAN). It is suitable for intensity-based sensors when it comes to sensing.

2.3.3 Fiber Optic Sensor

Fiber optic sensors are also known as optical fiber sensors (OFS(s)). They utilize OF as a sensing element. They are responsible for sensing various parameters such as; pressure, chemical concentrations, temperature, displacements or vibrations amongst many

others. Since fibers don't utilize electrical power at remote location and their tiny size, they are widely used in remote sensing and are suitable even for harsh condition (Gholamzadeh & Nabovati, 2008).

FOSs are super for unstable environments and insensitive conditions such as extreme temperatures, noise and high vibrating regions. They can be correctly and easily fixed in small areas when need for flexible fibers arises. The optical frequency-domain reflectometry (OFDR) aids in calculation of the wavelength shift while the optical time-domain Reflectometer (OTDR) helps in deciding the time-delay of FOSs.

Figure 2.4 is the diagrammatic representation of how a fiber-optic sensor works. It is made up of a light source, fiber under test (FUT), sensing element, photo detector and end-processing devices such as digital signal oscilloscope (DSO), optical-spectrum analyzer (OSA) and digital signal processor (DSP).

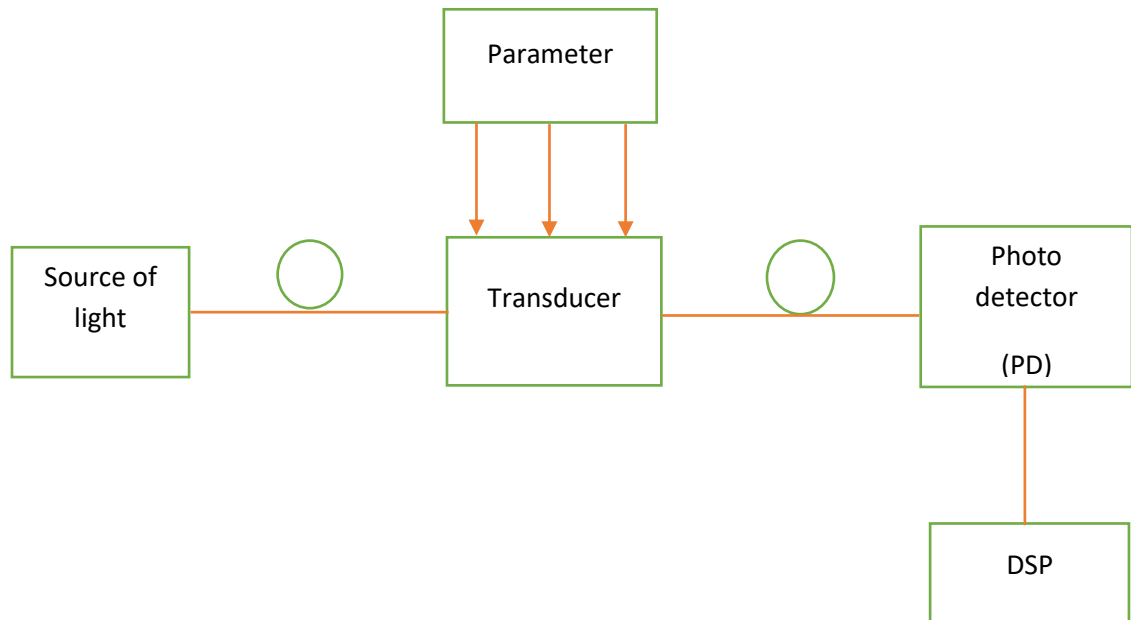


Figure 2.4: Diagrammatic representation of fiber-optic sensor

2.3.3.1 Fiber-Optic Sensor types

They are classified and described based on; sensor location, their operating principles and applications.

Classification of fiber optic sensors according to sensor location

They are classified as intrinsic and extrinsic FOSs. For the intrinsic sensors, sensing happens within the fiber. They rely on the features of the FUT itself in conversion of an environmental effect into a modulation of the light beam traversing it. In this sensor type, one of the physical features of light signal may be in the form of intensity, phase, frequency or polarization. It has an ability to provide sensing over long range distances that is distributed. The working principle of this FOS is illustrated in Figure 2.5.

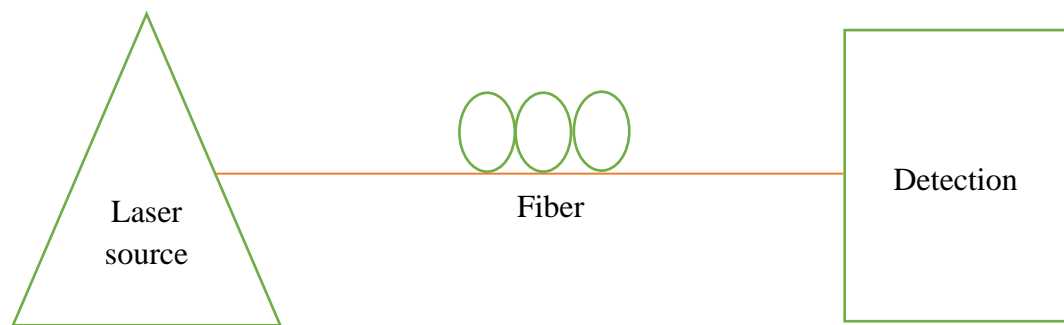


Figure 2.5: Intrinsic fiber optic sensor

In extrinsic sensors, the fiber is used as an information carrier leading to a black box to impress information on a light beam propagating to a remote receiver. The information arrived at the black box dictates the light signal generated. The black box can comprise up of mirrors, gases or any other mechanisms having an ability to generate an optical signal.

They are responsible for measuring the following parameters: displacement, vibration velocity, rotation, twist, torque and acceleration. An advantage of these sensors

is their capacity to access areas which are otherwise inaccessible (Elprocus, 2022). Internal temperature measurement of aircraft jet engine is a good illustration of this sensor since it utilizes a fiber in transmission of a radiation into a radiation pyrometer outside the engine. They provide excellent protection of measurement signals against noise corruption. Figure 2.6 illustrates how an extrinsic fiber optic sensor operates.

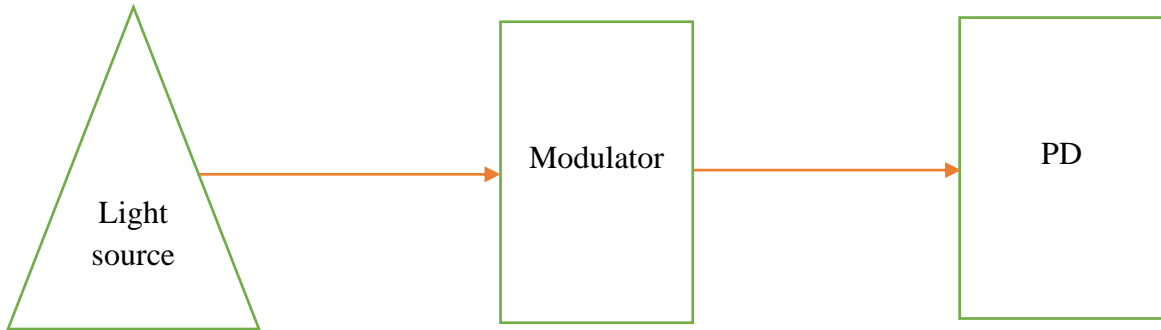


Figure 2.6: Extrinsic fiber optic sensor

Classification of fiber optic sensors according to their operating principles

They are classified as intensity, polarization and phase-based sensors.

(a) Intensity based Fiber Optic Sensor

In this type, a multi-mode-large core fiber which is lighter is employed. Figure 2.7 gives a simple closure or vibration sensor consisting of two optical fibers held in closeness to one another. When light is directed (incident) in one of the OFs; as it leaves, it spreads out into a cone of light whose angle relies on the difference (Yu & Yin, 2002). Figure 2.7 is an insight of how light intensity is utilized as a sensing parameter and how the fiber can work as a vibration sensor. In case of a vibration, light injected from one end to another end changes hence an intelligent measurement of the vibrational amplitude.

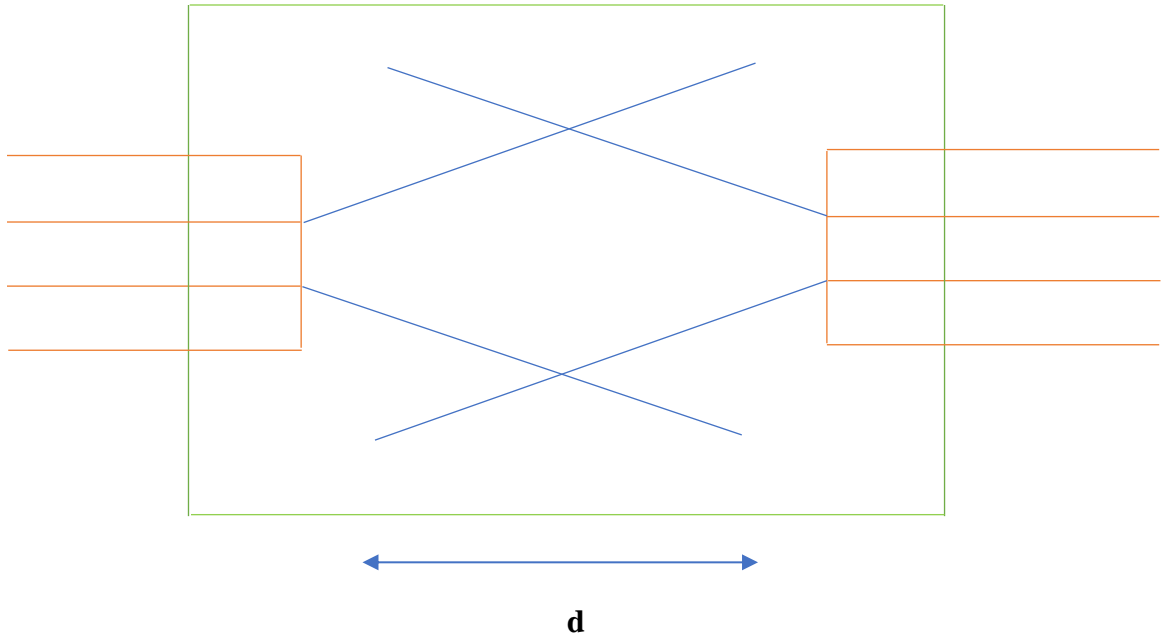


Figure 2.7: Intensity based fiber optic sensor

A normalized modulation index (m) for this class of sensors is given by:

$$m = \frac{\Delta I}{I_0 \cdot P} \quad (2.4)$$

Where, ΔI - change in optical power resulting from a modulation; I_0 - optical power that arrives at the detector in the absence of a modulation; and P - perturbation (Yu & Yin, 2002).

These sensors suffer the many limitations arising from variable losses in the system. These variable losses are; splices losses, micro and macro bending losses, connection losses at joints among others. Most of the higher-performing, intensity-based fiber sensors do utilize dual wavelengths so as to mitigate these problems. By bypassing the sensing region all the mistakes arising from unwanted intensity variations are calibrated out by one of these wavelengths (Davis *et al.*, 2006).

The strengths of these fiber optic sensors are that they: are cheaper, can work as real distributed sensors, its simplicity in use, can be multiplexed, etc. (Fenta *et al.*, 2021).

The variation of light intensity and relative measurements among others hinders this class of sensors.

(b) Fiber Optic Sensor based on polarization

They are crucial for a particular sensor type. These sensors are applicable in measuring various parameters because of their property to be modified by different external variables. Special fibers and other components of the same polarization features have been developed. They are applicable in various measurements, communication and signal processing.

Figure 2.8 shown is the optical setup for a fiber optic sensor based on polarization. The polarizer is used to polarize light emanating from the source. Injection of light that has been polarized is done at 45° to the selected axes of a length of birefringent polarization preserving fiber. It is in this section of the fiber that it acts as a sensor. In case of any external impact such as stress or strain, there will be a change in the phase difference between the two polarizing states (Rashleigh 1983, Wang *et al.*, 2004).

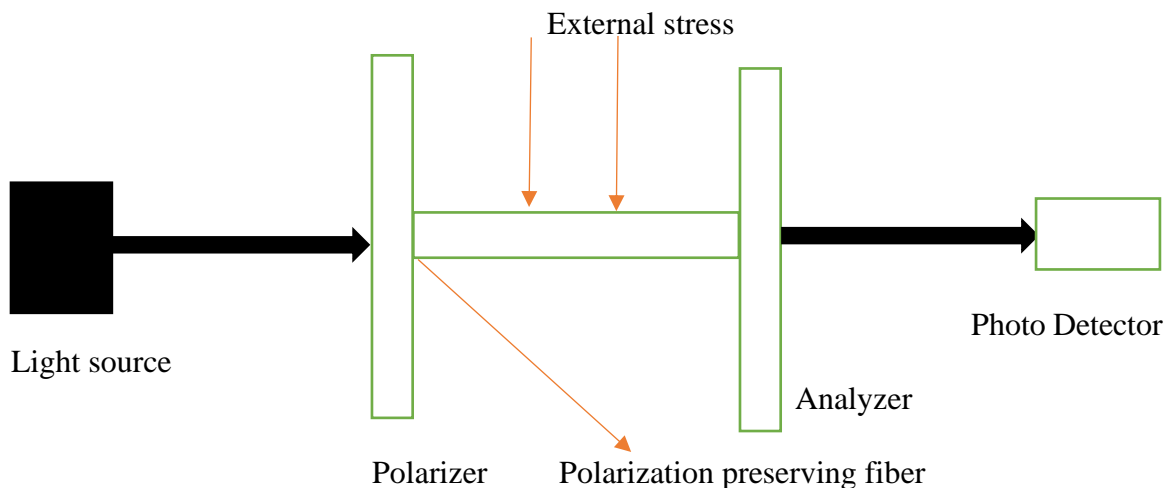


Figure 2.8: Fiber optic sensor based on polarization

It through this external impact that the output polarization changes. The detection of these external disturbances is then detected at the other end of the fiber through the output polarization state.

(c) Fiber Optic Sensor based on phase

They are utilized in transforming emitter light on the signal carrying information wherein the signal is studied using a FOS basing on the phase. Light splits into two beams when it is transmitted through an interferometer. One of these beams is subjected to the environment being sensed (under test) as the other is kept away from the environment being sensed, taken to be a reference. Later on, these beams recombine and move together (Byeong *et al.*, 2012). Michelson, Mach-Zehnder, Sagnac, grating and polarimetric interferometers are examples of the mostly employed interferometers.

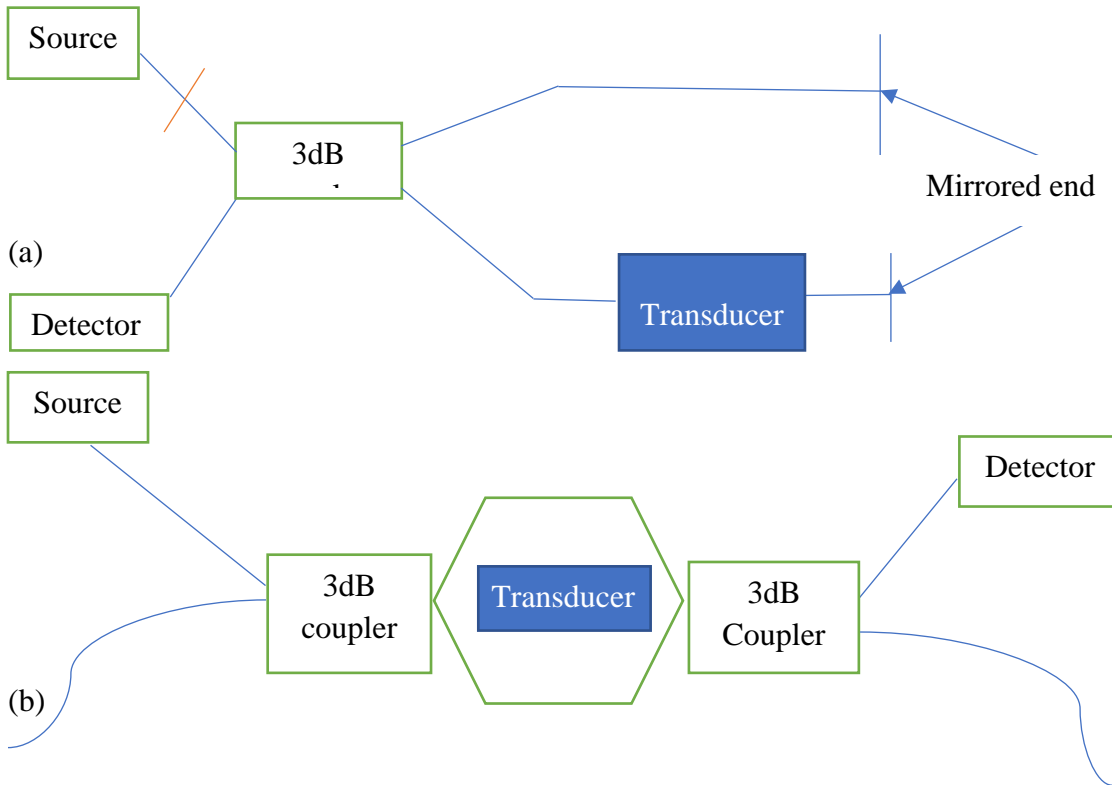


Figure 2.9: Fiber optic sensor based on phase: a) Mach Zehnder b) Michelson

Figure 2.9 illustrates the Mach Zehnder (a) and Michelson (b) interferometers. In most cases, the Michelson Interferometer is assumed to be a folded Mach Zehnder interferometer. For the Michelson interferometer to be configured it only adopts a single optical fiber coupler. Here, the optical phase shift per unit length is doubled due to light propagating twice through the sensing and reference fibers. This property places the Michelson at better place in terms of sensitivity. The ability of the Michelson to interrogate the sensor just with a single OF in between the source and the detector makes it advantageous. The only limitation for this interferometer is that a good-quality reflection mirror is needed.

The external perturbations can cause a change in the light field phase such that the fiber optic sensor can as well be constructed basing on the light field's phase changes (Gholamzadeh & Nabovati, 2008). The phase and optical path change are related by the equation below:

$$\phi(r, t) = \frac{2\pi}{\lambda} L(r, t) \quad (2.5)$$

Where, λ is the wavelength and $L(r, t)$ is the change in the optical. An insignificant change in the optical path can result in large phase change because of the tiny optical wavelength (Yu & Yin, 2002).

2.3.3.1.3 Classification of fiber optic sensors according to application

They are classified as chemical, physical and bio-medical sensors.

Chemical Sensor

It is used to convert a chemical information into a physical signal that can be measured and linked with the chemical concentration of a particular chemical family. It is an important component of an analyzer which may as well comprise up various devices

performing various functions such as: sampling, data and signal processing. An analyzer can be a crucial component of the automated system. Figure 2.10 is a schematic representation of a chemical sensor.

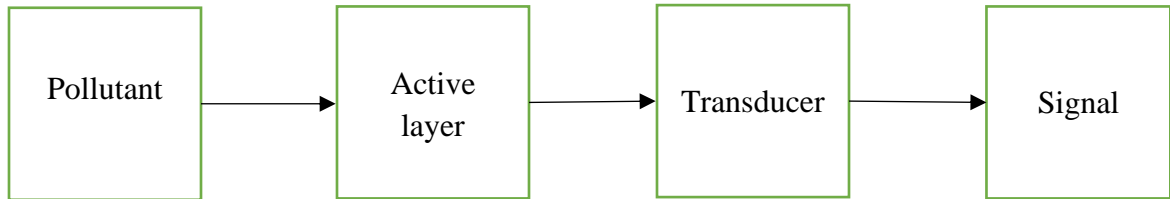


Figure 2.10: Illustration of the chemical sensor

According to a sampling plan, the analyzer is considered to be a monitor. These sensors are made up of two units that are functional; a receptor and transducer. Chemical information is converted to certain energy in the receptor part that can be measurable by the transducer. Chemical signal is converted to an analyzable signal that is insensitive at the transducer (Elprocus, 2022).

Physical Sensor

It is designed in regard to a physical property of a given element. It gives information about a certain physical feature of a material being investigated.

Bio Medical Sensor

Is capable of transmitting a variety of non- electrical quantities from the human body into electrical quantities that can be easily detected. This makes sensors very vital in the health sector.

2.3.4 Fiber Optic Sensors Applications

FOSs are widely used in our day-to-day life. Some of these applications include: measuring of physical properties of elements such as strain, displacement, velocity and temperature etc. They are employed in real time monitoring of physical structures. They

are also used large composite and concrete structures such as mines, aircrafts, etc. In medicine, they can be used for; blood monitoring, detection of cataract etc. They are applicable in monitoring electrical power load on electrical transmission cables. Used in oil and gas industry for monitoring pipelines. Can be utilized as crack sensors.

2.3.5 Optical Time-Domain Reflectometer (OTDR)

It is an optical tool for characterizing, troubleshooting and maintaining optical telecommunication networks. In order to test the performance of an OTDR, a pulse laser light is transmitted and analyzed as it propagates through an OF. Since light is injected at most extreme end of an OF cable link this measurement is considered unidirectional.

An OTDR acts as an optical radar system because it is capable of feeding the operator with adequate data on defects, splices condition and location and other properties that are of interest by utilizing the information gathered from the resulting light signature reflected or back scattered to the source.

2.3.5.1 OTDR working principles

An OTDR comprises of a laser diode source, a photodiode detector and time base as depicted in Figure 2.11. The laser gives out light pulse at a specified wavelength which then propagates.

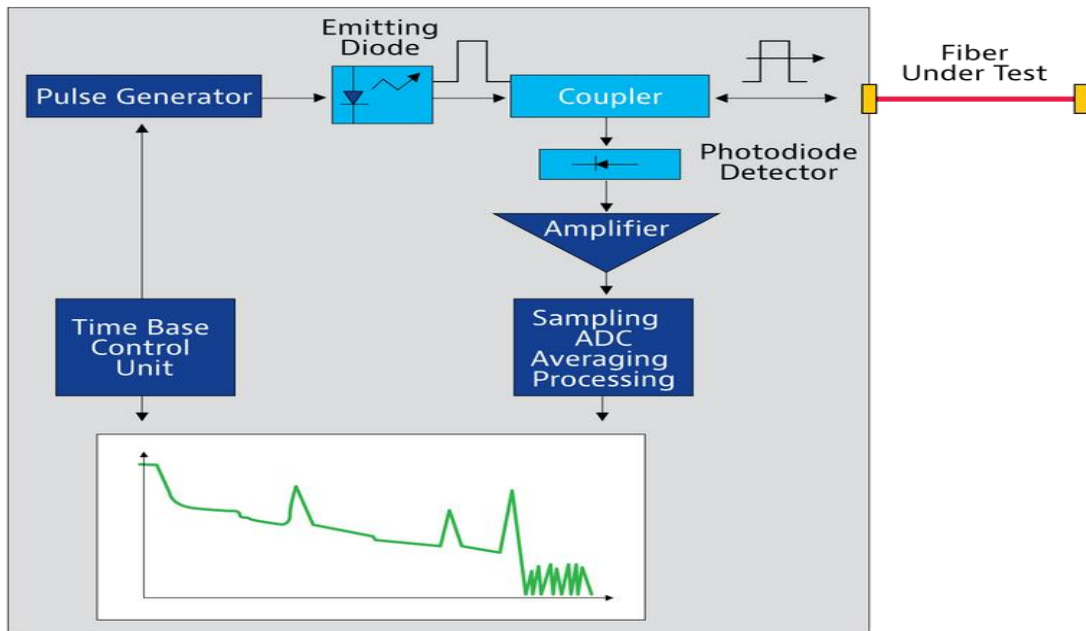


Figure 2.11: OTDR working principle (Courtesy of Viavi Solutions)

Some of the transmitted light is reflected or back scattered to the photodetector found in the OTDR. It is through the amount of this light getting back and the length of time it takes to reach the photo detector that we can report on the loss value, the type and location of phenomenon in a fiber as shown in Figure 2.12.

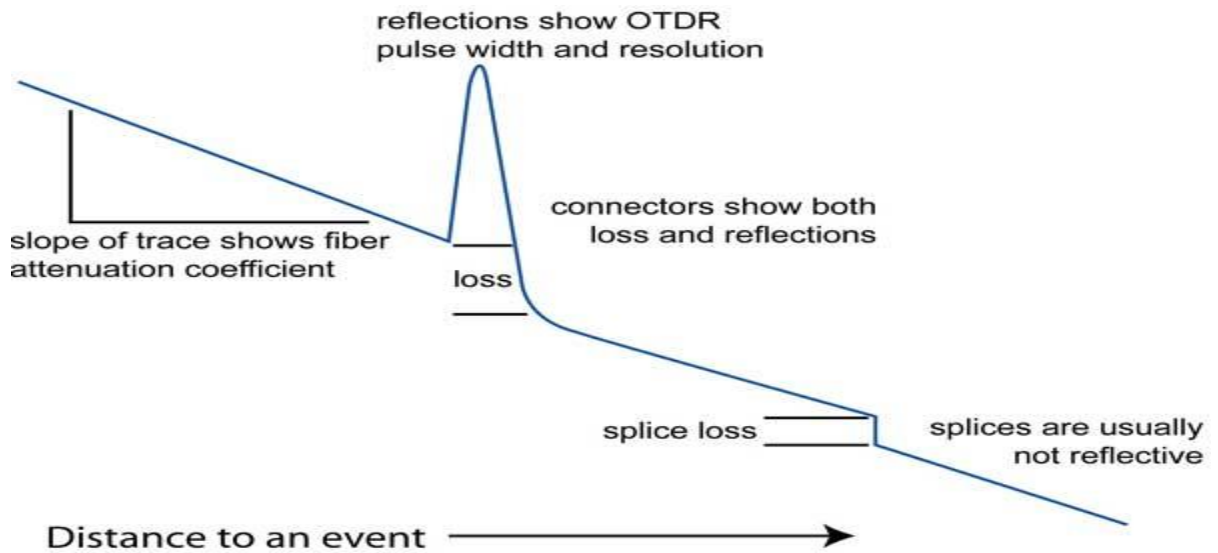


Figure 2.12: Information in the OTDR trace (Courtesy of Viavi Solutions)

Light gets back to the photo detector in various ways. These include:

Rayleigh Scattering and Backscattering

Rayleigh scattering is a process in which some incident light into a fiber split and move in different directions due to its interaction with tiny particles present in the fiber. Backscattering on the other hand refers to a scenario where some of the injected light scatters back in a direction that is opposite to the incident light as shown in Fig 2.13.

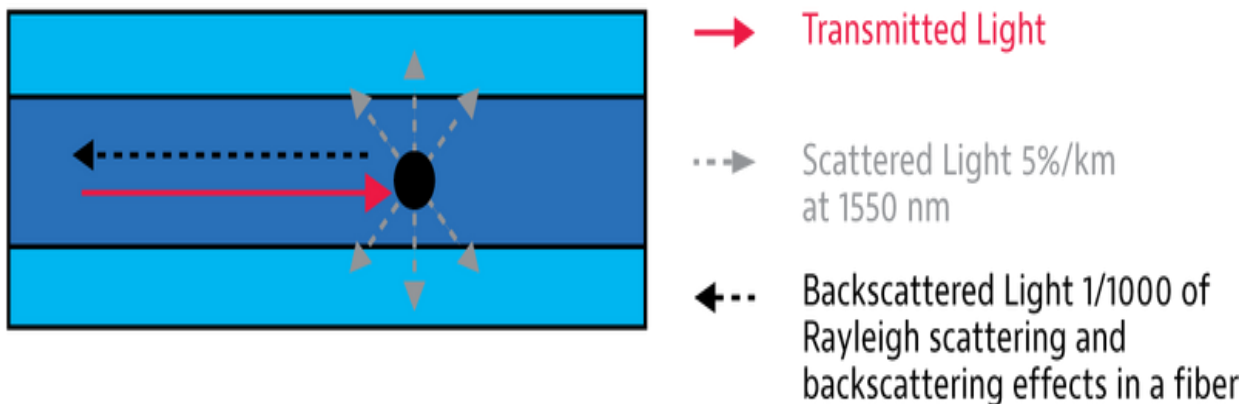


Fig 2.13: Illustration of Rayleigh scattering and backscattering (Courtesy of Viavi Solutions)

Rayleigh scattering has been adopted as the operational principle in OTDR because it is easily predicted. The quantity of light scattered back to the detector gives a picture of the attenuation and signal loss in the optical fiber.

Fresnel Reflection

Fresnel came up with the reflection coefficient; the ratio of the reflected light wave amplitude relative to the original source wave. Fresnel reflection is achieved when light bounces off an interface of two optically transmissive media with varied refractive index as in Figure 2.14. It is at a joint, a non-terminated fiber end, or break that this boundary can be realized.

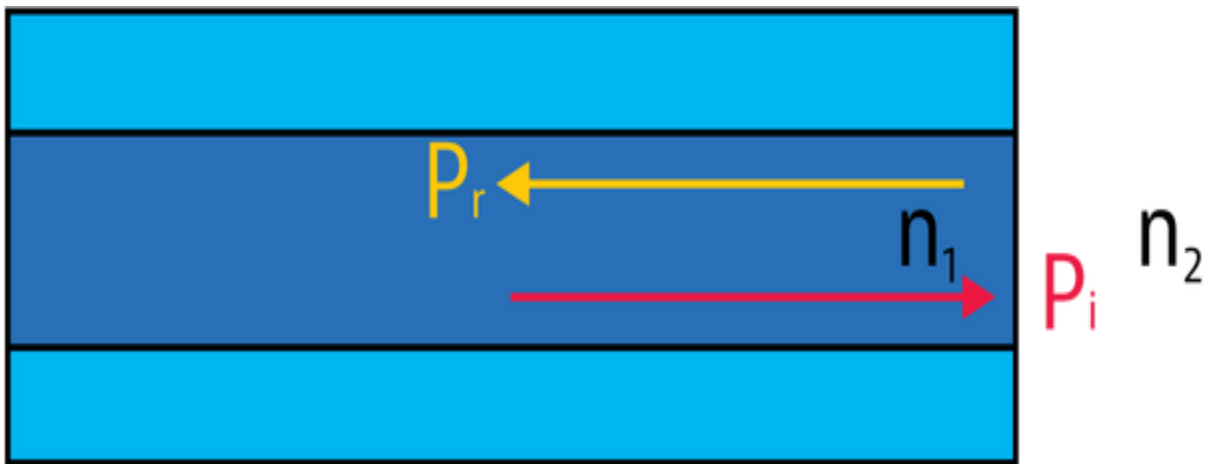


Figure 2.14: Illustration of Fresnel reflection (Courtesy of Viavi Solutions)

Fresnel reflection equations can be utilized in achieving the intensity, nature and position of various activities in a fiber link which include; breaks, splices, connections and terminations representing interaction of materials such as air and glass.

Absorption

Because of impurities presented in a fiber some of the light injected into it is absorbed by them. When a fiber has fewer impurities, it implies that the absorption rate will be low hence a higher quality material resulting in minimal loss of the signal.

2.3.5.2 Optical Frequency Domain Reflectometry (OFDR)

Optical Frequency Domain Reflectometry (OFDR) is responsible for analyzing light paths and the reflectional characteristics in optical fibers. Unlike Optical Time Domain Reflectometry (OTDR), OFDR operates in frequency domain utilizing continuous wave (CW) light sources hence higher signal to noise ratios (Pierce *et al.*, 2000, Palmieri & Schenato, 2013)

Light of a specific wavelength is injected into a fiber and after some time it's brought into interference with a reference arm. It's through the Fourier transformation of the resulting signal that the spatial distribution of the reflected light is obtained. It is through intrinsic Rayleigh scattering of the glass or enlargement that we obtain the reflection or it can undergo enlargement in the fiber which is low reflective hence continuous written Fiber Bragg Gratings. By monitoring the changes of the Rayleigh or FBG reflection pattern or peaks, strain and temperature measurements are recorded. It is advantageous to put in practice FBGs over Rayleigh because of their increased signal to noise ratio enhancing higher measurement speeds. Strain or temperature measurements can be obtained in sub-Millimeter resolution over several 10's of meters by the OFDR.

2.3.6 Fiber Bragg Grating Sensor

A fiber Bragg grating (FBG) sensor is just but a Bragg reflector built in a small section of an OF that is distributive in nature that reflect certain light wavelengths as the rest are transmitted as illustrated in figure 2.15. It is at the core of a fiber than an FBG is created due to varied period in its refractive indices.

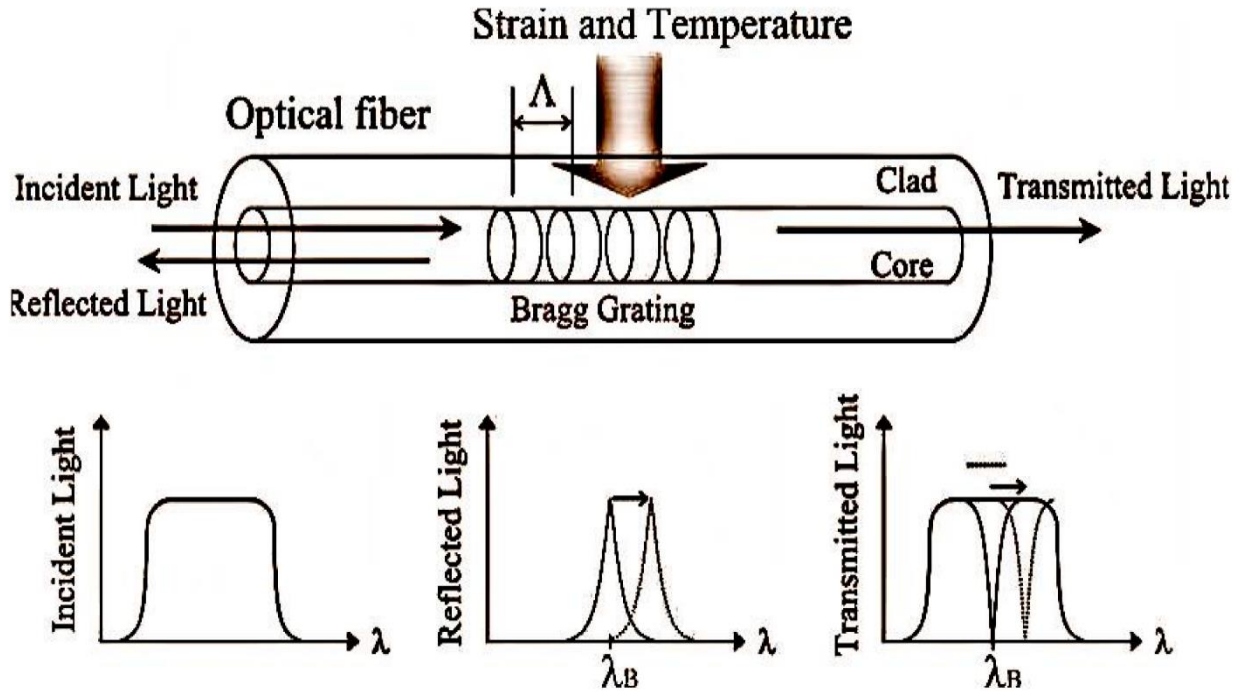


Figure 2.15: Fiber Bragg grating (FBGS, 2017)

Fresnel reflection is the major principle behind the working of an FBG, in that light traversing through media of varied refractive indices may reflect or refract at the interface (Hill & Meltz, 1997, Güemes, 2014). FBG resonance (or Bragg) wavelength (λ_B) is:

$$\lambda_B = 2n_{eff}\Lambda \quad (2.6)$$

Where the pitch grating (periodicity) is Λ , and the effective fiber's core refractive index is n_{eff} . The applied strain (ϵ) and temperature changes (T) causes a shift in the Bragg wavelength and is expressed as:

$$\frac{\Delta\lambda_B}{\lambda_B} = K_\epsilon\epsilon + K_T T \quad (2.7)$$

The fiber strain effect is catered for by the first term of Eq. (2.7) and the physical elongation of the grating pitch dictates the coefficient K_ϵ as well as the strain-optic coefficient of the

fiber. The temperature effect on the grating is represented by the second term and K_T is the temperature coefficient.

2.3.7 Polarization in fibers

Light is characterized by polarization since it's an electromagnetic wave. Polarization is described in terms of the pattern traced out in the transverse plane by the electric field vector as a function of time and its optical power is a scalar quantity that is proportional to the mean square of the electric field amplitude. If light is propagated in the z direction, then the polarization vector is in the x-y plane. By superposition of the x- and y-vector components at time t at any location, the polarization vector is expressed as (Collett, 1992);

$$E(t) = E_x(t) + E_y(t) \quad (2.8)$$

Where, $E_x(t)$ and $E_y(t)$ are the amplitudes of the x and y components of the electric field.

Polarization of light normally appears in three forms that is linear polarization, circular polarization and elliptical polarization. Generally, all polarized light takes the elliptical polarization state (Jena *et al.*, 2020) with the linear and circular states being special cases. Polarization and changes in states of polarization are described using a geometrical representation known as the Poincare' sphere (Walkenhorst & Nichols, 2020). Each state of polarization corresponds to a unique point on the sphere. Linearly polarized light is represented by the points on the equator while the two poles on the sphere represent left- and right-hand circularly polarized light. Elliptical state of polarization is represented by all other points on the sphere.

The Stokes parameters have a simple physical interpretation related to Poincare' sphere representation. They also have a physical interpretation related to intensity

measurement. In a given Oxyz reference system (Oz being the direction of propagation of light), the stokes vectors can be expressed as (Nabadda *et al.*, 2018):

$$S = \begin{bmatrix} S_0 \\ S_1 \\ S_2 \\ S_3 \end{bmatrix} = \begin{bmatrix} I_0 \\ I_x - I_y \\ I_{+45^\circ} - I_{-45^\circ} \\ I_L - I_R \end{bmatrix} \quad (2.9)$$

Where I_0 is the total power of light, I_x, I_y are the x and y linearly polarized light intensities, $I_{+45^\circ}, I_{-45^\circ}$ are the $+45^\circ$ and -45° linearly polarized light intensities and I_L, I_R are the left and right hand circularly polarized light intensities. Normalizing $\{S_1, S_2, S_3\}$ by S_0 , we will get the SOP $\{S_1, S_2, S_3\}$, which are the coordinates of one point on the Poincare' sphere; S_1, S_2 and S_3 being the states of polarization.

2.4 Identification of Knowledge gap

With the depletion of shallow reserves, continuous demand for minerals and precious metals and economic growth for miners, mining has shifted into deeper operations which poses various safety threats. Any significant increases in productivity and safety necessitate a dependable real-time monitoring system that offers more thorough data about multiple processes. There is limited data in the literature on developing a comprehensive mine disaster management system based on fiber optic sensor network, capable of early warning (real-time monitoring system) and control of mining hazard.

CHAPTER THREE

METHODOLOGY

3.1 Introduction

This section describes the materials and methodological procedures that were used to conduct the research.

3.2 Materials

For experimental investigation, a test-bed was built in the lab. The following materials were used; laser sources, optical fibers, power meter, polarization analyzer, personal computer (PC), Mach-Zehnder modulator (MZM), programmable pattern generator (PPG), Photodiode (PD), bit error rate tester (BERT) and digital signal oscilloscope (DSO). MATLAB software was adopted for offline signal processing.

3.3 Research Design

This study involved experimental analysis. The transmission performance of different laser sources was investigated over various fiber lengths. Figure 3.1 (a) below shows a schematic representation for investigating transmission performance over various fiber lengths.

The PPG was used to generate a pseudo-random bit stream (PBRs) pattern consisting of 0 and 1 bits. This is a typical representation of a digitized information/data. Light from a laser source was modulated with the generated pattern and then transmitted over a fiber under test (FUT). In this design, the fiber was utilized both as a signal propagating medium and sensing element (Tang & Cheng, 2018, Kipnoo *et al.*,2020).

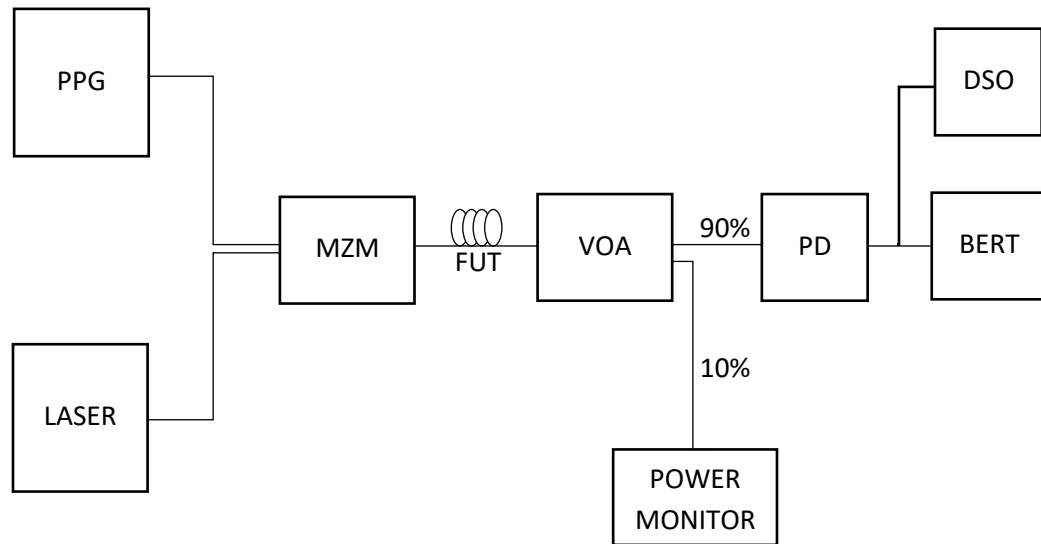


Figure 3.1 (a): Schematic representation for investigating transmission over various fiber lengths

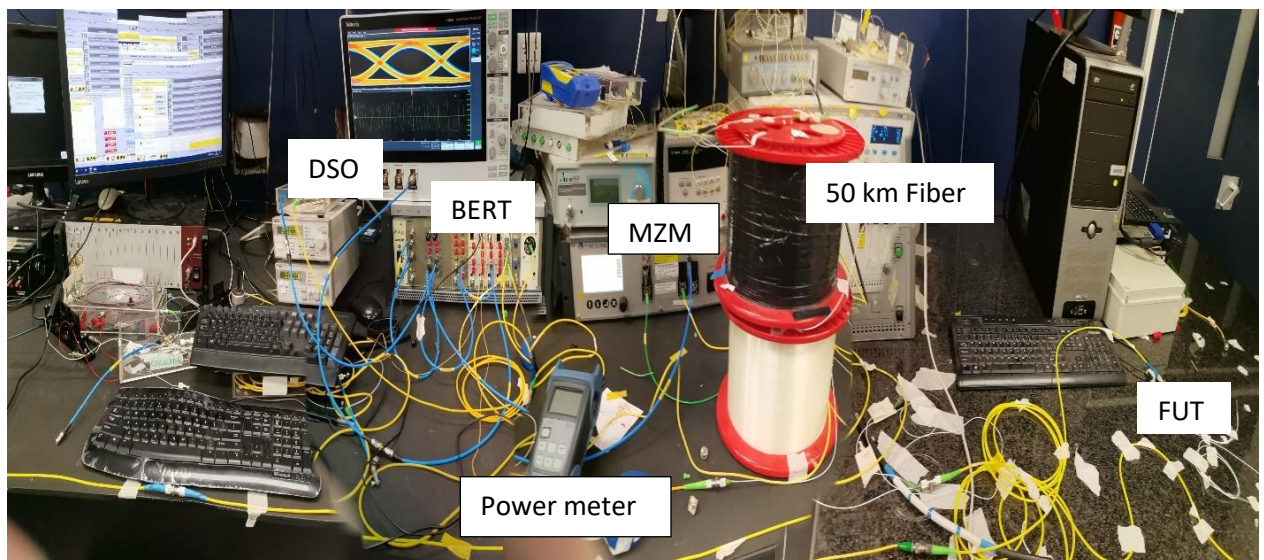


Figure 3.1 (b): A picture of experimental setup in investigating transmission over various fiber lengths.

Figure 3.1 (b) is a picture of the laboratory setup for investigating transmission performance. This was essential in determining the fiber length that an optical signal can be transmitted, ensuring maximum coverage of the risk potential area. The variable optical attenuator (VOA) was employed in stepping down the optical power as the bit error rates (BER) of the transmitted signal was monitored. 90% of the transmitted signal was fed into

the PD while 10% was utilized for monitoring purposes. A photodetector (PD) was used to convert the optical signal into electrical. The BERT was employed in establishing the transmitted BER. The DSO was used to visualize the eye and individual bits. Figure 3.2 (a) below shows the schematic representation of the proposed fiber optic sensor design.

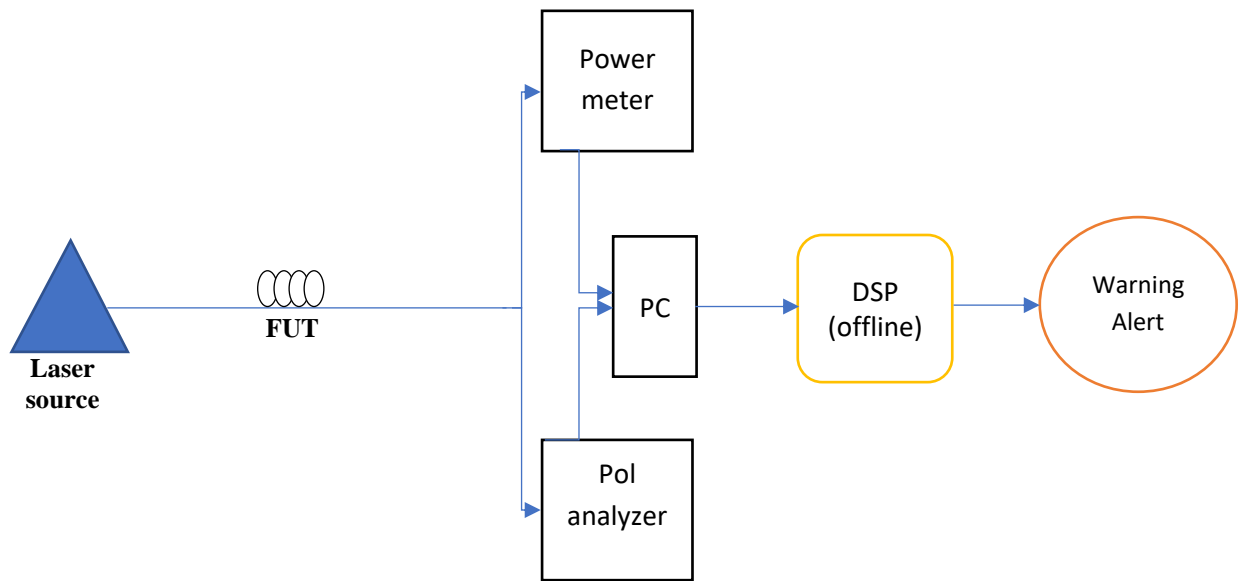


Figure 3.2 (a): schematic representation of the proposed fiber optic sensor design

Light emanating from a 1550 nm laser source was directed into a single-mode fiber (SMF) of about 3 m length. Three laser sources were put into consideration; Distributed Feedback (DFB), wavelength division multiplexing (WDM) and Mach-Zehnder modulator (MZM) sources. The monitoring process focused on a fiber under test (FUT), where a specific segment of the fiber underwent controlled strain during a laboratory experiment thus simulating the mine collapse conditions. In a typical mine collapse, a mass of soil falls on the fiber thus inserting stress/strain in it. This is in turn expected to affect the propagating signal in the medium. An optical fiber has an ability of detecting strain over a wide region, by increasing or reducing the length of the fiber, the area under monitorization

is controlled (Tang& Cheng, 2018). It is through this that the power and SOP of the transmitted signal were monitored so as to establish the effects of stress on a fiber. Four fiber types namely; G652 Corning, G655 Corning, G655 OFS and PMF Corning were put under investigation.

To examine the behavior of the signal's polarization, a polarization analyzer was employed, while a power meter simultaneously recorded the power readings. Subsequently, digital signal processing (DSP) facilitated the offline analysis of the transmitted signal. MATLAB was adopted in offline processing. This processed signal served as the basis for triggering an alarm in response to alterations in the soil profile thus ensuring the mine safety.

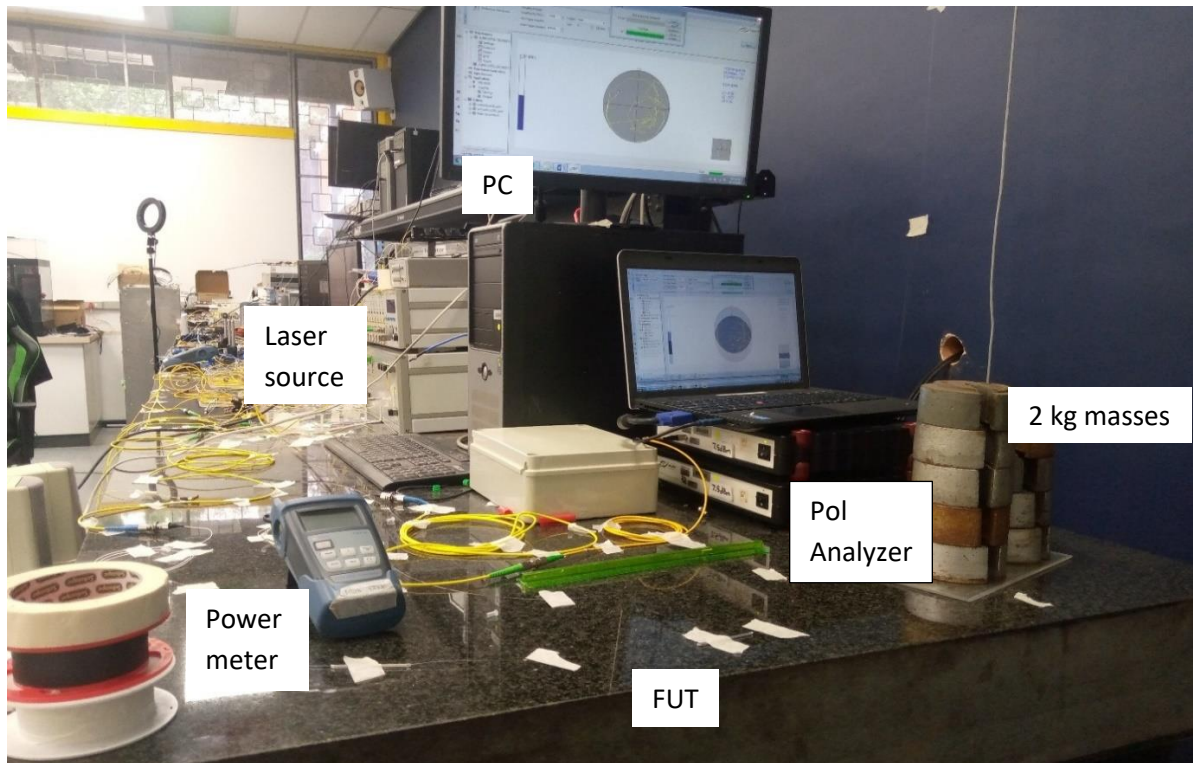


Figure 3.2 (b): A picture of a laboratory setup of the proposed fiber sensor design

In an experimental test-bed scenario, the Fiber Under Test (FUT) was subjected to gradual loading with 2kg masses up to 18 kg. This was done at an interval of 10 s. These masses were loaded on a straight and coiled fiber sections. This was critical in understanding how different configurations affect sensitivity. Simultaneously, the power levels and States of Polarization (SOPs) were closely monitored using a power meter and a polarization analyzer, respectively. A computer (PC) served as the interface for both visualizing and gathering the recorded SOP data as shown in figure 3.2 (b).

The collected SOP data was represented on a geometrical representation tool known as the Poincare sphere which then underwent offline digital signal processing (DSP) for analysis. This analysis was aimed at determining any changes or drift in SOP resulting from the applied strain/stress on the FUT. The system was configured in such a way that it triggers an alarm when the detected SOP drift exceeds a predefined threshold.

3.4 Location

A laboratory test-bed was built at the Centre for Broadband Communication, Physics Department, Nelson Mandela University, South Africa so as to investigate the proposed design.

CHAPTER FOUR

RESULTS AND DISCUSSIONS

4.1 Introduction

This chapter entails the results and the respective discussions of the findings obtained. Power and states of polarization fluctuations and transmission performance of the designed testbed have been reported.

4.2 Power and States of Polarization (SOP) Fluctuation

Light emanating from three laser sources namely; Distributed-feedback (DFB), Mach-Zehnder Modulator (MZM) and Wave-Division Multiplexing sources was each injected into four different fiber links at different time intervals. These fiber types were as follows: G655 OFS, G655 Corning, G652 Corning and Polarization Maintaining fiber (PMF) Corning. About 3 m of each of these fibers was put under investigation in a laboratory test-bed for purposes of monitoring. The choice of 3 m is because any fiber section with induced birefringence affects the signal propagating (Kipnoo *et al.*, 2020). In the entire link, a section of these fibers was subjected to loading of 2 kg masses at an interval of 10 s. This was done gradually with additional masses up to 18 kg due to tensile strength of the fiber. These masses mimic the potential strain/stress/pressure that is likely to be experienced in a section of a mine causing a collapse. A rectangular glass was placed on top of the fiber before loading was done, this was to ensure that there was uniform distribution of weight across the section of the fiber subjected to strain.

The essence of loading these fibers with masses was to establish the power and polarization fluctuations when the fiber is strained by loading. The power fluctuations were monitored using a power meter while the SOPs were collected simultaneously by the

polarization analyzer. The load was then removed at the same interval in which loading occurred so as to free the fiber from strain. The input and output powers before loading and after unloading were noted. This was used to establish power losses under different conditions i.e. linear and coiled fiber orientations. During unloading power readings were recorded as the masses were withdrawn from the fiber gradually. The sensitivity of these lasers and fiber types was also established so as to determine the most suitable laser source and fiber to be employed in our design.

4.2.1 Linear fiber orientation

4.2.1.1 Performance of different laser sources during loading on various fiber types

When the three laser sources; DFB source, WDM source and MZM source were employed on a G652 Corning, the input power recorded for these lasers was approximately 0.422 dBm, 0.479 dBm and 0.482 dBm respectively as shown in figure 4.1 (a).

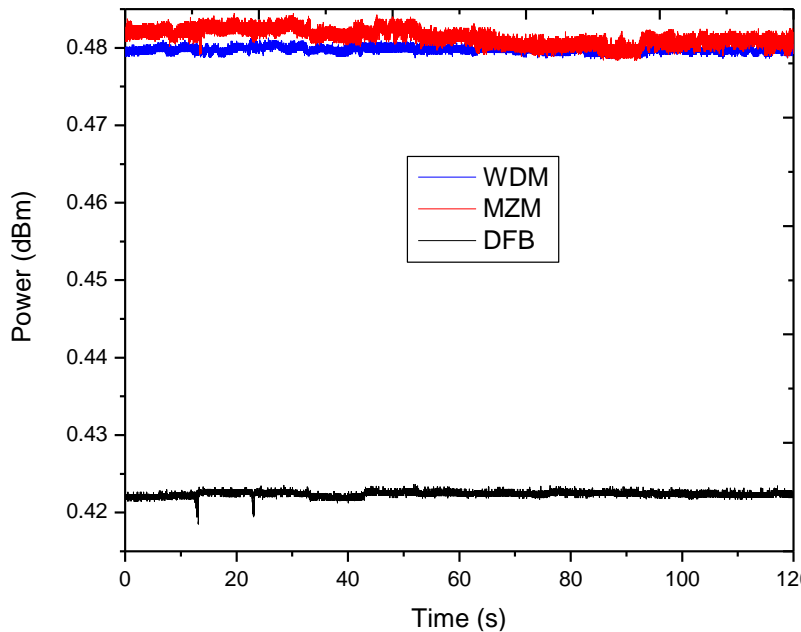


Figure 4.1 (a): Power fluctuation of light from each of the three laser sources; DFB, MZM and WDM sources injected on a G652 Corning fiber

The associated measurement error for power values was ± 0.0005 dBm and that of polarization was $\pm 0.5^\circ$. The output power for these sources was obtained to be close to 0.422 dB, 0.479 dB and 0.481 dB for the DFB source, WDM source and MZM source respectively. A slight power loss of about 0.001 dB was achieved on the MZM source which translated to a sensitivity of 0.00005 dBm/kg. It was evident that from figure 4.1 (a), there was some scattering of light since the trend/ trace was not smooth.

However, when the y-axis scale was enlarged, there was no significant power fluctuation and scattering noted as shown in figure 4.1 (b). The graphs obtained were perfectly linear for the three laser sources.

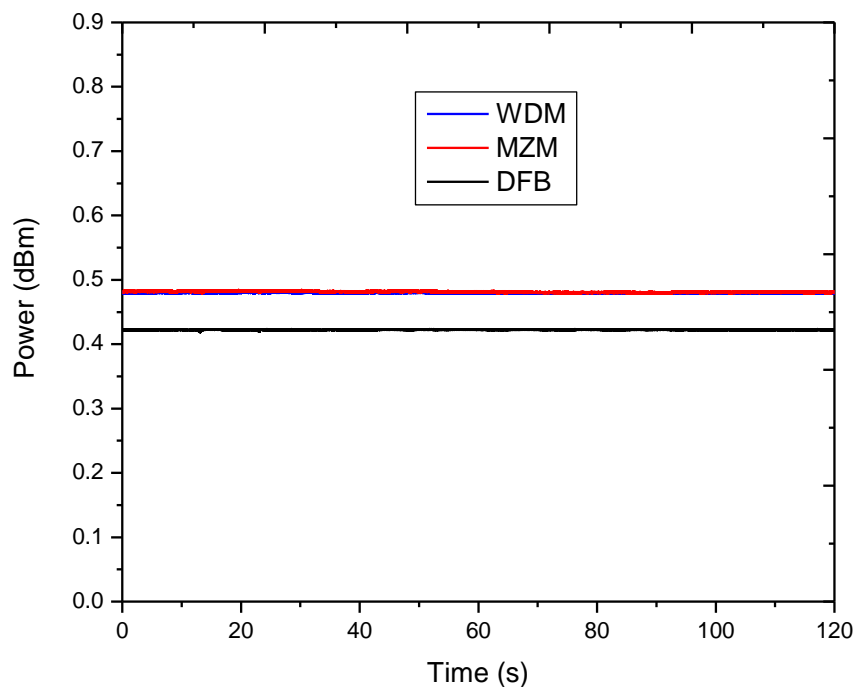


Figure 4.1 (b): Power fluctuation of light from each of the three laser sources; DFB, MZM and WDM sources injected on a G652 Corning fiber (y-axis scale enlarged)

The Poincare' sphere representation of the light from a DFB source propagating through a G652 Corning fiber in a linear orientation is shown in figure 4.1 (c). The normalized Stokes' parameters (S_1 , S_2 , S_3) as discussed in section 2.3.7 were used to plot

this information. From the trace it is evident that there was minimal distortion of the signal hence a low power fluctuation as depicted in 4.1 (a) and 4.1 (b).

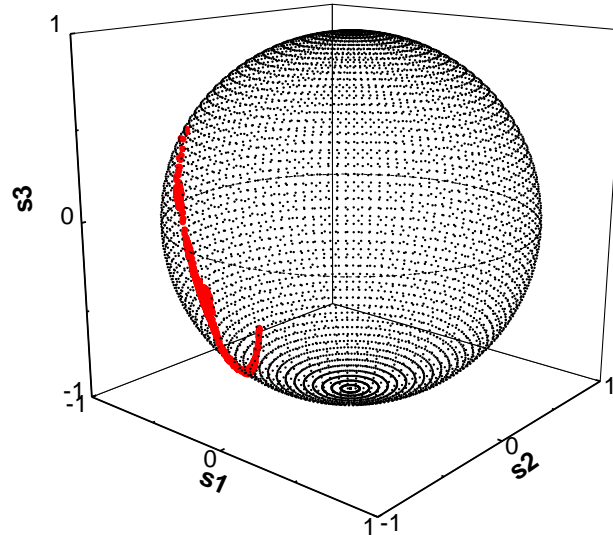


Figure 4.1 (c): Poincaré' sphere representation of SOP for DFB source injected on a G652 Corning fiber

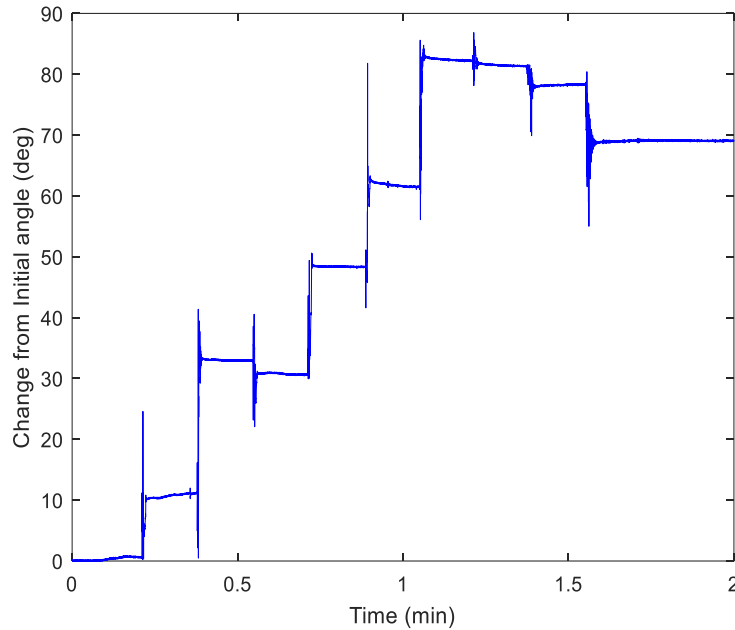


Figure 4.1 (d): A graph of SOP change with respect to time for DFB source injected on a G652 Corning fiber

The corresponding change in SOP of figure 4.1 (c) with respect to time is represented in figure 4.1 (d). This was enabled by the use of MATLAB software as

discussed in section 3.3. The initial angle before the fiber was strained was about 0° . A maximum change of about 85° was registered after approximately 63 s which translated to an instantaneous SOP speed of $1.35^{\circ}/\text{s}$. An overall SOP change of 499° was achieved after 120 s hence an average SOP speed of $4.16^{\circ}/\text{s}$.

Light emanating from these laser sources; DFB, WDM and MZM sources was also injected into a G655 corning fiber. The input power recorded before loading was done was approximately 0.539 dB, 0.504 dB and 0.502 dB for the DFB, WDM and MZM sources respectively as shown in figure 4.2 (a). After loading the fiber with the 18 kg mass the power recorded for these lasers sources was close to 0.534 dB, 0.493 dB and 0.499 dB for the DFB, WDM and MZM sources respectively. The DFB, WDM and MZM sources registered a power loss of about 0.005 dB, 0.011 dB and 0.003 dB respectively. This yielded a sensitivity of close to 0.0003 dBm/kg, 0.0006 dBm/kg and 0.0002 dBm/kg on the DFB, WDM and MZM sources respectively.

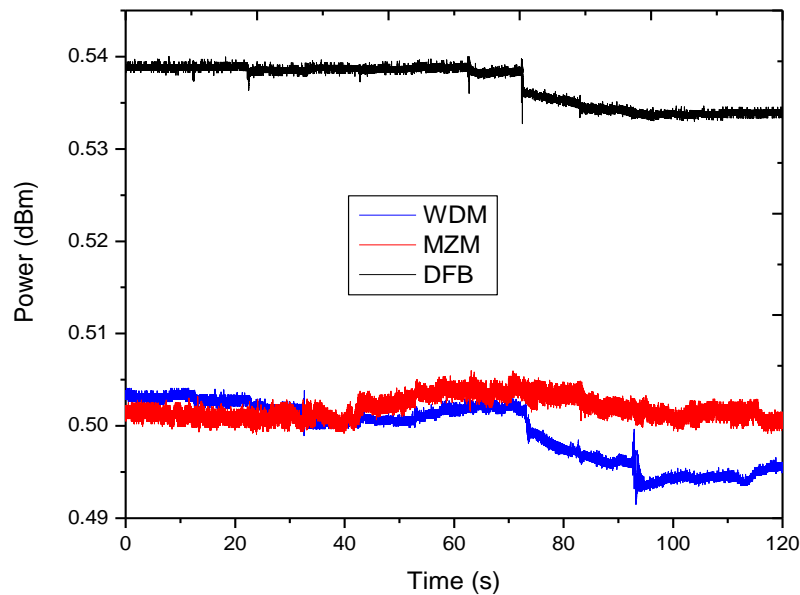


Figure 4.2 (a): Power fluctuation of light from each of the three laser sources; DFB, MZM and WDM sources injected on a G655 Corning fiber during loading.

When this data was plotted using an enlarged y-axis scale, a very slight fluctuation was noted on the graph as shown in figure 4.2 (b) unlike for the graph presented on figure 4.2 (a) above.

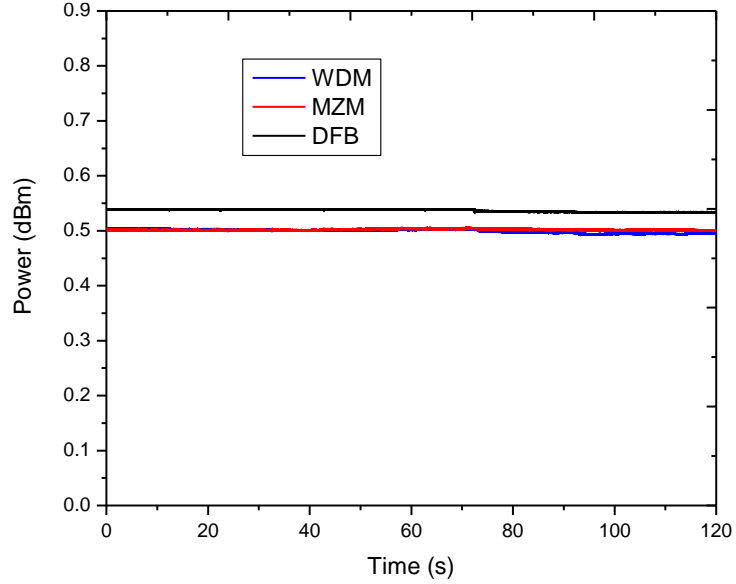


Figure 4.2 (b): Power fluctuation of light from each of the three laser sources; DFB, MZM and WDM sources injected on a G655 Corning fiber (enlarged y-axis scale)

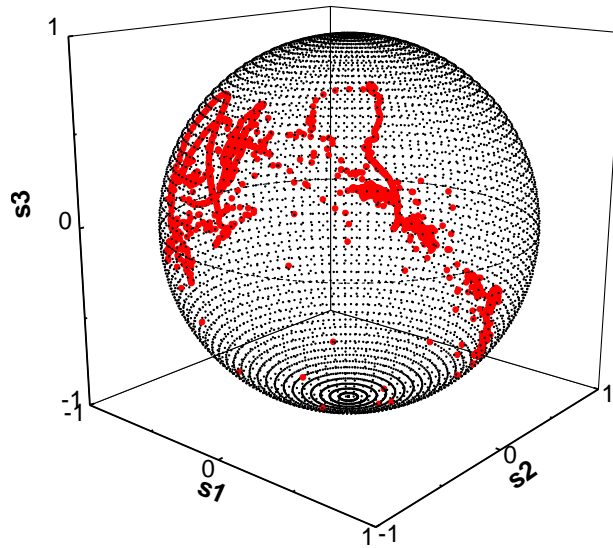


Figure 4.2 (c): Poincaré sphere representation of SOP change for a signal from WDM source propagating through a G655 Corning fiber during loading

Figure 4.2 (c) is the Poincare' sphere representation of the SOP change of WDM source. A random fluctuation was observed from the trace implying a significant distortion of the signal as shown in figure 4.2 (a) (refer to WDM source – blue in color). This implies a significant power loss in power during transmission. It is also evident the S_3 Stoke's parameter was dominant. Figure 4.2 (d) is a graph of change of SOP against time and maximum value recorded was approximately 130° after 52.5 s resulting to an instantaneous SOP speed of about $2.48^{\circ}/s$.

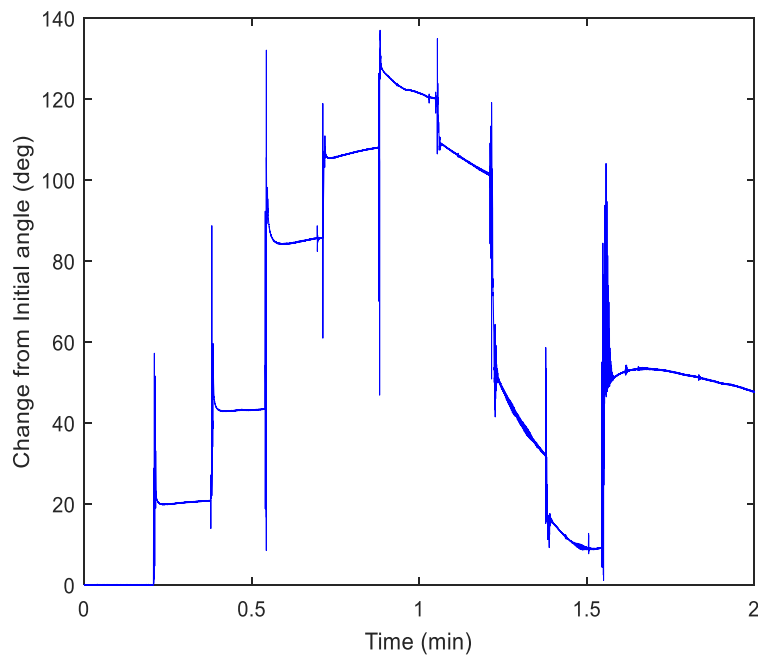


Figure 4.2 (d): A graph of SOP change with respect to time for the WDM source employed on a G655 Corning fiber

An overall change of 633° was attained after 120 s. This translated to average SOP speed of about $5.28^{\circ}/s$.

A G655 OFS fiber was also considered, the power recorded before loading was approximately 0.565 dB, 0.564 dB and 0.551dB on the DFB, MZM and WDM sources respectively. Fig 4.3 (a) shows the power recorded after loading the fiber with 18 kg mass

was about 0.564 dB, 0.555 dB and 0.523 dB on the DFB, MZM and WDM sources respectively. This was equivalent to a power loss of about 0.001 dB, 0.009 dB and 0.028 dB on the DFB, MZM and WDM sources respectively. A corresponding sensitivity of 0.00005 dBm/kg, 0.00050 dBm/kg and 0.00156 dBm/kg was achieved. This shows that a G655 OFS is sensitive to small strain changes making it valuable in the mining application.

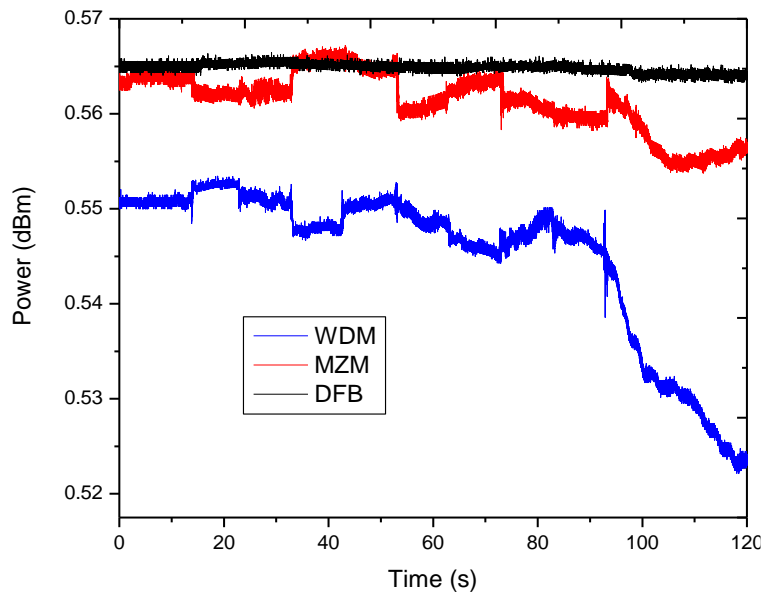


Figure 4.3 (a): Power fluctuation of light from each of the three laser sources; DFB, MZM and WDM sources injected on a G655 OFS fiber

The information of signal propagation from a WDM source through a G655 OFS fiber on a linear orientation was represented on a Poincare' sphere as shown in figure 4.3 (b).

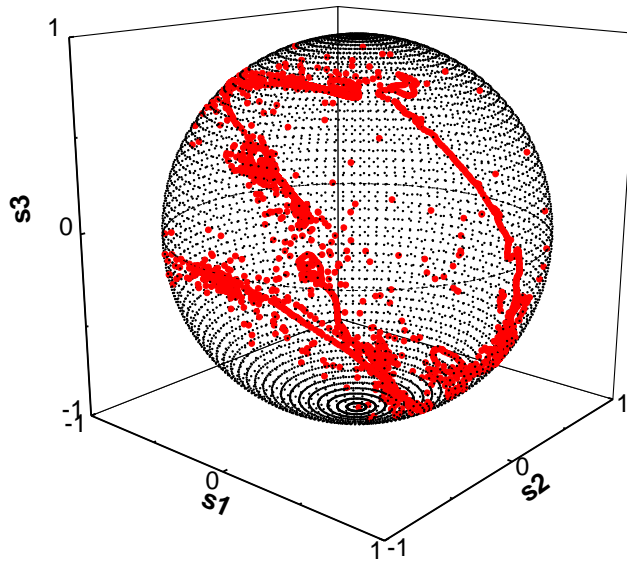


Figure 4.3 (b): Poincare' sphere representation of a signal from a WDM source propagation through a G655 OFS

More random fluctuations were observed on the trace as compared to figures 4.1 (c) and 4.2 (c). This is a clear indication of higher power loss due to the random change in SOP as shown in figure 4.3 (a) (WDM source – blue color).

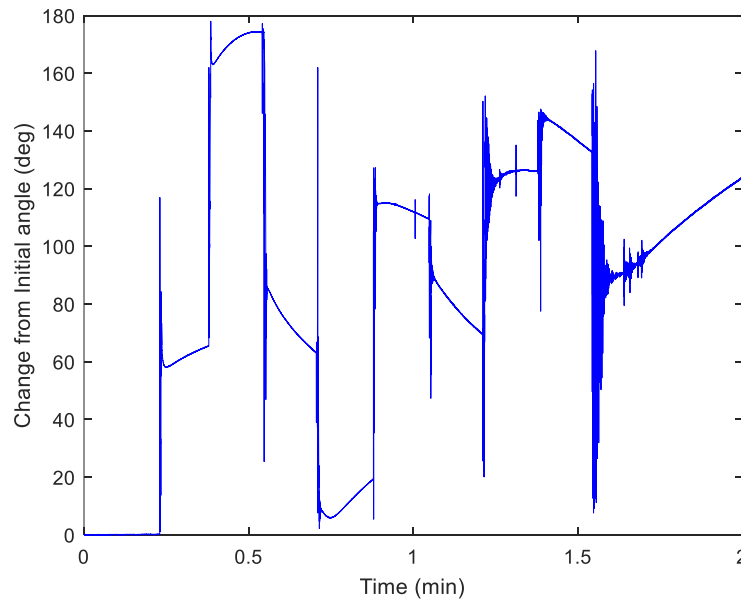


Figure 4.3 (c): A graph of SOP change with respect to time for the WDM source employed on a G655 OFS fiber

The corresponding graph of the information on trace in figure 4.3 (b) is given by figure 4.3 (c). The maximum change in SOP from the graph is approximately 175° attained after 33 s resulting to an instantaneous SOP speed of $5.30^{\circ}/s$. It was observed that the change in SOP on the Poincare' sphere corresponds with the rate of change of SOP that is the bigger the trace the higher the change from the initial angle. An overall change of 940° was achieved hence an overall SOP speed of $7.83^{\circ}/s$.

An input power of about 0.501 dBm, 0.480 dBm and 0.434 dBm was recorded when the MZM source, DFB source and WDM source were employed on the PMF respectively as shown in figure 4.4 (a).

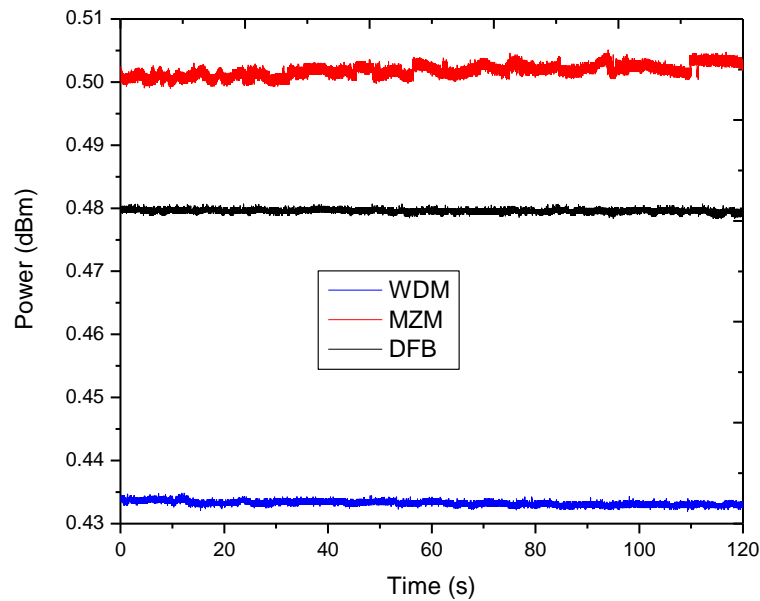


Figure 4.4 (a): Power fluctuation of light from each of the three laser sources; DFB, MZM and WDM sources injected on a PMF Corning fiber

The power readings when the fiber was subjected to the 18 kg mass was close to 0.500 dBm, 0.479 dBm and 0.433 dBm for the MZM, DFB and WDM sources respectively. A power loss of about 0.001 dB on all the laser sources was obtained. A sensitivity of 0.00005 dBm/kg was achieved on the three laser sources.

The Poincare' sphere representation of a light from an MZM source propagating through a PMF Corning fiber is represented in figure 4.4 (b).

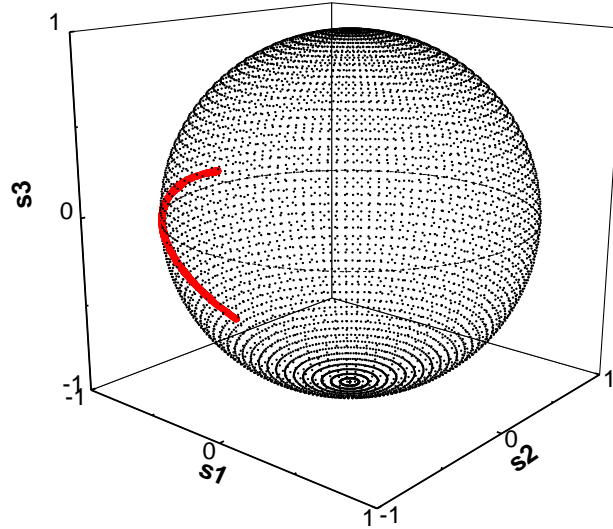


Figure 4.4 (b): Poincare' sphere representation of a signal from an MZM source propagation through a PMF Corning

There were no random fluctuations observed on the trace in fig 4.4 (b). This is because the PMF Corning fiber is tailored in such a way that it maintains the polarization state of the signal propagating along it (Furukawa 2009, Nabadda *et al.*, 2018).

The graphical representation of the change in SOP with respect to time corresponding to figure 4.4 (b) is given in figure 4.4 (c). A maximum change of about 75° was achieved after 52.5 s resulting to an instantaneous SOP speed of $1.43^\circ/\text{s}$. The overall SOP change was about 514° hence an average speed of $4.28^\circ/\text{s}$. The values of PMF Corning fiber showed to be the lowest in polarization change therefore not suitable in the design because of minimized fluctuation. Typically, PMFs are designed to maintain particular orientation if a fiber (Rashleigh, 1983).

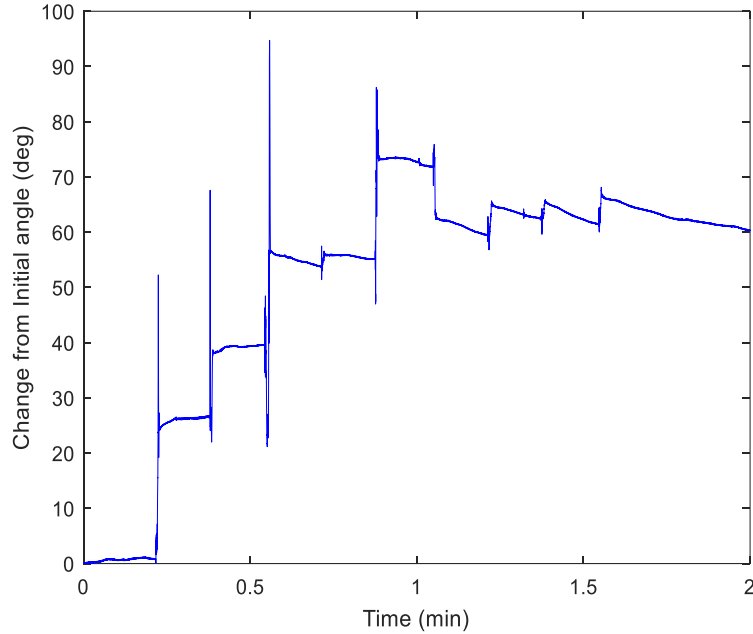


Figure 4.4 (c): A graph of SOP change with respect to time for the MZM source employed on a PMF Corning fiber

4.2.1.2 Performance of the signal during the mass unloading for different laser sources

The power readings were recorded when the load was removed from the fiber. This aimed at studying the power fluctuation of the fiber when freed of strain. This is not the real picture of the possible collapse but was just a guide on the investigation of the performance.

The initial power registered by the G652 Corning fiber before removing the strain was 0.421 dBm, 0.479 dBm and 0.479 dBm for the DFB, WDM and MZM sources respectively as shown in figure 4.5. The resulting power after unloading was established to be approximately 0.421 dBm, 0.480 dBm and 0.480 dBm for the DFB, WDM and MZM laser sources respectively. This translated to a power gain of about 0.001 dB for both the WDM and MZM source. This yielded a sensitivity of about 0.00005 dBm/kg. There was no power gain noted on the DFB laser source. However, a sharp power fluctuation was

observed between around the 84th and 94th second corresponding to the 9th 2 kg mass. A sudden application of weight can cause a quick spike in strain hence an increased scattering which translates to a significant power loss (Lu *et al.*,2019).

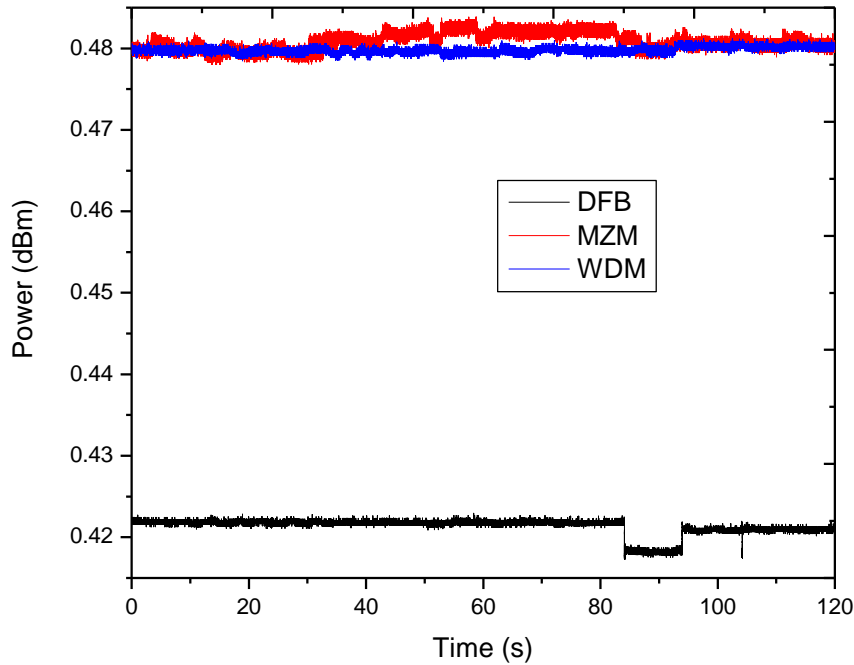


Figure 4.5: Power fluctuation of light from each of the three laser sources; DFB, MZM and WDM sources injected on a G652 Corning fiber

A G655 Corning fiber was also considered. An input of 0.496 dBm, 0.503 dBm and 0.537 dBm was recorded for the WDM, MZM and DFB sources respectively. Figure 4.6 shows the power recorded after unloading was approximately 0.503 dBm for both the WDM and MZM sources and 0.539 for the DFB source. This corresponds to a power gain of about 0.006 dB and 0.002 dB for the WDM and DFB source respectively. This yielded a sensitivity of 0.00033 dBm/kg and 0.00011 dBm/kg for the WDM and DFB source respectively.

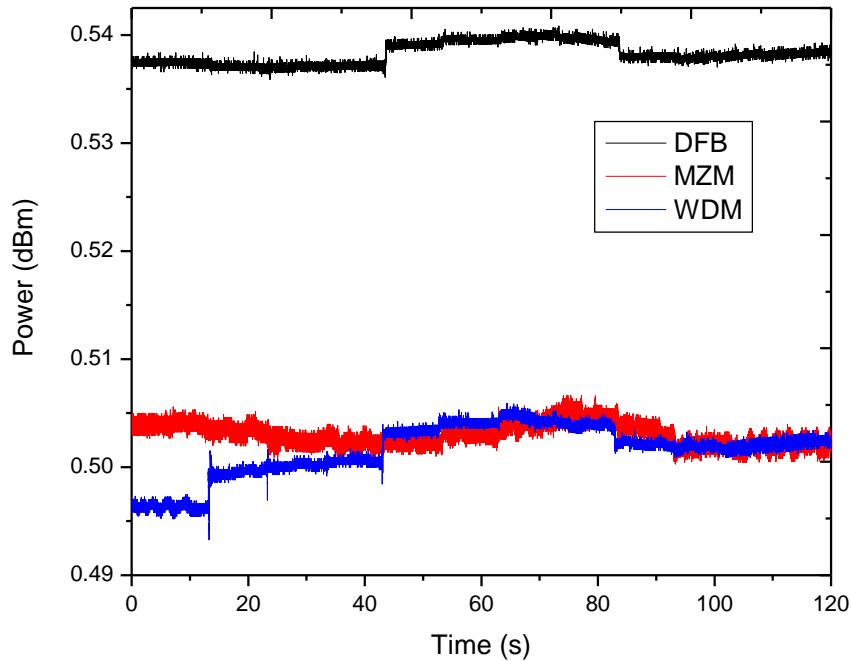


Figure 4.6: Power fluctuation of light from each of the three laser sources; DFB, MZM and WDM sources injected on a G655 Corning fiber

When the G655 OFS fiber was employed, the power recorded before unloading the masses was approximately; 0.518 dBm, 0.552 dBm and 0.564 dBm for the WDM, MZM and DFB sources respectively. Upon unloading masses completely from this fiber, the power recorded was close to 0.551 dBm, 0.562 dBm and 0.565 dBm for the WDM, MZM and DFB sources respectively. From figure 4.7 it is clear that there was a significant power gain on the G655 OFS fiber of about 0.033 dB, 0.010 dB and 0.001 dB for the WDM, MZM and DFB sources respectively. This is because the G655 OFS is optimized for low-loss, offering a better strain sensitivity.

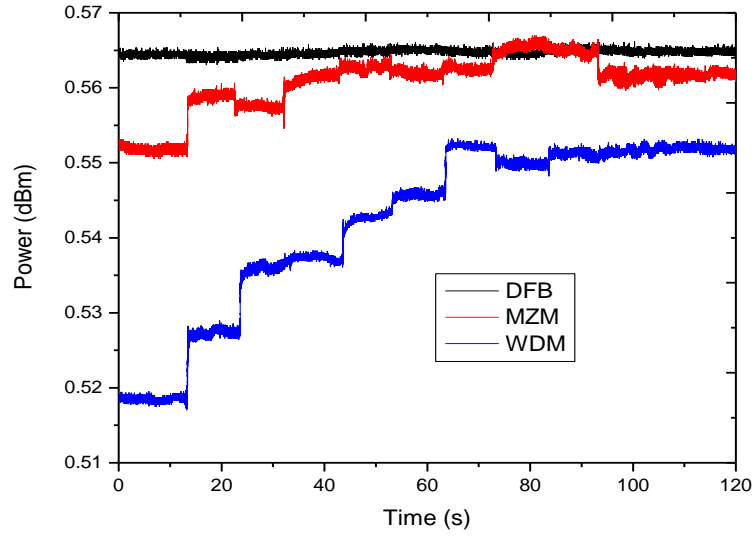


Figure 4.7: Power fluctuation of light from each of the three laser sources; DFB, MZM and WDM sources injected on a G655 OFS fiber

The PMF Corning fiber was also considered and the initial power recorded before unloading was recorded to be 0.433 dBm, 0.478 dBm and 0.502 dBm for the WDM, DFB and MZM sources respectively as shown in figure 4.8.

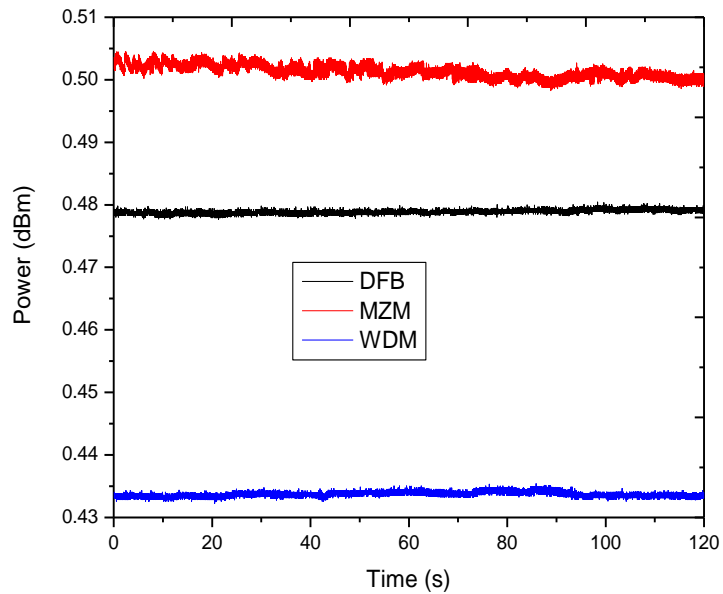


Figure 4.8: Power fluctuation of light from each of the three laser sources; DFB, MZM and WDM sources injected on a PMF Corning fiber

The final power recorded when the fiber was completely freed of strain was approximately 0.433 dBm, 0.478 dBm and 0.500 dBm for the WDM, DFB and MZM sources completely. There was no power fluctuation noted on the WDM and DFB laser source. However, a power loss of about 0.002 dB was registered on the MZM.

4.2.1.3 Investigation of SOP and Power fluctuation on various fiber types during loading

The sensitivity of the four fiber types namely; the G652 Corning, G655 Corning, G655 OFS and PMF Corning fiber was also evaluated. This was to enable us to settle on the most sensitivity fiber to strain. Light from the three laser sources DFB, WDM and MZM sources was coupled into these fiber types at different times. The power readings before loading and after unloading to establish the power fluctuation trends. This also was important in establishing the sensitivities of these fiber types per kilogram both when loaded and unloaded with the 18 kg mass.

Light from a DFB laser source was directed into these four fiber types; G652 Corning, G655 Corning, G655 OFS and PMF fiber at a wavelength of 1550 nm. The initial power recorded before loading of the four fiber types was recorded to be approximately; 0.421 dBm, 0.480 dBm, 0.540 dBm and 0.565 dBm for the G652 Corning, PMF, G655 Corning and G655 OFS respectively as shown in figure 4.9.

These fiber types were then loaded with 2 kg masses at an interval of 10 s additionally up to 18 kg mass. The power readings after loading were close to 0.421 dBm, 0.479 dBm, 0.537 dBm and 0.563 dBm for the G652 Corning, PMF, G655 Corning and G655 OFS respectively. There was no significant power loss noted on the G652 Corning fiber. A power loss of about 0.001 dB, 0.003 dB, 0.002 dB was recorded on the PMF, G655

Corning and G655 OFS fibers respectively. This translated to a sensitivity of about 0.00005 dB/kg, 0.00017 dB/kg and 0.00011 dB/kg for the PMF, G655 Corning and G555 OFS respectively.

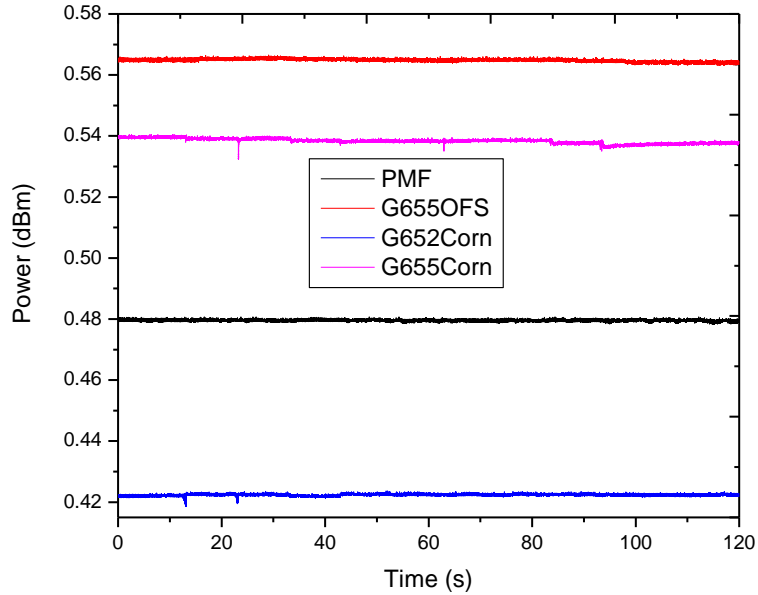


Figure 4.9: Performance of the four fiber types when coupled with a DFB laser

When light emanating from a 1550 nm MZM source was injected into the four fiber types it was noted that the input power was approximately 0.482 dBm, 0.501 dBm, 0.501 dBm and 0.563 dBm for the G652 Corning fiber, PMF, G655 Corning and G655 OFS respectively. The power readings after the fiber was loaded were about 0.479 dBm, 0.500 dBm, 0.502 dBm and 0.555 dBm for the G652 Corning, G655 Corning, PMF and G655 OFS respectively as shown on figure 4.10. A power loss of about 0.003 dB, 0.001 dB, and 0.008 dB for the G652 Corning, G655 Corning and G655 OFS respectively. This was equivalent to a sensitivity of close to 0.00017 dB/kg, 0.00005 dB/kg and 0.00044 dB/kg on the G652 Corning, G655 Corning and G655 OFS respectively. A power gain of about 0.001 dB was recorded on the PMF Corning fiber. This could be because of the light that

had been scattered being aligned properly on the PMF Corning hence minimizing power loss.

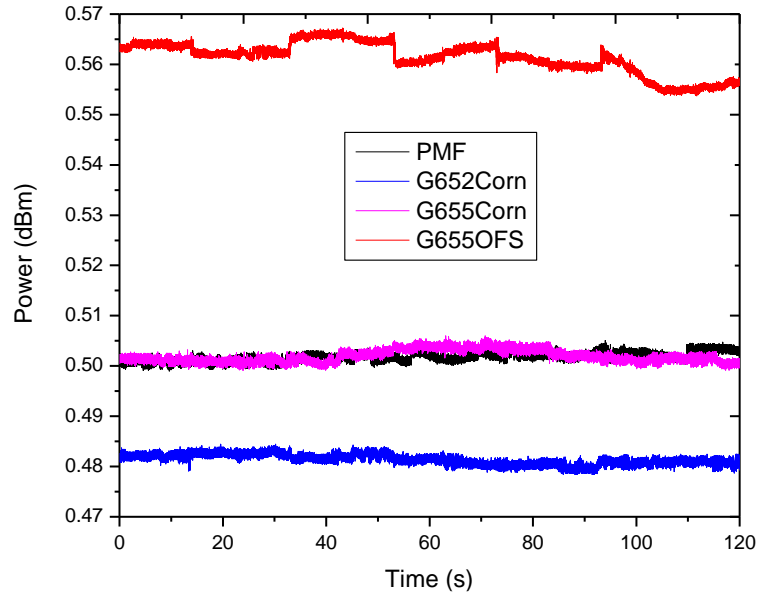


Figure 4.10: Performance of the four fiber types when coupled with an MZM laser source

A 1550 nm WDM source was also employed on the four fiber types on a linear orientation. It noted that the input power was approximately 0.433 dBm, 0.480 dBm, 0.504 dBm and 0.551 dBm for the PMF Corning, G652 Corning, G655 Corning and G655 OFS as shown in figure 4.11. The power readings after loading were approximately 0.433 dBm, 0.479 dBm, 0.499 dBm and 0.523 dBm for the PMF Corning, G652 Corning, G655 Corning and G655 OFS respectively. There was no power loss recorded on the PMF Corning and G655 OFS respectively. This translated to a power loss of about 0.001 dB, 0.005 dB and 0.028 dB for the G652 Corning, G655 Corning and G655 OFS respectively. A sensitivity of about 0.00005 dB/kg, 0.00028 dB/kg and 0.00156 dB/kg for the G652 Corning, G655 Corning and G655 OFS respectively.

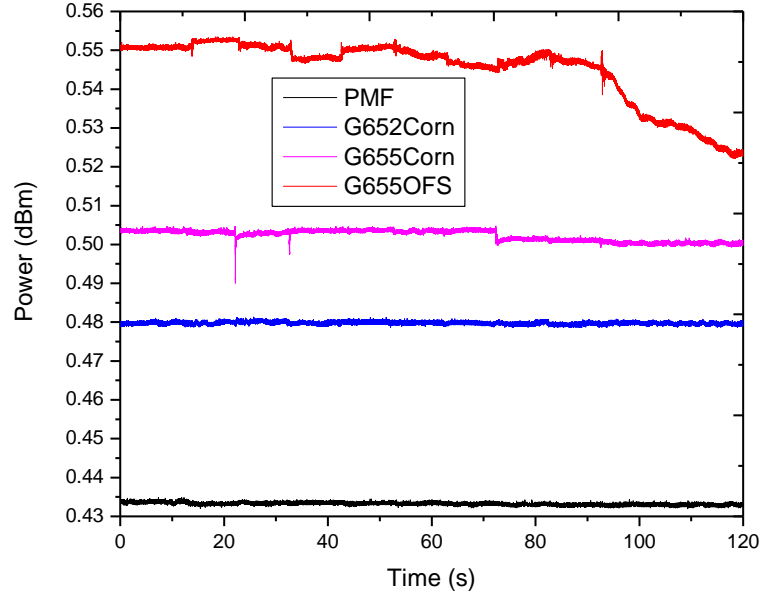


Figure 4.11: Performance of the four fiber types when coupled with a WDM laser source

4.2.1.4 Investigation of SOP and Power fluctuation on various fiber types during unloading

The performance of the four fiber types; G652 Corning, G655 Corning, G655 OFS and PMF Corning was also evaluated when the load was removed freeing the fiber from strain. The power readings before unloading and after unloading was recorded so as to establish the trend on power fluctuation.

When light from a 1550 nm DFB source was injected on the four fiber types, the power reading when the fiber was loaded with 18 kg mass was approximately; 0.421 dBm, 0.478 dBm, 0.536 dBm and 0.564 dBm for the G652 Corning, PMF Corning, G655 Corning and G655 OFS respectively. The power readings after the load was completely removed was close to 0.421 dBm, 0.478 dBm, 0.539 dBm and 0.565 dBm for the G652 Corning, PMF Corning, G655 Corning and G655 OFS respectively. There was no significant power gain noted on the G652 Corning and G655 Corning. However, there was

a sharp fluctuation between the 84th and 94th minute as shown in figure 4.12. This could be as a result of the nature in which the 2 kg mass was being removed at that instant.

A power gain of about 0.003 dB and 0.001 dB on the G655 Corning and G655 OFS respectively. This yielded a sensitivity of about 0.00017 dB/kg and 0.00005 dB/kg for the G655 Corning and G655 OFS respectively.

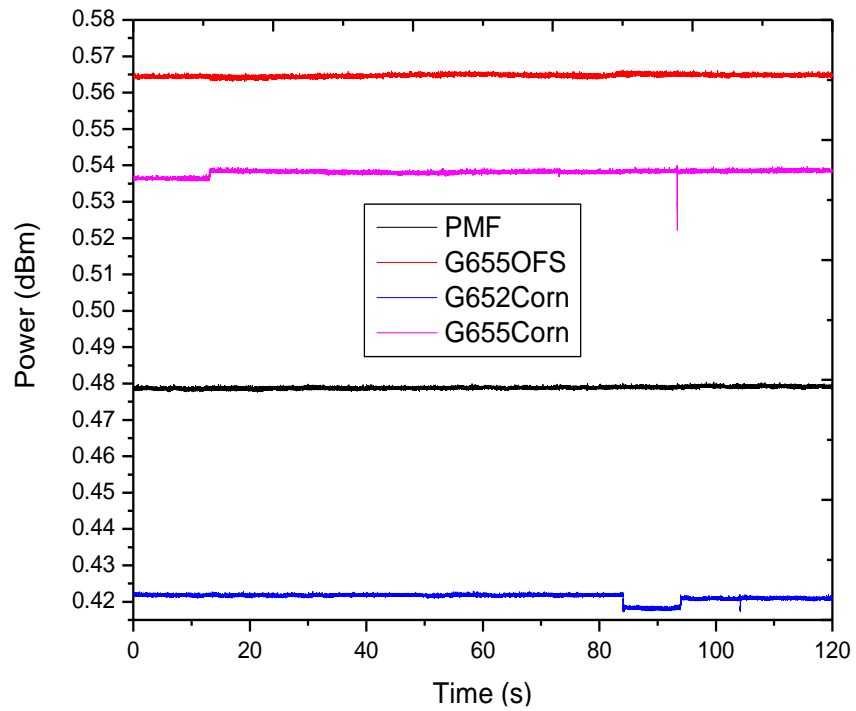


Figure 4.12: Performance of the four fiber types when coupled with a DFB laser source

Light from a 1550 nm MZM source was also injected into the four fiber types. The power readings before unloading were close to 0.479 dBm, 0.502 dBm, 0.503 dBm and 0.551 dBm for the G652 Corning, PMF Corning, G655 Corning and G655 OFS respectively as shown in figure 4.13. The power readings after the masses were unloaded was approximately 0.480 dBm, 0.500 dBm, 0.503 dBm and 0.562 dBm for the G652 Corning, PMF Corning, G655 Corning and G655 OFS respectively.

A power gain of approximately 0.001 dB and 0.011 dB was registered on the G652 Corning and G655 OFS respectively. This yielded a sensitivity of about 0.00005 dB/kg and 0.00061 dB/kg for the G652 Corning and G655 OFS respectively. There was no significant power gain on the G655 Corning and PMF Corning during unloading of the masses from the fiber.

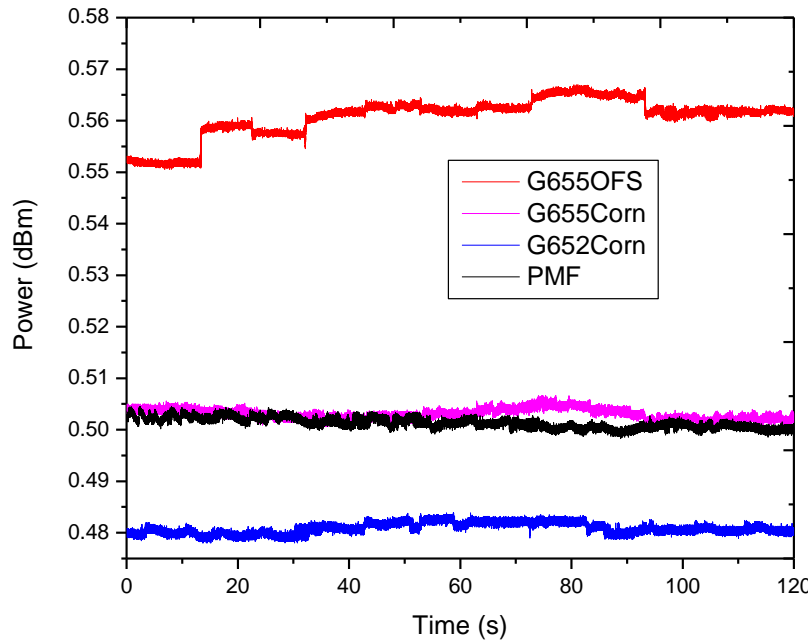


Figure 4.13: Performance of the four fiber types when coupled with an MZM laser source

A 1550 nm WDM source was also employed on these four fiber types when unloading was done. The readings before removing the load were approximately 0.432 dBm, 0.479 dBm, 0.501 dBm and 0.518 dBm for the PMF Corning, G652 Corning, G655 Corning and G655 OFS respectively. Figure 4.14 shows the power fluctuation trend when the masses were unloaded from the fibers. This showed that the power increased as the mass on the fiber reduced.

The power readings when the fiber was free of strain was approximately 0.433 dBm, 0.480 dBm, 0.503 dBm and 0.551 dBm for the PMF Corning, G652 Corning, G655 Corning and G655 OFS respectively. This translated to a power gain of about 0.001 dB, 0.001 dB, 0.002 dB and 0.033 dB for the PMF Corning, G652 Corning, G655 Corning and G655 OFS respectively. A sensitivity of approximately 0.00005 dB/kg was achieved on the PMF Corning and G652 Corning. The G655 Corning and G655 OFS fibers yielded a sensitivity of about 0.00011 dB/kg and 0.00183 dB/kg respectively.

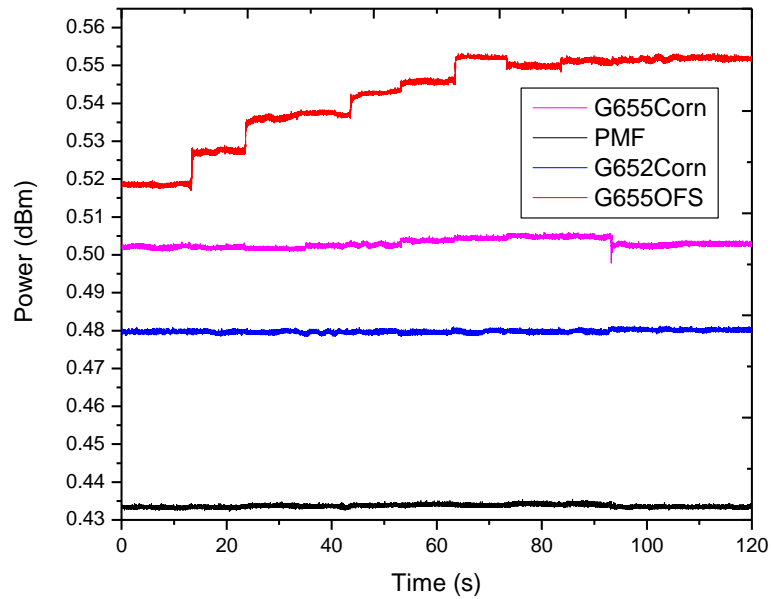


Figure 4.14: Performance of the four fiber types when coupled with a WDM laser source

4.2.2 Coiled Fiber Orientation

In the linear orientation, the strain on the fiber was not sufficient to demonstrate a large fluctuation expected in a typical mine collapse hence the transition to coiled orientation. The coiled orientation depicted a greater SOP and power fluctuation because of more birefringence due to torsional and compressional force (Isoe *et al.*, 2020).

The same 3 m fiber that was used initially on the linear/straight fiber orientation was bent or coiled four times at a diameter of about 3.5 cm as shown in figure 4.15. This was essential in investigating the contributions of some optical effects such as scattering and bending loss. The curved shape of the waveguide alters the propagation of light in the fiber core. When a fiber is bent or coiled, the light prefers to carry on in a straight line so wants to shoot right out the cladding at the bend. This makes the light weakly confined in a coiled fiber than a straight one, causing some degree of loss (Fokoua *et al.*, 2023). The mechanical stress induced by bending causes a change in the refractive index of the fiber, further impacting light transmission (Nagano *et al.*, 1978). The choice on the 3.5 cm was to minimize the chances of the fiber breaking because the fibers under investigation are bend sensitive unlike the G657 fiber which is bend insensitive.

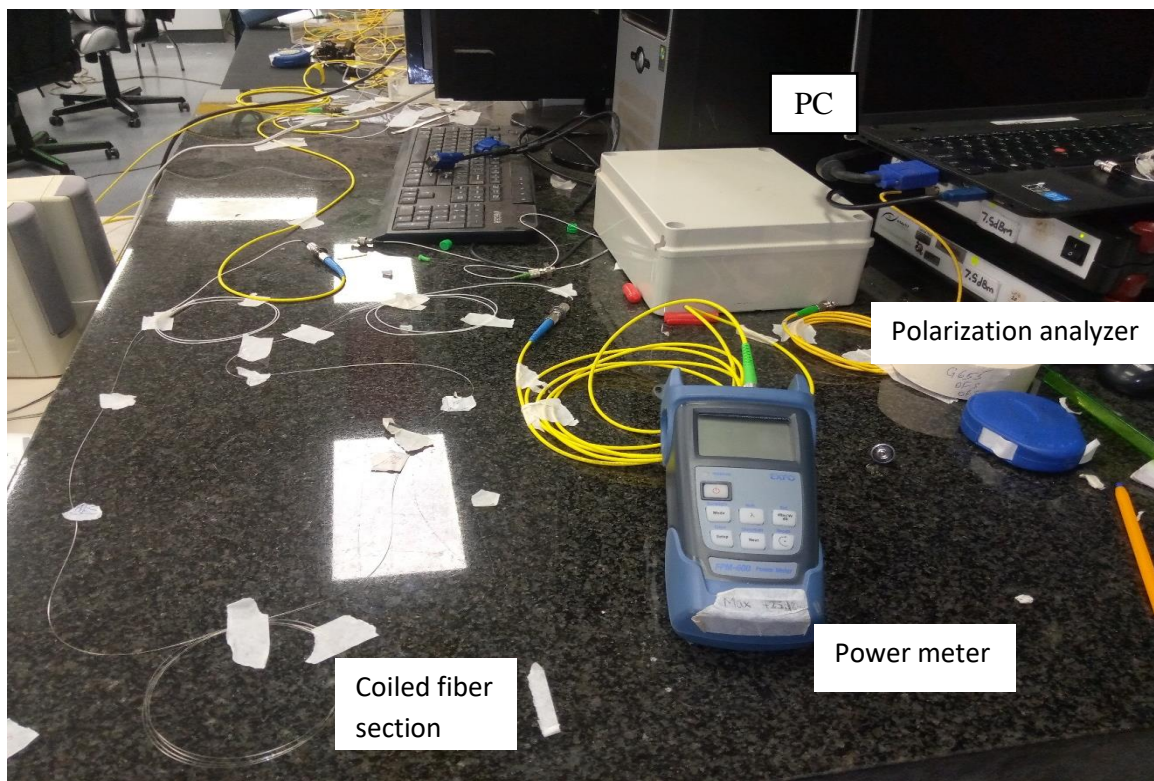


Figure 4.15: A picture of a coiled fiber section in the laboratory

The three laser sources DFB, WDM and MZM sources were also considered. This laser sources were employed on the four fiber types; G655 OFS, G652 Corning, G655 Corning and the PMF Corning. Light emanating from three laser sources; DFB, MZM and WDM was coupled into the four coiled fiber links at different times. A rectangular glass block was placed on top of the coils so as to enhance uniform distribution of force when loading. The 2 kg masses were loaded additionally up to 18 kg on the coiled section of the fiber at an interval of 10 s. The power readings were recorded during loading and later on when the load was gradually removed. This was important in establishing the power fluctuations when the fiber is loaded and unloaded. It is also through this that the sensitivity of the fiber and laser source was calculated. It was noted that as loading was done gradually there was decrease in power this could be because of the induced mechanical stress by the weights.

4.2.2.1 Investigation of SOP and Power fluctuation of fiber types during loading

Light from a 1550 nm DFB laser source was directed into the four coiled fiber at different times. The power readings before loading were approximately; 0.81 dBm, 0.54 dBm, 0.50 dBm and 0.48 dBm for the G652 Corning, PMF Corning, G655 Corning and G655 OFS respectively. On the other-hand, the output power readings after loading were 0.08 dBm, 0.01 dBm, 0.17 dBm and 0.03 dBm for the G652 Corning, PMF Corning, G655 Corning and G655 OFS in that order. The power loss of each fiber was calculated after loading them with 18 kg mass. It is from this that we were able to deduce the sensitivity of each fiber per kilogram.

A power loss of about 0.73 dB, 0.53 dB, 0.33 dB and 0.45 dB on the G652 Corning, PMF Corning, G655 Corning and G655 OFS respectively as shown in figure 4.16 (a). A

sensitivity of about 0.041 dB/kg, 0.029 dB/kg, 0.025 dB/kg and 0.018 dB/kg was achieved on the G652 Corning, PMF Corning, G655 OFS and G655 Corning respectively. From the graph, it is evident that power reduces with increase in mass due to more significant stress experienced on the bent fiber when coiled, this adds the signal optical changes due to strain. The bend allows more light scattering resulting to higher losses.

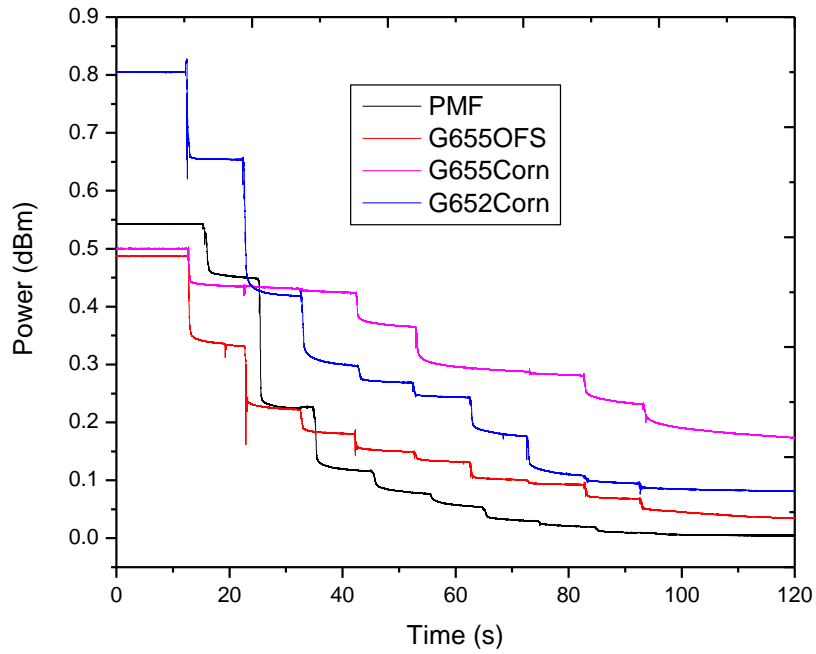


Figure 4.16 (a): Performance of the four fiber types when coupled with a DFB laser source

The Poincare' sphere representation when light from a DFB source was coupled with a G652 Corning fiber with a coiled section is represented in figure 4.16 (b). The dominant Stoke's parameter was S_3 .

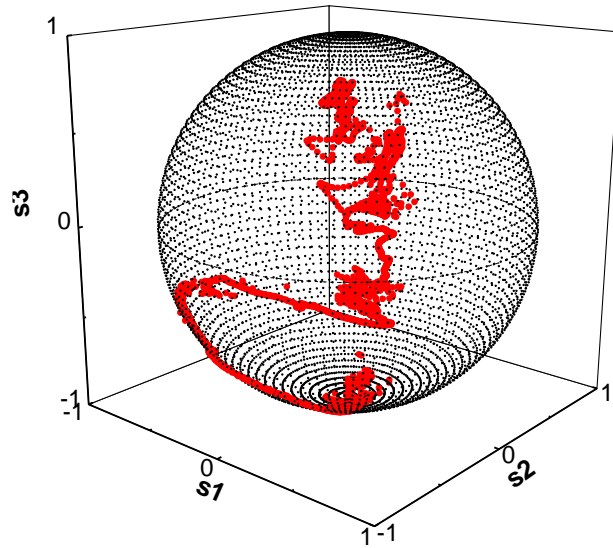


Figure 4.16 (b): Poincaré representation of SOP change for light from a DFB source propagating through a G652 Corning fiber

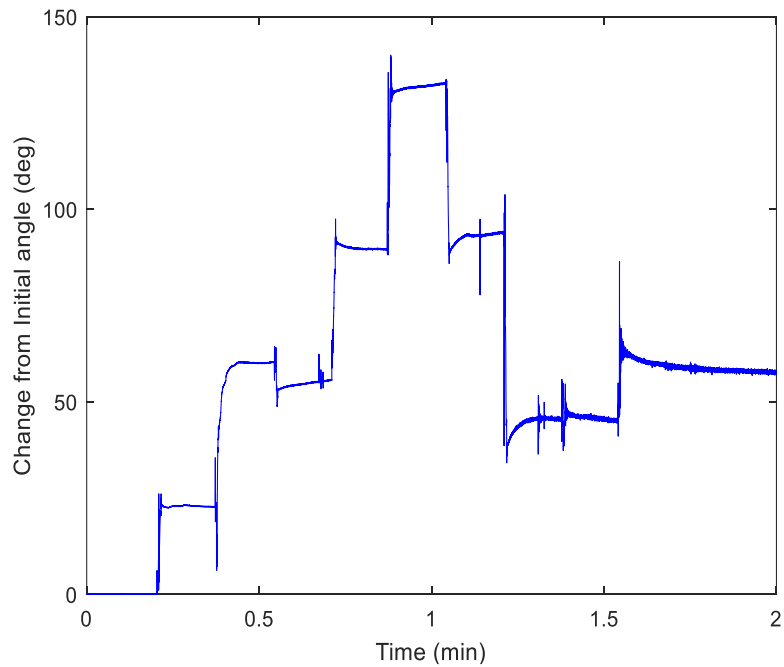


Figure 4.16 (c): A graph of SOP change with respect to time for light from a DFB source propagating through a G652 Corning fiber

The change in SOP with respect to time is given in figure 4.16 (c). A maximum SOP change of about 135° was achieved after 63 s translating to an instantaneous SOP

speed of $2.14 \text{ }^\circ/\text{s}$. An overall SOP change of about 622° was realized. This resulted to an average SOP speed of $5.18 \text{ }^\circ/\text{s}$.

The signal from Mach-Zehnder Modulator (MZM) laser source was also coupled into the different fibers while being subjected to a strain. The same procedures were done as for the DFB laser source. The input power for these fiber types were 0.87 dBm, 0.50 dBm, 0.49 dBm, 0.47 dBm for the G652 corning, PMF Corning, G655 OFS and G655 Corning respectively. The reading at the power meter after loading was 0.06 dBm, 0.12 dBm, 0.25 dBm and 0.50 dBm for the G655 OFS, PMF Corning, G655 corning and G652 corning respectively as shown in figure 4.17 (a). This yielded a power loss of approximately 0.37 dB, 0.38 dB, 0.43 dB and 0.22 dB on the G652 Corning, PMF Corning, G655 OFS and G655 Corning respectively. A sensitivity of about 0.021 dB/kg was achieved on the G652 Corning and PMF corning. The G655 OFS and G655 Corning yielded a sensitivity of close to 0.024 dB/kg and 0.012 dB/kg respectively.

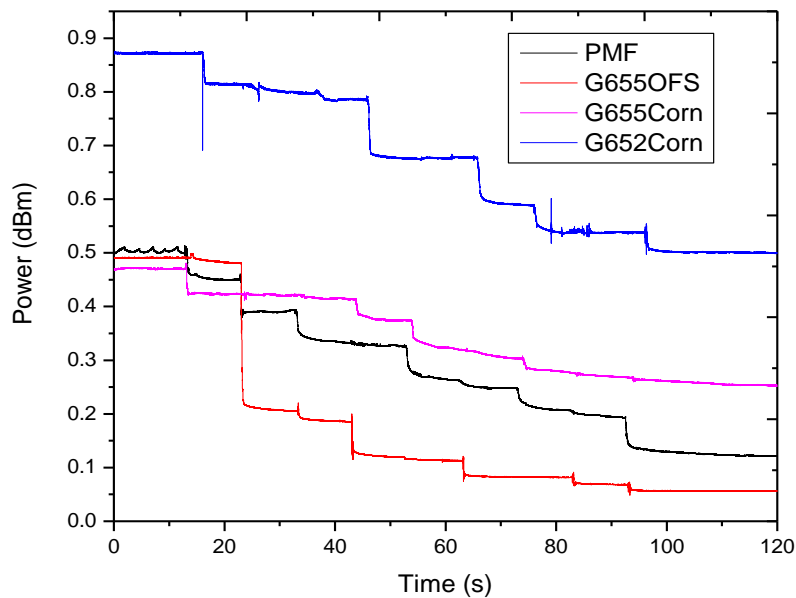


Figure 4.17 (a): Performance of the four fiber types when coupled with an MZM laser source

The SOP fluctuation of light from the MZM source injected into a G655 OFS was represented in a Poincare' sphere as shown in figure 4.17 (b).

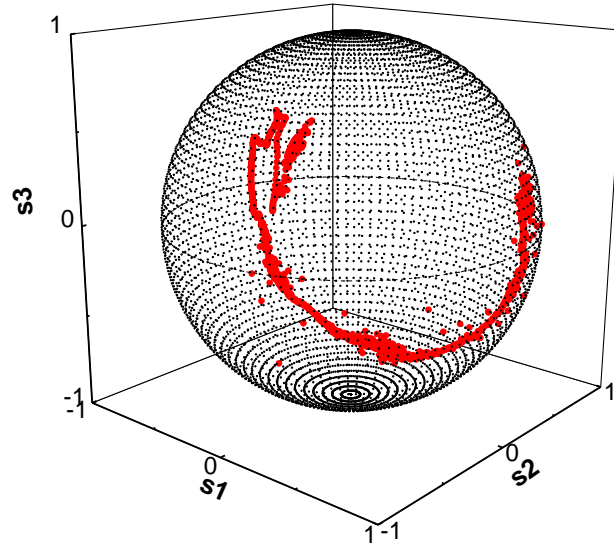


Figure 4.17 (b): Poincare' representation of SOP change for light from an MZM source propagating through a G655 OFS fiber

The information on figure 4.17 (b) was processed in MATLAB resulting to a maximum change of approximately 160° after 75 s as shown in figure 4.17 (c). An instantaneous SOP speed of $2.13^\circ/\text{s}$ was achieved. An overall SOP change of about 875° was attained. This resulted to an overall SOP speed of $7.29^\circ/\text{s}$. The dominant stokes parameter was S3 (refer to appendix 3 – blue color). This is evident from the trace of SOP fluctuation trace shown in figure 4.17 (b).

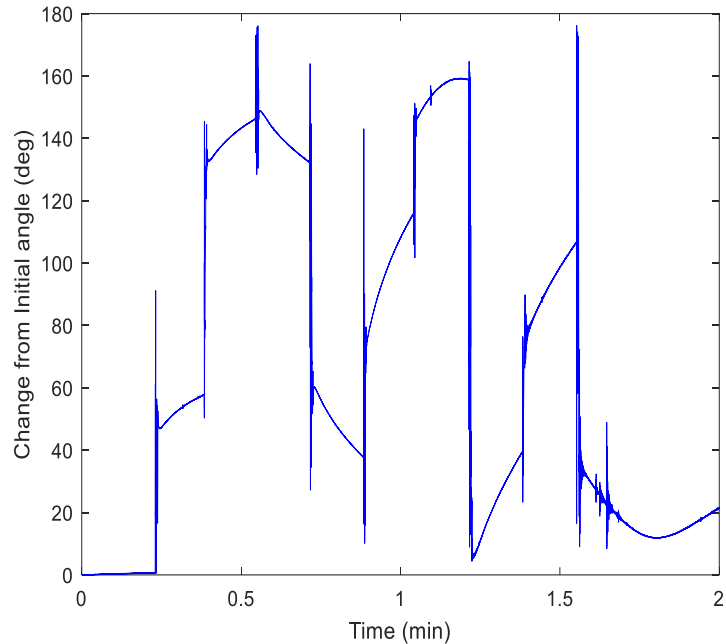


Figure 4.17 (c): A graph of SOP change with respect to time for light from an MZM source propagating through a G655 OFS fiber

The research also evaluated the performance of these fibers when utilizing signal from a Wavelength Division Multiplexing (WDM) laser source. From figure 4.18 (a), the initial power readings before mass loading were 0.83 dBm, 0.54 dBm, 0.49 dBm, 0.44 dBm for the G652 corning, PMF Corning, G655 OFS and G655 corning in that manner. The output power after straining the fiber with 18 kg was about 0.00 dBm, 0.04 dBm, 0.15 dBm and 0.52 dBm for the PMF Corning, G655 OFS, G655 corning and G652 corning. These contributed to a power loss of about 0.31 dB, 0.54 dB, 0.45 dB and 0.29 dB on the G652 Corning, PMF Corning, G655 OFS and G655 Corning in that order. A sensitivity of about 0.017 dB/kg, 0.030 dB/kg, 0.025 dB/kg and 0.016 dB/kg was registered by the G652 Corning, PMF Corning, G655 OFS and G655 Corning respectively.

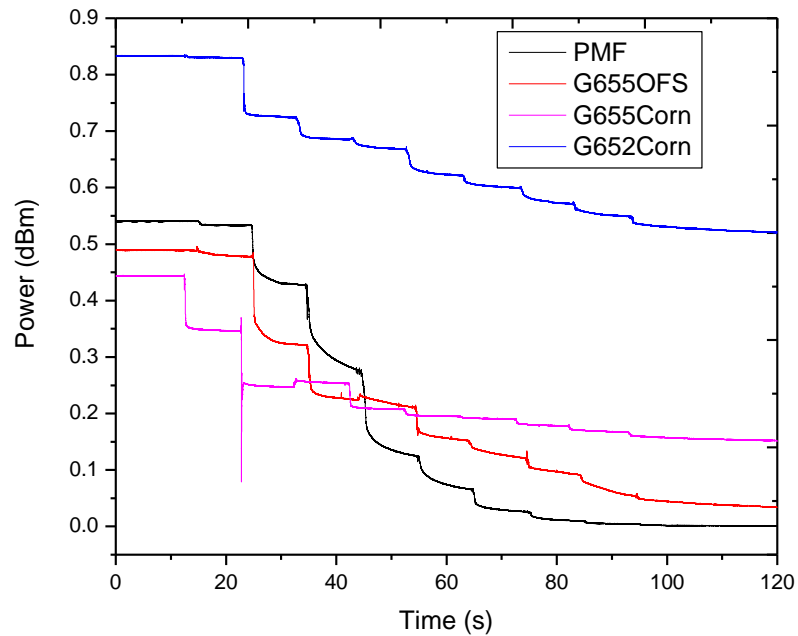


Figure 4.18 (a): Performance of the four fiber types when coupled with a WDM laser source

The SOPs of light propagated through a PMF Corning fiber from a WDM source is given by figure 4.18 (b). It was observed that the fluctuations on the trace followed a singular path smoothly. This is because of the nature of the fiber to maintain the polarization state of the signal propagated through it.

A maximum SOP change of about 160° was attained after 38 s hence an instantaneous SOP speed of $4.21^\circ/\text{s}$. A total SOP change of about 925° was achieved resulting to an overall SOP change of $7.71^\circ/\text{s}$. It is noted from figure 4.18 (c) that a lot of scattering occurred at around 75 s onwards. This was a clear indication that the fiber was approaching deformation due to the induced mechanical stress. It is evident from the graph that the PMF fiber has low tolerance to weight.

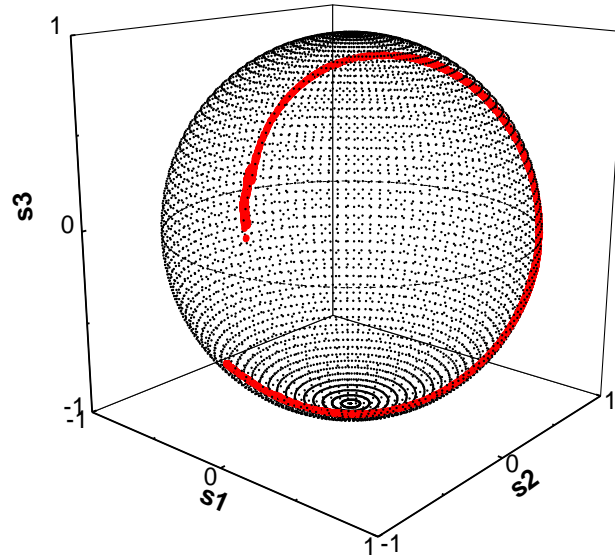


Figure 4.18 (b): Poincare' representation of SOP change for light from a WDM source propagating through a PMF Corning fiber

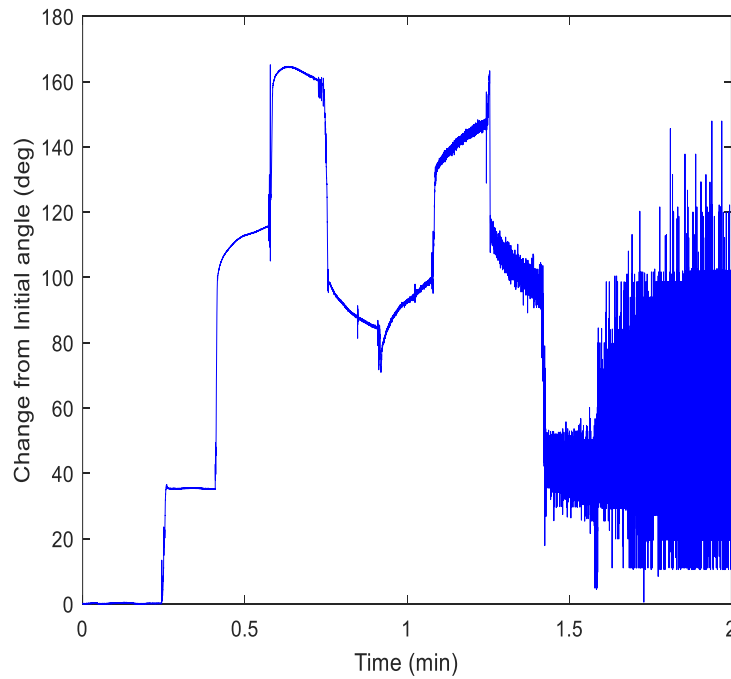


Figure 4.18 (c): A graph of SOP change with respect to time for light from a WDM source propagating through a PMF Corning fiber

4.2.2.2 Investigation of SOP and Power fluctuation of fiber types during unloading

The 18 kg mass that was initially loaded on the coiled fiber types was later on removed gradually at an interval of 10 s. The power readings before and after the load was removed were recorded so as to establish the power fluctuation trends. This was also essential in achieving the sensitivity of the four fibers when utilized on the three laser sources when freed of strain. It was noted that as the masses were removed gradually, there was a significant increase in power. This was as a result of withdrawal of the induced stress on the fiber.

From figure 4.19, when the DFB source was utilized, the power readings before the load was removed was approximately 0.00 dBm, 0.02 dBm, 0.04 dBm and 0.12 dBm on the PMF Corning, G655 OFS, G652 Corning and G655 Corning respectively. The power went almost to the same level before loading (refer to figure 4.16 (a)).

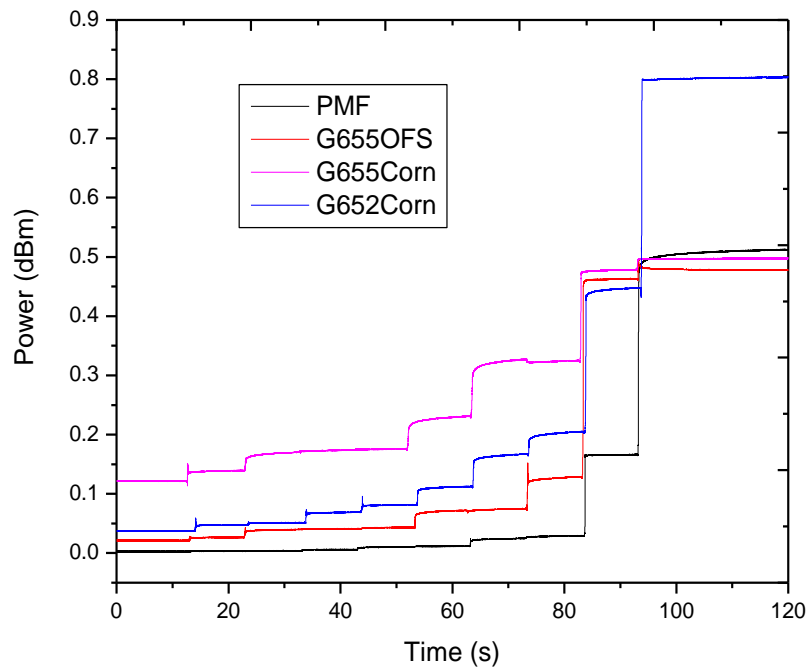


Figure 4.19 (a): Performance of the four fiber types when coupled with a DFB laser source

The final power readings when the fiber was free of strain was approximately 0.48 dBm, 0.50 dBm, 0.52 dBm and 0.80 dBm for the G655 OFS, G655 Corning, PMF Corning and G652 Corning in that order. This translated to a power gain of about 0.76 dB, 0.52 dB, 0.46 dB and 0.38 dB on the G652 Corning, PMF Corning, G655 OFS and G655 Corning respectively. A sensitivity of 0.042 dB/kg, 0.029 dB/kg, 0.026 dB/kg and 0.021 dB/kg was achieved on the G652 Corning, PMF Corning, G655 OFS and G655 Corning in that order.

The Poincare' sphere representation of a coiled G652 Corning fiber coupled with a DFB source during unloading is given in figure 4.19 (b).

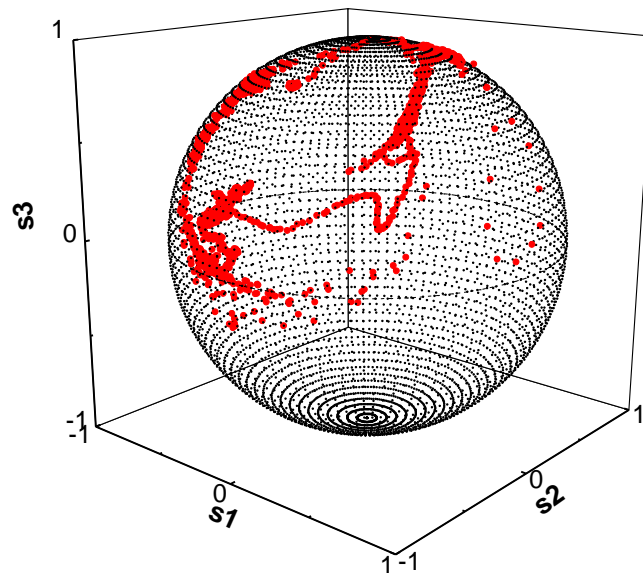


Figure 4.19 (b): Poincare' sphere representation of SOP change for light from a DFB source coupled with a G652 Corning fiber

A plot on SOP change with respect to time corresponding to figure 4.19 (b) is given by figure 4.19 (c). A maximum change of about 105° was attained after 75 s translating to an instantaneous SOP speed of $1.4^\circ/\text{s}$. An overall change of 525° was reached hence an average SOP speed of $4.38^\circ/\text{s}$.

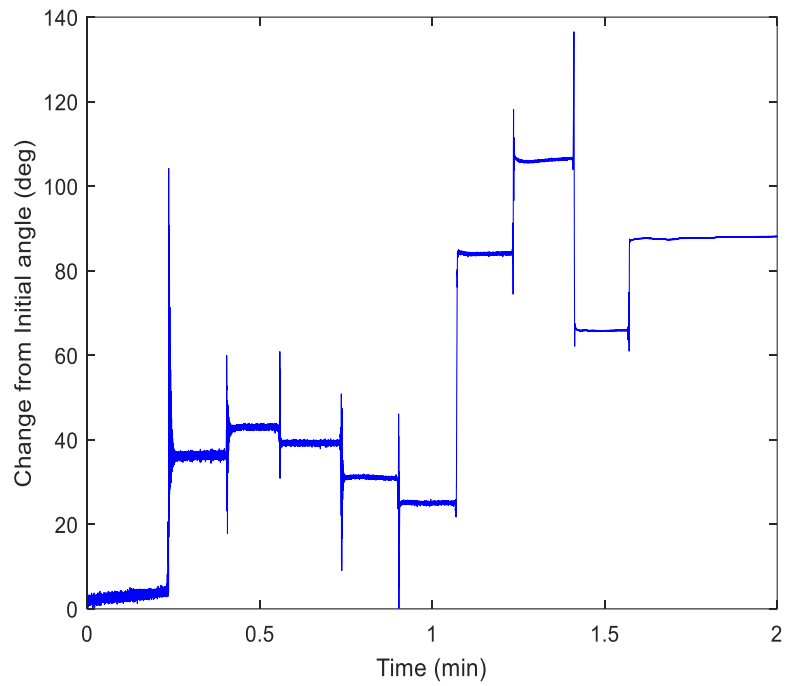


Figure 4.19 (c): A graph SOP change with respect to time of light from a DFB source coupled with a G652 Corning fiber

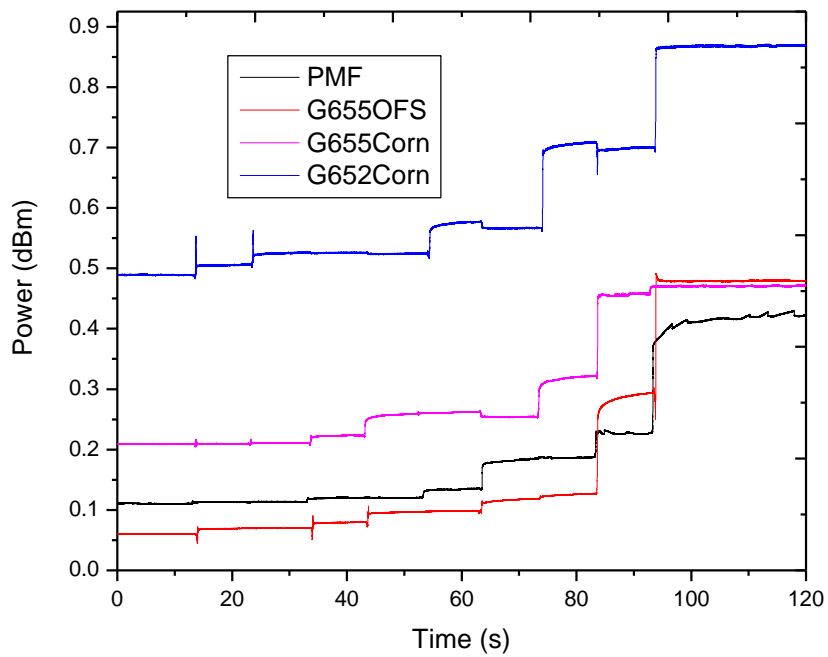


Figure 4.20: Performance of the four fiber types when coupled with an MZM laser source

On the other hand, when the MZM source was employed, the initial power readings before unloading were taken to be close to 0.06 dBm, 0.11 dBm, 0.21 dBm and 0.49 dBm on the G655 OFS, PMF Corning, G655 Corning and G652 Corning respectively. The power readings when the load was removed was 0.43 dBm, 0.47 dBm, 0.48 dBm and 0.87 dBm for the PMF Corning, G655 Corning, G655 OFS and G652 Corning respectively as depicted in figure 4.20.

It is evident from figure 4.20, there was a power rise of about 0.42 dB, 0.38 dB, 0.32 dB and 0.26 dB on the G655 OFS, G652 Corning, PMF Corning and G655 Corning respectively. This yielded a sensitivity of about 0.023 dB/kg, 0.021 dB/kg, 0.018 dB/kg and 0.014 dB/kg on the G655 OFS, G652 Corning, PMF Corning and G655 Corning respectively.

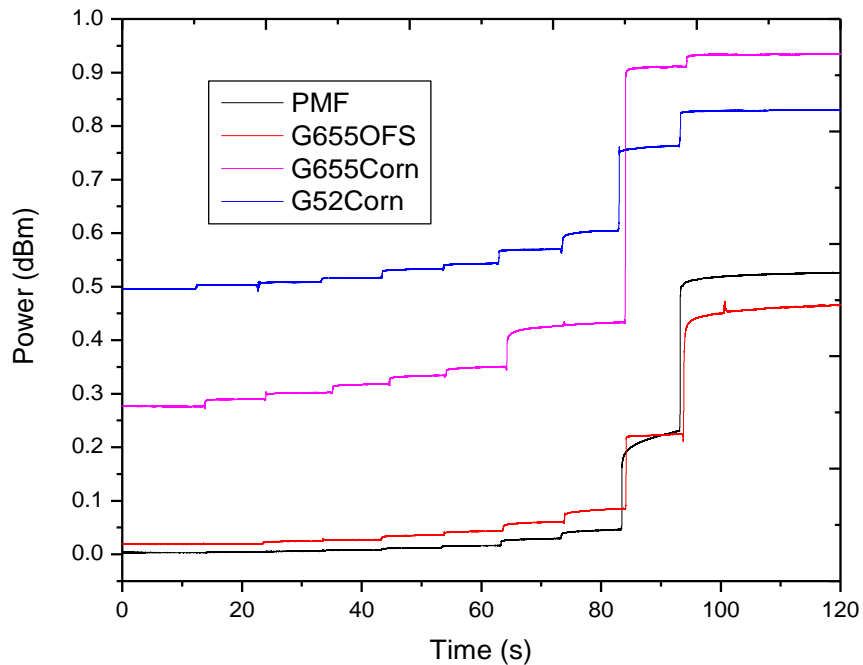


Figure 4.21: Performance of the four fiber types when coupled with a WDM laser source

The WDM source was also employed on the four unloaded coiled fiber types. The power readings before the load was removed was close to 0.00 dBm, 0.02 dBm, 0.28 dBm and 0.50 dBm on the PMF Corning, G655 OFS, G655 Corning and G652 Corning respectively as shown in figure 4.21. From figure 4.21, the power recorded when the 18 kg load was removed from the fibers was approximately 0.47 dBm, 0.53 dBm, 0.83 dBm and 0.93 dBm for the G655 OFS, PMF Corning, G652 Corning and G655 Corning respectively. This led to a power gain of about 0.33 dB, 0.45 dB, 0.53 dB and 0.65 dB for the G652 Corning, G655 OFS, PMF Corning and G655 Corning respectively. This translated to a sensitivity of about 0.018 dB/kg, 0.025 dB/kg, 0.029 dB/kg and 0.036 dB/kg on the G652 Corning, G655 OFS, PMF Corning and G655 Corning in that order.

4.2.2.3 Performance of different laser sources during loading

The performance of the three laser sources; DFB, WDM and WZM sources was also investigated. This was helpful in determining the most suitable laser source to be utilized.

Light emanating from each of the sources was separately injected into a coiled G652 Corning fiber. The fiber was then loaded with 2 kg mass additionally up to 18 kg mass at an interval of 10 s. The power readings were taken before and after the fiber was loaded.

Figure 4.22 shows the initial power reading before loading was approximately 0.80 dBm, 0.83 dBm and 0.87 dBm for the DFB, WDM and MZM sources respectively. The power readings when the load was removed was close to 0.08 dBm, 0.50 dBm and 0.52 dBm on the DFB, MZM and WDM sources respectively. This gave a power gain of about 0.31 dB, 0.37 dB and 0.72 dB on the WDM, MZM and DFB sources in that order. This

yielded a sensitivity of about 0.017 dB/kg, 0.021 dB/kg and 0.040 dB/kg on the WDM, MZM and DFB sources respectively.

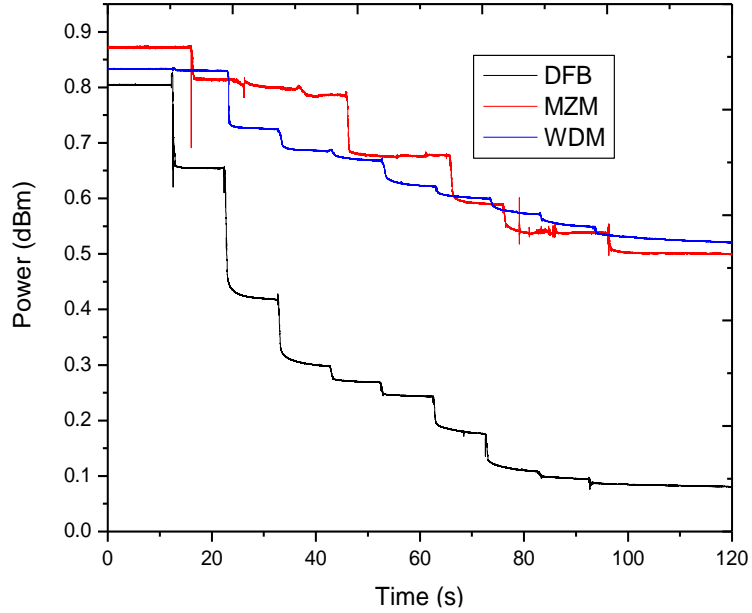


Figure 4.22: Power fluctuation of light from each of the three laser sources; DFB, MZM and WDM sources injected on a G652 Corning fiber

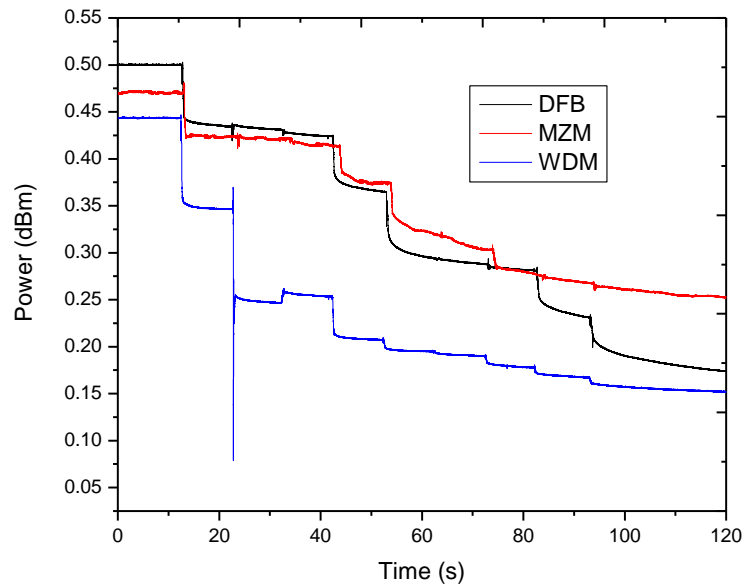


Figure 4.23: Power fluctuation of light from each of the three laser sources; DFB, MZM and WDM sources injected on a G655 Corning fiber

Light from the three laser sources; DFB, WDM and MZM sources also propagated through a G655 Corning fiber. The initial power readings before the fiber was subjected to loading was approximately; 0.44 dBm, 0.47 dBm and 0.50 dBm for the WDM, MZM and DFB sources respectively as shown in figure 4.23. A major event was noticed after the second mass was placed. This might have been as a result of greater birefringence induced at a particular point of a fiber due to a twist (Kaminow, 1981).

After applying masses on the fiber, the power reading was approximately 0.15 dBm, 0.17 dBm and 0.25 dBm on the WDM, DFB and MZM sources respectively. This resulted to a power loss of about 0.22 dB, 0.29 dB and 0.33 dB on the MZM, WDM and DFB sources respectively. This yielded a sensitivity of about 0.012 dB/kg, 0.016 dB/kg and 0.018 dB/kg on the MZM, WDM and DFB sources respectively.

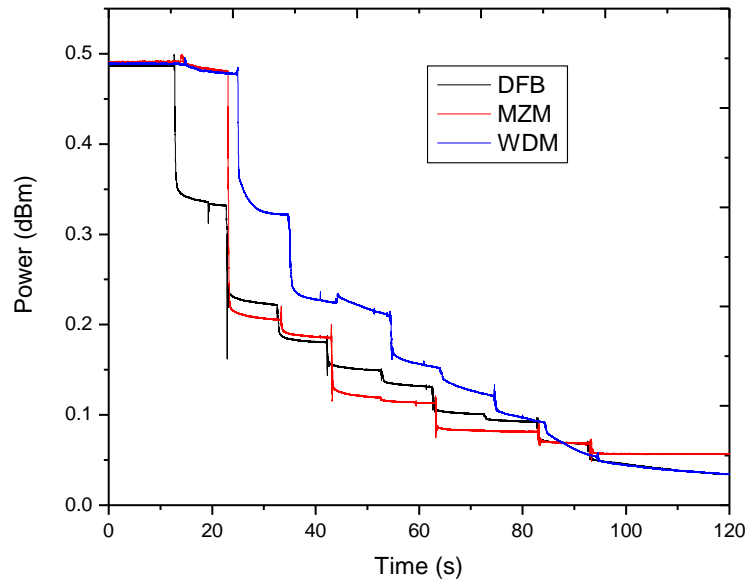


Figure 4.24: Power fluctuation of light from each of the three laser sources; DFB, MZM and WDM sources injected on a G655 OFS fiber

When light from the three laser sources was simultaneously injected into a G655 OFS fiber with a coiled section, the power reading was approximately 0.49 dBm for all the

power sources as depicted in figure 4.24. The power recorded when the fiber was loaded was approximately 0.04 dBm for the MZM, WDM and DFB sources. The MZM source recorded a power reading of about 0.06 dBm. A power loss of about 0.45 dB was recorded on the WDM and DFB while the MZM recorded 0.43 dB loss. A sensitivity of about 0.024 dB/kg was achieved on the MZM source. The DFB and WDM sources yielded a sensitivity of about 0.025 dB/kg. This shows that the G655 OFS provided consistent and reliable data when employed by the three laser sources on different configurations hence suitable for use in mining applications where conditions can change rapidly.

Light from the three laser sources was differently coupled into a coiled PMF Corning fiber. The power reading before the fiber was subjected to strain was approximately 0.50 dBm for the MZM source as shown in figure 4.25.

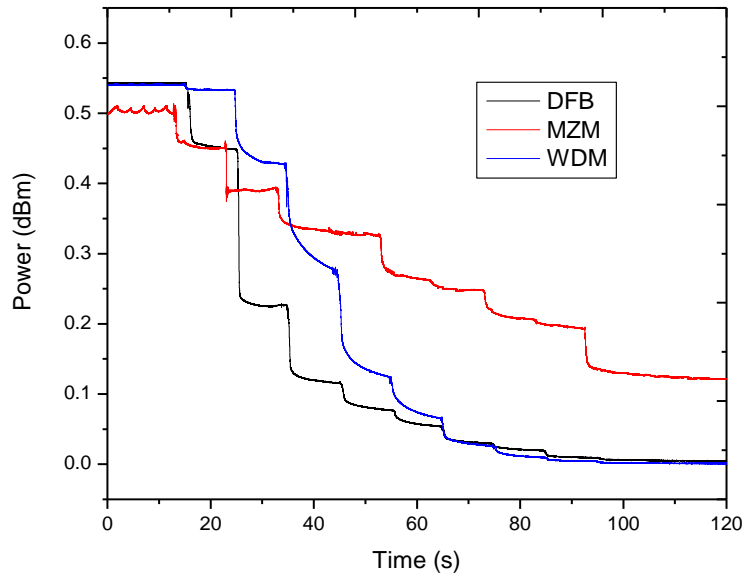


Figure 4.25: Power fluctuation of light from each of the three laser sources; DFB, MZM and WDM sources injected on a PMF Corning fiber

The WDM and DFB sources recorded a power of about 0.54 dBm. When the fiber was subjected to strain, the power readings were approximately; 0.12 dBm for the MZM

and 0.00 dBm for both the DFB and WDM sources. Figure 4.25 is a clear indication that there was a power loss about 0.38 dB on the MZM source and 0.54 dB for both the WDM and DFB sources. A sensitivity of about 0.021 dB/kg was achieved on the MZM source. Both the DFB and WDM sources yielded a sensitivity of 0.030 dB/kg.

4.2.2.4 Evaluation of laser sources during unloading on different fiber types

Similar procedure as in section 4.1 (b) was followed. It was noted that as the unloading was done gradually, there was a significant gain in power. It was evident that the power increased in steps at an interval of time. This was a clear sign that as the 2 kg masses were unloaded after 10 s each, there was a power rise corresponding to the strain lifted from the fiber. This clearly indicates that power is proportionate to strain. The power readings before and after the load was removed were recorded.

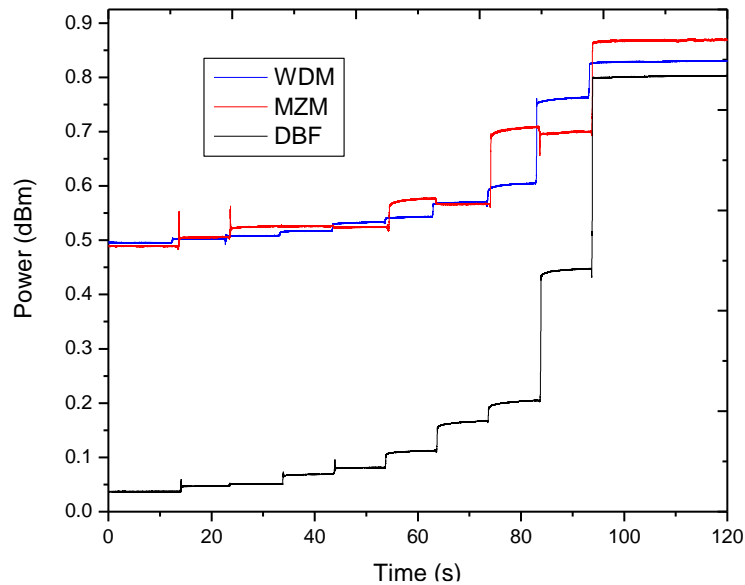


Figure 4.26: Power fluctuation of light from each of the three laser sources; DFB, MZM and WDM sources injected on a G652 Corning fiber

The three laser sources were considered on the various fiber types. On the G652 Corning fiber, the power reading before the load was removed was; 0.04 dBm, 0.49 dBm

and 0.50 dBm on the DFB, MZM and WDM sources respectively. Figure 4.26 shows that the power reading after the load was removed was approximately; 0.80 dBm, 0.83 dBm and 0.87 dBm on the DFB, WDM and MZM sources respectively. A power gain of 0.33 dB, 0.38 dB and 0.76 dB was registered on the WDM, MZM and DFB sources respectively. This yielded sensitivity of 0.018 dB/kg, 0.021 dB/kg and 0.042 dB/kg on the WDM, MZM and DFB sources respectively.

Light from the different laser sources was then injected into a G655 Corning fiber with a coiled section. The initial power readings were; 0.12 dBm, 0.21 dBm and 0.28 dBm for the DFB, MZM and WDM respectively. The resultant power readings after completely unloading were 0.47 dBm, 0.50 dBm and 0.93 dBm for the MZM, DFB and WDM respectively. Figure 4.27 shows the power gain was approximately 0.26 dB, 0.38 dB and 0.65 dB on the MZM, DFB and WDM respectively. This resulted to a sensitivity of about 0.014 dB/kg, 0,021 dB/kg and 0.036 dB/kg on the MZM, DFB and WDM respectively.

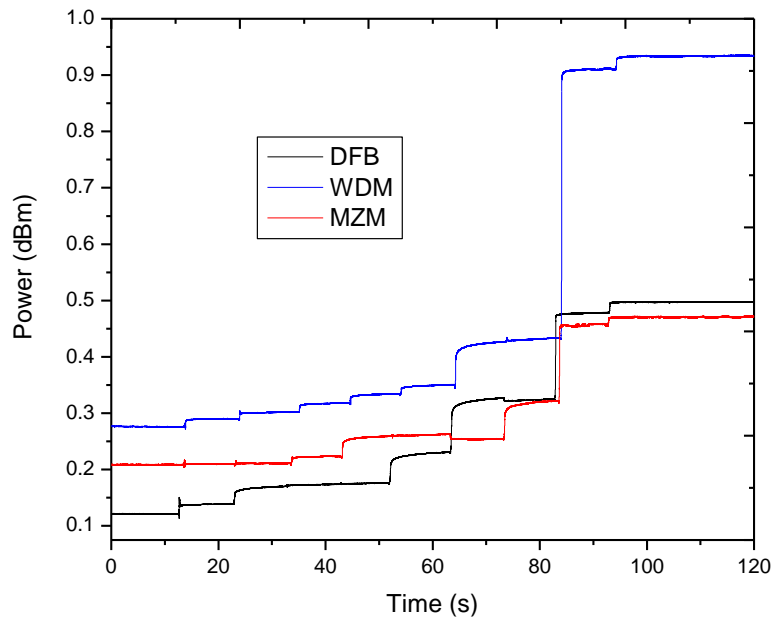


Figure 4.27: Power fluctuation of light from each of the three laser sources; DFB, MZM and WDM sources injected on a G655 Corning fiber

When light from the DFB, WDM and MZM sources were propagated on the G655 OFS fiber, the initial power readings were about 0.02 dBm for the DFB and WDM and 0.06 dBm for MZM. On removing the load, the power readings were close to 0.46 dBm for the WDM and 0.48 dBm for the MZM and DFB respectively as shown in figure 4.28. This yielded a power gain of about 0.42 dB, 0.44 dB and 0.46 dB on the MZM, WDM and DFB respectively. A response of 0.023 dB/kg, 0.024 dB/kg and 0.026 dB/kg on the MZM, WDM and DFB respectively.

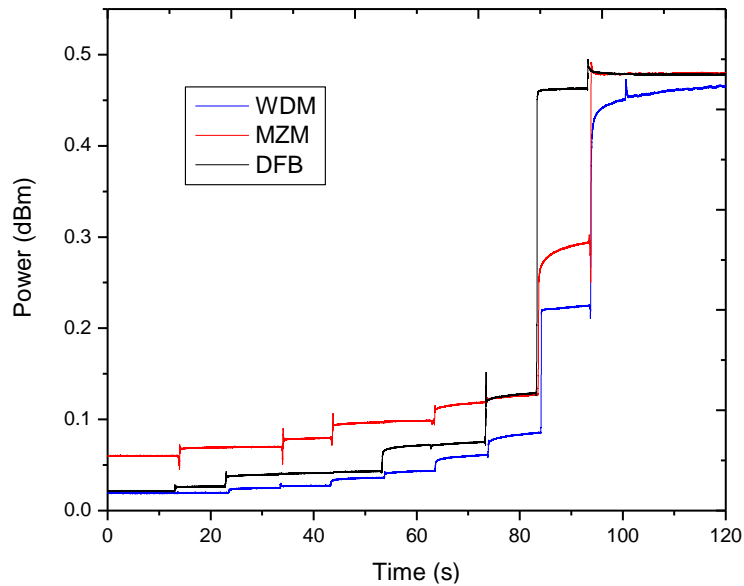


Figure 4.28: Power fluctuation of light from each of the three laser sources; DFB, MZM and WDM sources injected on a G655 OFS fiber

On the PMF Corning fiber with a coiled section, the initial power readings before the load was removed was approximately 0.11 dBm for the MZM and 0.00 dBm for the WDM and DFB respectively as depicted in figure 4.29. The final power reading when the fiber was freed of strain by unloading was 0.43 dBm, 0.51 dBm and 0.53 dBm for the MZM, DFB and WDM respectively as shown in figure 4.29. This translated to a power gain of about 0.32 dB, 0.51 dB and 0.53 dB on the MZM, DFB and WDM respectively

corresponding to sensitivities of 0.018 dB/kg, 0.028 dB/kg and 0.029 dB/kg on the MZM, DFB and WDM respectively.

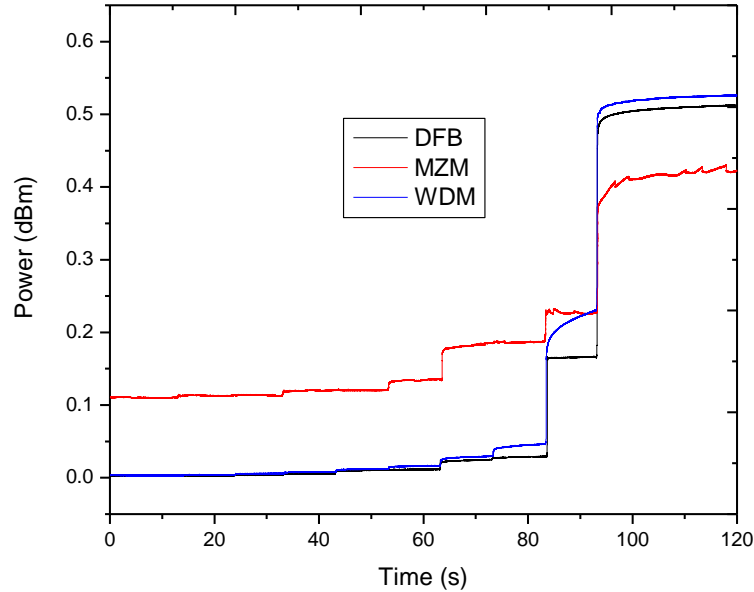


Figure 4.29: Power fluctuation of light from each of the three laser sources; DFB, MZM and WDM sources injected on a PMF Corning fiber

4.3 Transmission of the designed link

This section describes the transmission performance of the designed testbed. Three light sources were considered; a Distributed Feedback (DFB), Wave Division Multiplexing (WDM) source and Mach-Zehnder Modulator (MZM) source. Light emanating from the three laser sources was coupled with a Single Mode Fiber (SMF) of different lengths up to 75 km so as to establish BER of transmitted signal as discussed in section 3.3.

Figure 4.30 gives the various measurements performed on the DFB source. Figure 3.1 was employed in achieving these results. B2b refers to the back-to-back measurement. This is used to quantify the receiver sensitivity. It characterizes the photodiode used. The other fiber lengths were used to quantify the contribution of optical effects to the clarity of the signal transmitted. The receiver sensitivity was -13.97 dBm (refer to B2b).

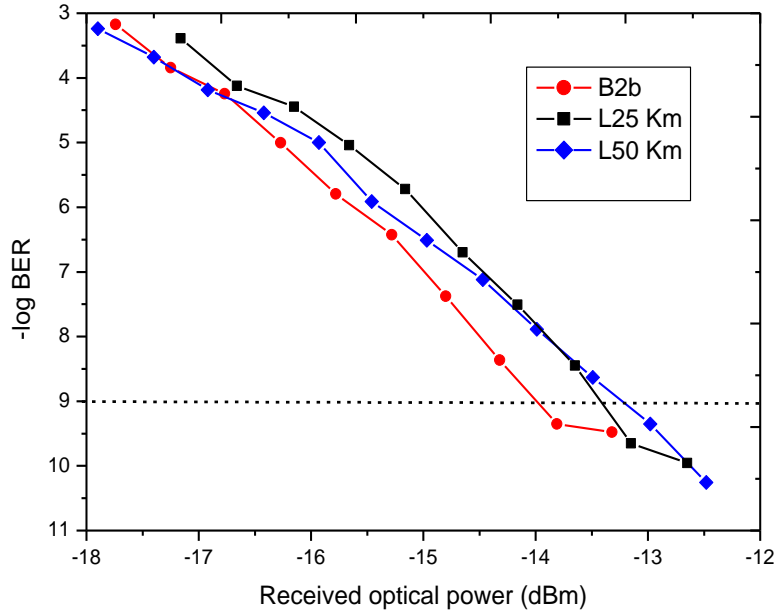


Figure 4.30: Transmission performance of a DFB laser source

The DFB laser source had the capability to transmit up to 50 km with zero error. At the 25 km and 50 km transmission, the BER at telecommunication threshold of 10^{-9} was measured at an incident power of -13.42 dBm and -13.16 dBm indicating a 0.55 dB and 0.81 dB power penalty respectively. The source of the power penalty was as a result of cumulative dispersion effects over the fiber length.

When the WDM source was employed, it also managed transmitting up to a length of 50 km error free as depicted in figure 4.31. The received incident optical power was established to be -19.13 dBm, -18.94 dBm and -18.87 dBm for the B2b, 25 km, and 50 km transmission respectively. This resulted to transmission penalties of 0.19 dB and 0.26 dB for the 25 km and 50 km respectively.

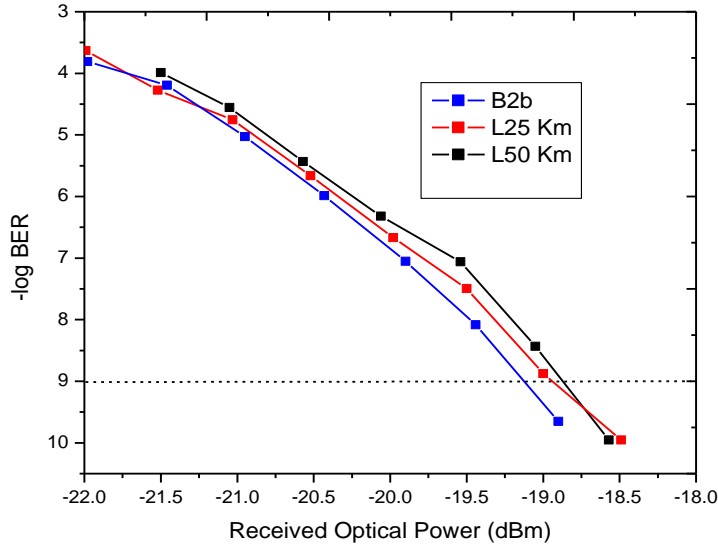


Figure 4.31: Transmission performance of a WDM laser source

The MZM source managed to transmit up to a length of 75 km error free unlike the DFB and WDM sources which did 50 km. Figure 4.32 shows the incident optical power at the B2b, 25 km, 50 km and 75km transmission was -19.36 dBm, -19.33 dBm, -19.15 dBm and -19.10 dBm respectively. The 25 km, 50km and 75 km transmission yielded transmission penalties of 0.03 dB, 0.21 dB and 0.26 dB respectively.

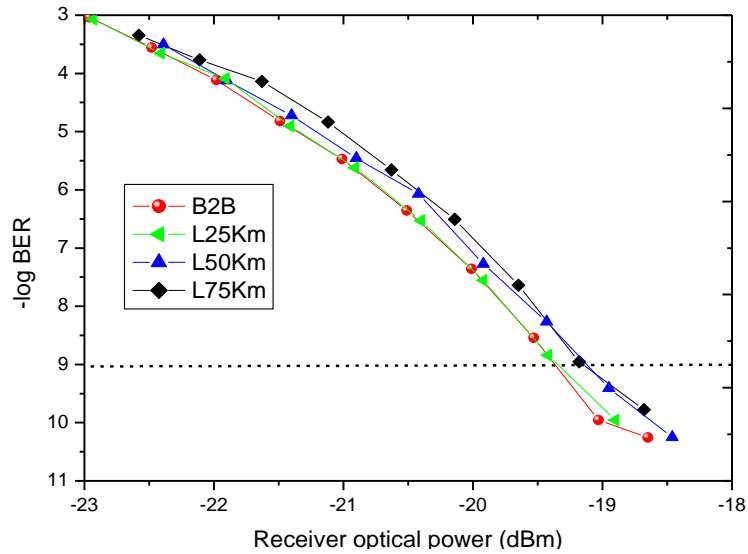


Figure 4.32: Transmission performance of an MZM laser source

CHAPTER FIVE

SUMMARY, CONCLUSIONS AND RECOMMENDATIONS

5.1 Introduction

This chapter provides conclusions and recommendations of the conducted research including the transmission performance, SOP and Power fluctuations. In addition, it provides suggestions for future studies regarding the design.

5.2 Summary

The G652 Corning fiber depicted a highest power fluctuation of 0.73 dB when coupled with the DFB laser source however it was not the best fiber for our design. The G655 OFS turned out to be the most suitable fiber because of its consistency in terms of power fluctuations when employed with all the three laser sources as shown in figure 4.24.

This study shows that all the three laser sources that were employed are suitable both for small scale and large-scale mining since they were in a capacity to transmit an optical signal over a 50 km length. This is a clear indication that the risk potential area covered. The research found out that a fiber with a coiled section would result to a greater power loss when subjected to strain unlike a fiber on a straight orientation hence a higher sensitivity. However, in a typical mine a straight fiber would be wound on the tunnel because a mine collapse does not occur suddenly but instead it happens gradually. Any stress that will be induced at any point on the fiber laid in a mine will lead to a significant power loss and SOP fluctuation hence the signal transmitted along the fiber will be altered.

All the fiber types were found out to be suitable for the design since they were all sensitivity to the any mechanical stress induced on them. However, the PMF fiber could

not be employed because of its nature to maintain polarization and the minimal fluctuation noted. After careful investigation, G655 OFS fiber was found to be the most suitable for distributed sensor design because it's optimized for low loss at 1550 nm window and its ability to detect small optical changes due to strain. It also has the smallest effective area of $52 \mu\text{m}^2$ compared to the other fibers giving a high-density power. Typically, the G655 OFS exhibits a low attenuation making it suitable for long distance-distance sensing. Its design optimizes performance for reduced loss over extended reaches. The MZM laser source was best suited for this design because of the extended reach enhancing wider span of sensing. However, any of the three laser sources can be applied for a 50 km length. This clearly shows that the top laser-fiber combination for the design was MZM- G655 OFS offering an extended reach and superior sensitivity to minor variations in strain. The designed sensor is mounted on the walls of a mine site to enhance monitoring.

The design needs to be customized to perform its sensing. A program was developed with set threshold of power and polarization values. Whenever the parameters surpass the set threshold an alarm is turned on. This is a real time monitoring scheme. Basing on the G655 OFS fiber which is the best for our design, the system was configured such that when power drops past 0.2 dB and SOPs below 100^0 then an alarm is turned on automatically (refer to appendix 5). This notifies those in the mines that there is need to make an escape plan from the mine because of a possible collapse. This alarm is placed in the mine site so that it can alert the miners and rescuers on a possible danger.

5.3 Conclusions

The current study employed an optical fiber both as a transmission medium and a sensing element. The aim of this study was to investigate a design of a distributed optical

fiber sensor for early hazard detection in mining so as to enhance safety in the mines. An optical fiber was considered because of its high speeds, non-corrosive, immune to harsh conditions and electromagnetic conditions. These advantages make it suitable for use in mining sites.

A laboratory testbed was built so as to investigate the transmission performance of various laser sources over different fiber lengths so as to ascertain capabilities. Three laser sources; DFB, WDM and MZM sources were considered. The designed distributed optical fiber sensor had a capacity of successfully transmitting a 10 Gbps signal through an optical fiber link extending up to 75 km successfully with a power penalty of 0.03 dB, 0.21 dB and 0.26 dB on the 25 km, 50 km and 75 km respectively. The MZM source had a capability of transmitting up to a length of 75 km with a zero error unlike the DFB and WDM sources which could manage a fiber length of 50 km. This is a clear illustration that an MZM source extends a longer reach than the DFB and WDM sources. The MZM source is suited more for extended reach distributed sensing compared to DFB and WDM sources. This implies that a fiber stretch of up to 75 km can be laid down in a mining area ensuring extensive coverage of the risk potential area. From the transmission performance, it is evident that the three light sources can be used for both large scale and small-scale mining thus enhancing safety in mines.

The states of polarization (SOP) fluctuation of the transmitted signal were monitored in real time using a polarization analyzer and presented in a Poincare' sphere. It was noted that the signal propagating was affected at any fiber section with induced birefringence. The change in relative angle (SOPs) with respect to time was plotted so as enhance calculation of SOP speeds. In the case of linear fiber orientation, the graphs

showed small displacements (change in relative angle) between consecutive points unlike fibers with coiled sections which depicted a very high fluctuation. This research found out that the SOP change is proportional to stress induced on an optical fiber. The greater the angle between two points, the higher the SOP speed. This is a clear indication that the fibers with coiled sections depicted a greater SOP speed than those in a linear orientation.

This study also looked into the effect of stress on a signal propagating through an optical fiber. The power fluctuations of the transmitted signal were monitored when the fiber was subjected to laboratory strain. These masses symbolized the strain/stress/pressure that is likely to be experienced in a section of a mine causing a collapse. The initial power readings before and after loading were recorded so as to establish power trends. This was done both for the linear and coiled orientation. The power fluctuation on a linear orientation was very minimal unlike a fiber with a coiled section. This shows that the fiber on a linear configuration was limited in its ability to translate small mechanical changes to detectable optical signals. On the other hand, coiled fibers depicted high sensitivities to strain because of increased mechanical stress due to bending and increased fiber length exposed to strain. This indicates that an increased mechanical stress on a fiber intensifies an optical power loss in a link. Graphs of power against time for each of these fibers and laser sources were plotted. It was evident from the graphs that as loading was done gradually there was a decrease in power because of the mechanical stress induced on the fiber.

5.4 Recommendations

In this design, loading of masses was systematic unlike an actual mine collapse where the walls of a mine just fall abruptly without following a particular sequence. This study suggests loading of masses be done randomly during the monitoring process.

In this study, monitoring was done for a period of 120 s only however, the time in which a collapse is likely to occur in a mine is not defined. This research recommend that monitoring can be done for an extended period of time.

This study suggests the use of a different laser source which can manage a transmission beyond 75 km enhancing effective coverage of large mines. This will maximize the sensing performance on the potential risk area.

REFERENCES

Amadala, B., (2021, May 13). *The death traps that are Kakamega's gold mines.*

Retrieved from ([The death traps that are Kakamega's gold mines | Nation](#))

Buimistryuk G.Y. (2005). *Information-Measuring Equipment and Technology Based on Fiber-Optic Sensors and Systems.* St. Petersburg, FL, USA: Monograph; IVA, GROT's Minatom.

Buimistryuk G.Y. (2013). *Fiber-optic sensors for extreme conditions.* Control Eng. Russ. 3, 34–40.

Byeong H.L, Young H.K., Kwan S.P., Joo B.`E., Myoung J.K., Byung S.R., and Hae Y.C., *Interferometric Fiber Optic Sensors.* Sensors 2012, 12, 2467-2486.

Collett, E. (1992). Polarized light. Fundamentals and applications. *Optical Engineering.*

Davis, C. M., Carome, E. F., Weik, M. H., Ezekiel, S., & Einzig, R. E. (2006). *Fiberoptic Sensor Technology Handbook, Optical Technologies (OPTECH).* A Division of Dynamic Systems. Inc., Herndon, Virginia, 304-307.

Elprocus (2022). *Introduction to Fiber Optic Sensors and their Types with Applications.*

Retrieved from (<https://www.elprocus.com/different-types-of-fiber-optic-sensors/>)

FBGS. (2017). *Fiber Bragg Grating Principle.* Retrieved from (http://www.lazoc.jp/english/technical/principle/assets_c/2017/05/FBG-thumb-300xauto-374.jpg)

- Fenta, M. C., Potter, D. K., & Szanyi, J. (2021). *Fibre optic methods of prospecting: A comprehensive and modern branch of geophysics*. *Surveys in Geophysics*, 42(3), 551-584.
- Fritz M., McQuilken J., Collins N. and Weldegiorgis F. (2018). *Global Trends in Artisanal and Small-Scale Mining (ASM)*. Retrieved from (<https://www.iisd.org/system/files/publications/igf-asm-global-trends.pdf>)
- Furukawa, R. (2009). *Polarization maintaining and phase retarding properties of a birefringence controlled plastic optical fiber*.
- Gholamzadeh, B., & Nabovati, H. (2008). *Fiber optic sensors*. *International Journal of Electronics and Communication Engineering*, 2(6), 1107-1117.
- Güemes A. (2014). *Fiber Optics Strain Sensors*. Retrieved from (<https://www.sto.nato.int/publications/STO%20Educational%20Notes/STO-EN-AVT-220/EN-AVT-220-03.pdf>.)
- Hill, K. O., & Meltz, G. (1997). *Fiber Bragg grating technology fundamentals and overview*. *Journal of lightwave technology*, 15(8), 1263-1276.
- Isoe, G. M., Jena, J. F., Julie, R. P. M., & Kapp, F. B. (2020). *Distributed SOP tracking fault detection technique for MeerKAT radio telescope array sub-metre single mode fibre link health monitoring*. *Optics Communications*, 466, 125673.
- Jena, J., Wassin, S., Bezuidenhout, L., Doucouré, M., & Gibbon, T. (2020). *Polarization-based optical fiber acoustic sensor for geological applications*. *JOSA B*, 37(11), A147-A153.

- Kaminow, I. (1981). Polarization in optical fibers. *IEEE Journal of Quantum Electronics*, 17(1), 15-22.
- Kipnoo, E. R., Isoe, G. M., Boiyo, D. K., Kuja, S., Waswa, D., Gibbon, T. B., & Leitch, A. W. R. (2020). *All optical polarization-based and DSP-Assisted distributed fiber sensor for earth mass movements caused by environmental factors*. *Optik*, 206, 163691.
- Komane, B. L., & Mathonsi, T. E. (2019). *A review of wireless sensor networks: Early accident detection models for South African mine industries*. 2019 Open Innovations (OI), 36-41.
- Kuang, K. S. C., Cantwell, W. J., & Thomas, C. (2003). *Crack detection and vertical deflection monitoring in concrete beams using plastic optical fibre sensors*. *Measurement Science and Technology*, 14(2), 205.
- Lanciano, C., & Salvini, R. (2020). *Monitoring of strain and temperature in an open pit using Brillouin distributed optical fiber sensors*. *Sensors*, 20(7), 1924.
- Li, H. N., Li, D. S., & Song, G. B. (2004). *Recent applications of fiber optic sensors to health monitoring in civil engineering*. *Engineering structures*, 26(11), 1647-1657.
- Liu, T., Wang, C., Wei, Y., Zhao, Y., Huo, D., Shang, Y., Wang, Z., & Ning, Y. (2009). *Fibre optic sensors for mine hazard detection*. In *Journal of Physics: Conference Series* (Vol. 178, No. 1, p. 012004). IOP Publishing.

- Liu, T., Wei, Y., Song, G., Hu, B., Li, L., Jin, G., Wang, J., Li, Y., Song, C., Shi, Z., Zhao L., Hu, J., Zhao, W., Hou, M., Li, R., & Wang, J. (2018). *Fibre optic sensors for coal mine hazard detection*. *Measurement*, 124, 211-223.
- Lu, P., Lalam, N., Badar, M., Liu, B., Chorpening, B. T., Buric, M. P., & Ohodnicki, P. R. (2019). *Distributed optical fiber sensing: Review and perspective*. *Applied Physics Reviews*, 6(4).
- Mekhtiyev, D., Neshina, E. G., Madi, P. S., & Gorokhov, D. A. (2021). *Automated fiber-optic system for monitoring the stability of the pit quarry mass and dumps*. *Bezop. Tr. Promyshlennosti*, 2021, 19-26.
- Nabadda, E., Ireeta, W. T., & Gibbon, T. B. (2018). *Angular displacement and SOP speeds in aerial and buried single mode and polarisation maintaining fibers*. *Optik*, 168, 77-85.
- Nagano, K., Kawakami, S., & Nishida, S. (1978). *Change of the refractive index in an optical fiber due to external forces*. *Applied optics*, 17(13), 2080-2085.
- Palmieri, L., & Schenato, L. (2013). *Distributed optical fiber sensing based on Rayleigh scattering*. *The Open Optics Journal*, 7(1).
- Pierce, S. G., MacLean, A., & Culshaw, B. (2000). *Optical frequency domain reflectometry for interrogation of microbend-based optical fiber sensors*. In *Smart Structures and Materials 2000: Sensory Phenomena and Measurement Instrumentation for Smart Structures and Materials* (Vol. 3986, pp. 352-361). SPIE.

- Rashleigh, S. (1983). *Origins and control of polarization effects in single-mode fibers*. *Journal of Lightwave Technology*, 1(2), 312-331.
- Reddy, N. S., Saketh, M. S., & Dhar, S. (2016). *Review of sensor technology for mine safety monitoring systems: A holistic approach*. In 2016 IEEE First International Conference on Control, Measurement and Instrumentation (CMI) (pp. 429-434). IEEE.
- Schenato, L. (2014). *Fiber-optic sensors for geo-hydrological applications: Basic concepts and applications*. *Rendiconti Online della Società Geologica Italiana*, 30, 51-54.
- Tang, B., & Cheng, H. (2018). *Application of distributed optical fiber sensing technology in surrounding rock deformation control of TBM-excavated coal mine roadway*. *Journal of Sensors*, 2018, 1-10.
- United States Mine Rescue Association (2022). *Optical Fiber Monitoring Systems*. Retrieved from https://miningquiz.com/pdf/Technology/Optic_fiber_monitoring_systems.pdf.
- Viavi Solutions. (n.d.). *What are working principles and characteristics of OTDRs?* Retrieved from <https://www.viavisolutions.com/en-us/what-are-working-principles-and-characteristics-of-otdrs#:~:text=The%20laser%20emits%20a%20pulse,photo%20detector%20in%20the%20OTDR.>) Accessed July 2024.

- Walkenhorst, B. T., & Nichols, S. (2020). *Revisiting the Poincaré sphere as a representation of polarization state*. In 2020 14th European Conference on Antennas and Propagation (EuCAP) (pp. 1-5). IEEE.
- Wang, J., Shi, S. Q., Chen, L. Q., Li, Y., & Zhang, T. Y. (2004). *Phase-field simulations of ferroelectric/ferro elastic polarization switching*. *Acta Materialia*, 52(3), 749-764.
- Yu, F. T., & Yin, S. (2002). *Fiber optic sensors*. Marcel-Dekker.
- Yugay, V., Mekhtiyev, A., Madi, P., Neshina, Y., Alkina, A., Gazizov, F., Afanaseva, O., & Ilyashenko, S. (2022). *Fiber-Optic System for Monitoring Pressure Changes on Mine Support Elements*. *Sensors*, 22(5), 1735.
- Zeni, L., Picarelli, L., Avolio, B., Coscetta, A., Papa, R., Zeni, G., Di Maio, C., Vassallo, L., & Minardo, A. (2015). *Brillouin optical time-domain analysis for geotechnical monitoring*. *Journal of Rock Mechanics and Geotechnical Engineering*, 7(4), 458-462.
- Zhang, X., Zhu, H., Jiang, X., & Broere, W. (2024). *Distributed fiber optic sensors for tunnel monitoring: A state-of-the-art review*. *Journal of Rock Mechanics and Geotechnical Engineering*.
- Zhu, H. H., Yin, J. H., Zhang, L., Jin, W., & Dong, J. H. (2010). *Monitoring internal displacements of a model dam using FBG sensing bars*. *Advances in Structural Engineering*, 13(2), 249-261.

APPENDICES

Appendix I: Power fluctuations for various fiber types in a coiled orientation

G652 CORNING LOADING

FIBER TYPE	INPUT POWER (dBm)	OUTPUT POWER (dBm)	POWER LOSS (dBm)	SENSITIVITY (dBm/Kg)
DFB	0.80	0.08	0.72	0.04
MZM	0.87	0.50	0.37	0.02056
WDM	0.83	0.52	0.31	0.01722

G652 CORNING UNLOADING

FIBER TYPE	INPUT POWER (dBm)	OUTPUT POWER (dBm)	POWER GAIN (dBm)	SENSITIVITY (dBm/Kg)
DFB	0.04	0.80	0.76	0.0422
MZM	0.49	0.87	0.38	0.0211
WDM	0.50	0.83	0.33	0.0183

G655 CORNING LOADING

LASER SOURCE	INPUT POWER (dBm)	OUTPUT POWER (dBm)	POWER LOSS (dBm)	SENSITIVITY (dBm/Kg)
DFB	0.50	0.17	0.33	0.0183
MZM	0.47	0.25	0.22	0.0122
WDM	0.44	0.15	0.29	0.0161

G655 CORNING UNLOADING

LASER SOURCE	INPUT POWER (dBm)	OUTPUT POWER (dBm)	POWER GAIN (dBm)	SENSITIVITY (dBm/Kg)
DFB	0.12	0.50	0.38	0.0211
MZM	0.21	0.47	0.26	0.0144
WDM	0.28	0.93	0.65	0.0361

G655 OFS LOADING

LASER SOURCE	INPUT POWER (dBm)	OUTPUT POWER (dBm)	POWER LOSS (dBm)	SENSITIVITY (dBm/Kg)
DFB	0.49	0.04	0.45	0.025
MZM	0.49	0.06	0.43	0.024
WDM	0.49	0.04	0.45	0.025

G655 OFS UNLOADING

LASER SOURCE	INPUT POWER (dBm)	OUTPUT POWER (dBm)	POWER GAIN (dBm)	SENSITIVITY (dBm/Kg)
DFB	0.02	0.48	0.46	0.026
MZM	0.06	0.48	0.42	0.023
WDM	0.02	0.46	0.44	0.024

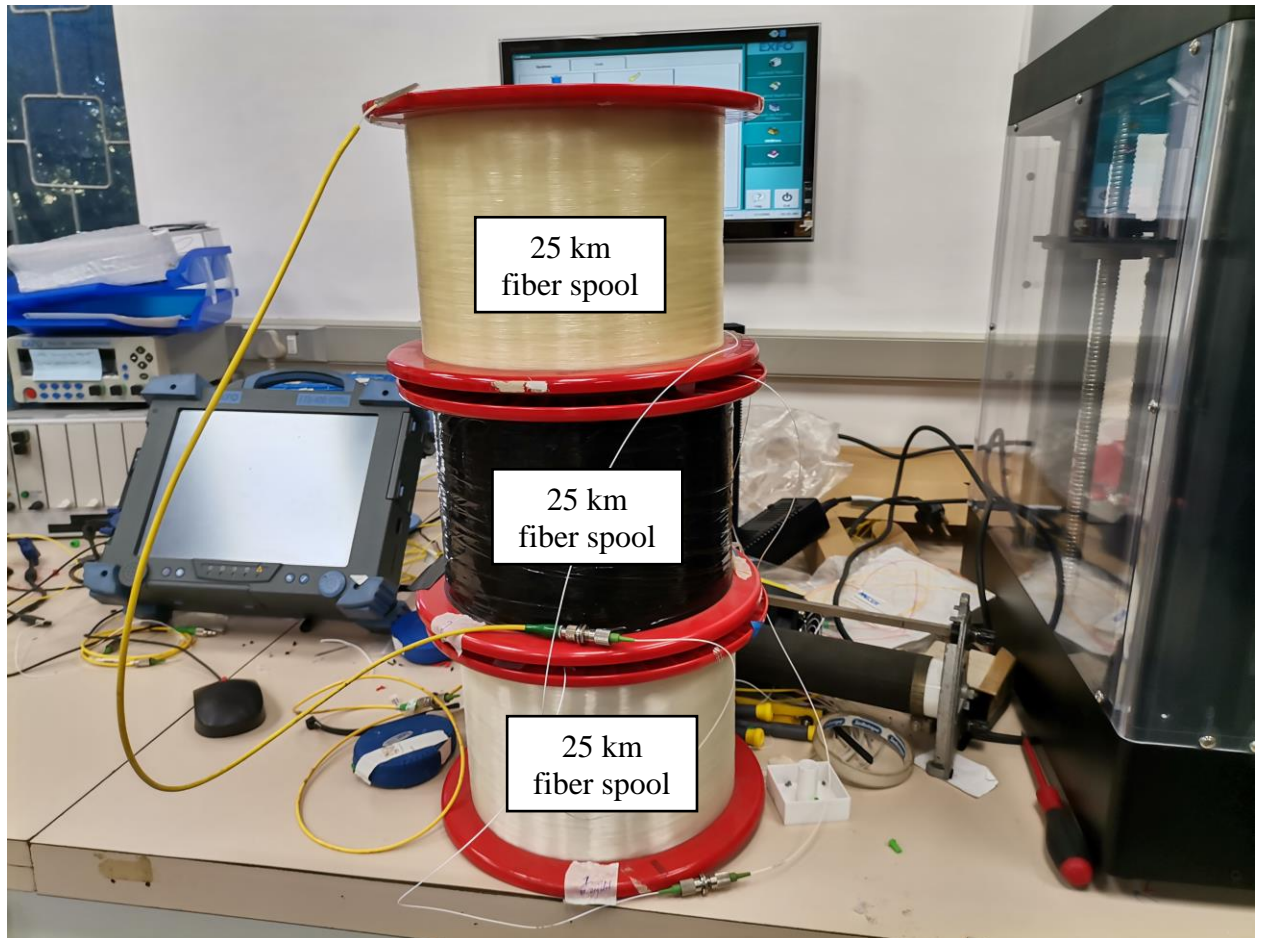
PMF CORNING LOADING

LASER SOURCE	INPUT POWER (dBm)	OUTPUT POWER (dBm)	POWER LOSS (dBm)	SENSITIVITY (dBm/Kg)
DFB	0.54	0.00	0.54	0.03
MZM	0.50	0.12	0.38	0.02
WDM	0.54	0.00	0.54	0.03

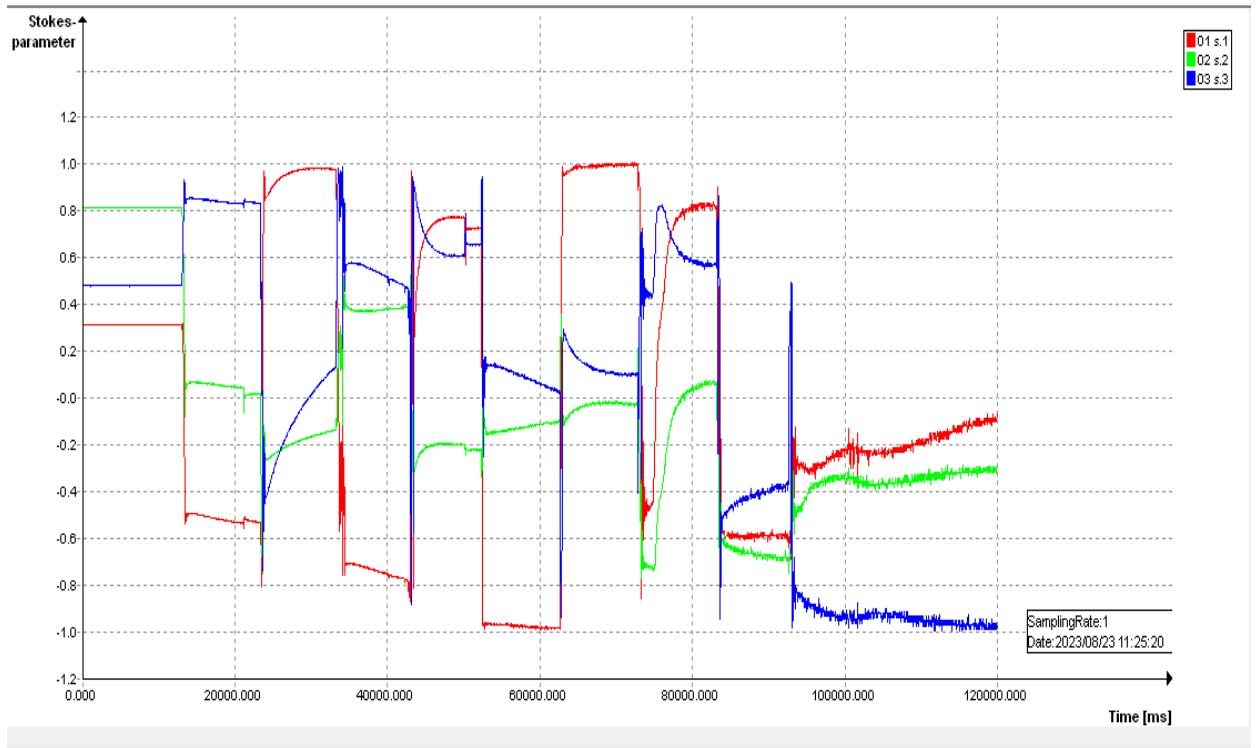
PMF CORNING UNLOADING

LASER SOURCE	INPUT POWER (dBm)	OUTPUT POWER (dBm)	POWER GAIN (dBm)	SENSITIVITY (dBm/Kg)
DFB	0.00	0.51	0.51	0.028
MZM	0.11	0.43	0.32	0.018
WDM	0.00	0.53	0.53	0.029

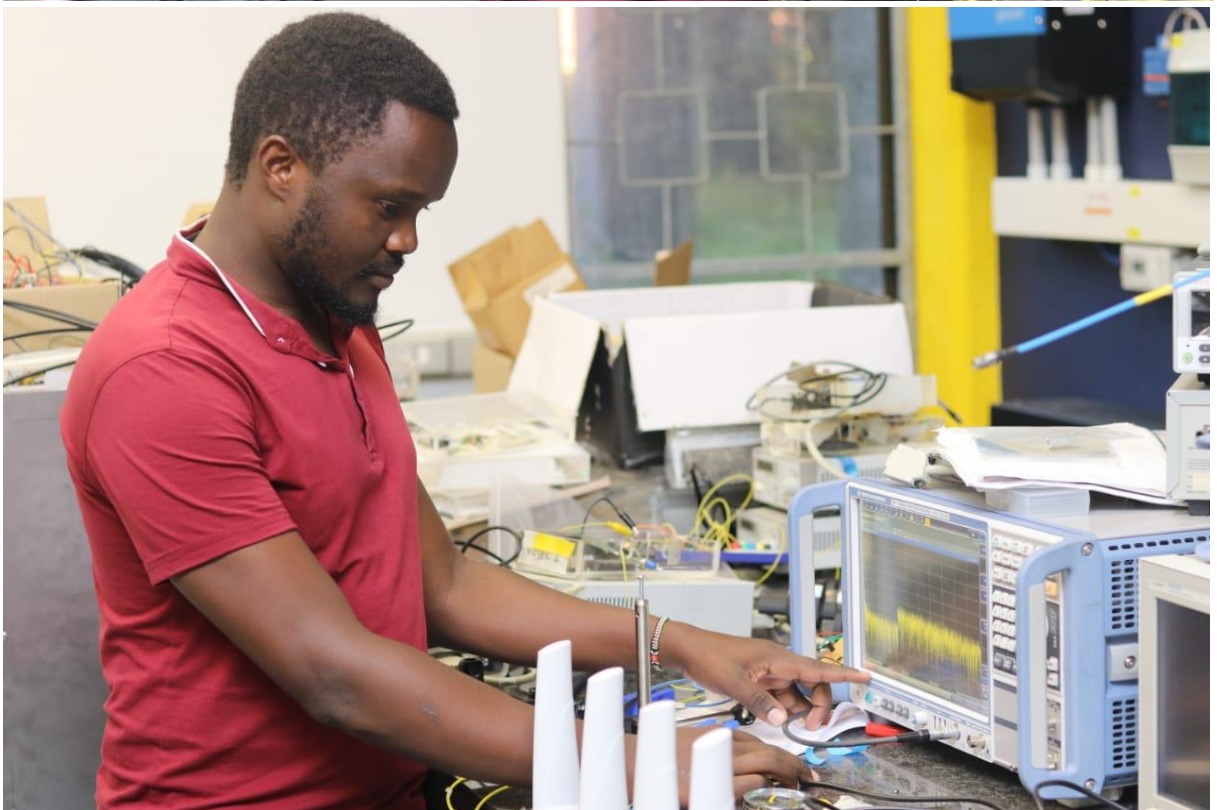
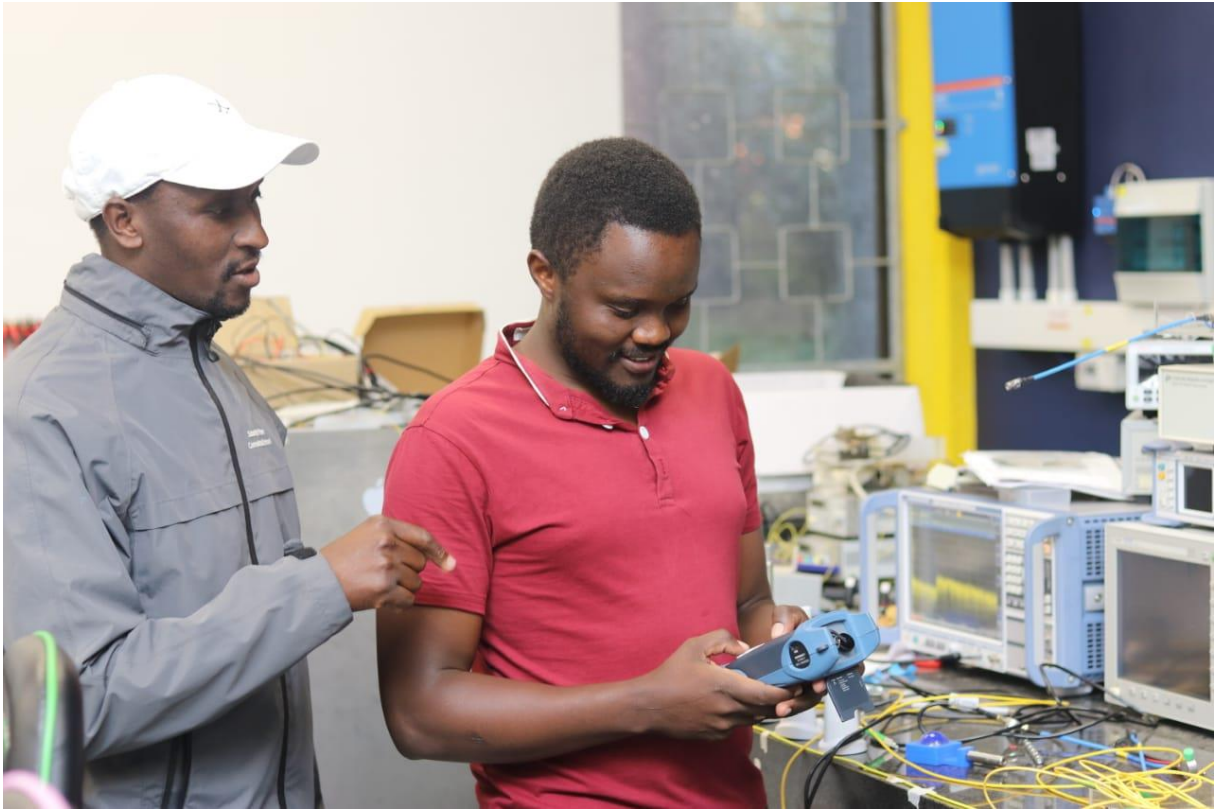
Appendix II: Fiber spools



Appendix III: Stokes' parameter changes for MZM on G655 OFS



Appendix IV: Data collection



Appendix V: Program for turning on an alarm

```
import serial

import time

# Define thresholds for power and polarization

MinPowerThreshold = 0.2

PolarizationThreshold = 100.0

def read_power_meter():

    """

    Function to read data from a Thorlabs PM100D power meter connected via serial

    port.

    Modify the serial port and baud rate as per your device configuration.

    """

    try:

        ser = serial.Serial('/dev/ttyUSB0', 115200, timeout=1)

        ser.write(b"MEAS:POW?\n")

        response = ser.readline().decode('utf-8')

        ser.close()

        return float(response.strip())

    except Exception as e:

        print(f"Error reading power meter: {e}")

        return None

def read_polarization_analyzer():

    """

    Function to read data from a Thorlabs PAX5710 polarization analyzer connected

    via serial port.
```


Modify the serial port and baud rate as per your device configuration.

```
"""  
  
try:  
  
    ser = serial.Serial('/dev/ttyUSB1', 9600, timeout=1)  
  
    ser.write(b"MEAS:POL?\n")  
  
    response = ser.readline().decode('utf-8')  
  
    ser.close()  
  
    return float(response.strip())  
  
except Exception as e:  
  
    print(f"Error reading polarization analyzer: {e}")  
  
    return None
```

```
def trigger_alarm(alarm_type):
```

```
    """  
  
    Function to trigger an alarm when a threshold is crossed.  
  
    """  
  
    if alarm_type == 'Power':  
  
        print('Power threshold crossed! Triggering alarm...')  
  
        # Implement additional alarm mechanisms here (e.g., sound, email alert)  
  
    elif alarm_type == 'Polarization':  
  
        print('Polarization threshold crossed! Triggering alarm...')  
  
        # Implement additional alarm mechanisms here (e.g., sound, email alert)  
  
    elif alarm_type == 'Both':  
  
        print('Both thresholds crossed! Triggering alarm...')  
  
        # Implement additional alarm mechanisms here (e.g., sound, email alert)
```

```

def monitor_fiber():
    """
    Main function to continuously monitor the fiber and trigger alarms based on
    thresholds.
    """
    while True:
        power_data = read_power_meter()
        polarization_data = read_polarization_analyzer()

        power_alarm = power_data is not None and power_data < MinPowerThreshold
        polarization_alarm = polarization_data is not None and polarization_data <
        PolarizationThreshold

        if power_alarm and polarization_alarm:
            trigger_alarm('Both')
        elif power_alarm:
            trigger_alarm('Power')
        elif polarization_alarm:
            trigger_alarm('Polarization')

        time.sleep(1) # Adjust the interval as needed

if __name__ == '__main__':
    monitor_fiber()

```

Appendix VI: List of publications

Nyarangi, W. K., Kipnoo, E. R., Masinde, F. W., Rop, R. K., Gibbon, T. B., & Cherutoi, H. C. (2023, September). Towards the Design of a Distributed Fiber Optical Sensor for Mining Applications. In *2023 IEEE AFRICON* (pp. 1-4). IEEE (**Published**)

Nyarangi, W. K., Kipnoo, E.R., Masinde, F. W., Waswa, D., & Jena, J. Demonstration of a distribution optical fiber strain sensor using a G655 OFS SMF for mining application. *SATNAC 2024* (**Accepted**)

Nyarangi, W. K., Kipnoo, E.R., Masinde, F. W., Waswa, D., & Jena, J. Experimental demonstration of a polarization-based distributed optical fiber sensor using a G652 SMF for mining applications (**Under review**)

Appendix VII: Clearance by Board of Graduate Studies



UNIVERSITY OF KABIANGA
ISO 9001:2015 CERTIFIED
OFFICE OF THE DIRECTOR, BOARD OF GRADUATE STUDIES

REF: PGC/PHY/0003/2021

DATE: 14TH MAY, 2024

Wilfred Kibet Nyarangi,
MAPS Department,
University of Kabianga,
P.O Box 2030- 20200,
KERICHO.

Dear Mr. Nyarangi,

RE: CLEARANCE TO COMMENCE FIELD WORK/DATA COLLECTION

I am pleased to inform you that the Board of Graduate Studies has considered and approved your Masters Research proposal entitled "**Design and Evaluation of a Distributed Optical Fiber Sensor for Hazard Detection in Mining**". Subsequently the Board has also approved the following supervisors for appointments.

1. Dr. Enoch K. Rotich Kipnoo, PhD
2. Dr. Fred Wekesa Masinde, PhD

You may now proceed to commence field work/data collection on condition that you obtain a research permit from NACOSTI and /or an ethical review permit from a relevant ethics review board.

You are also required to publish one (1) article in a peer reviewed journal, with all your supervisors, before your oral defense of thesis and to submit through your supervisors, and HoD, progress reports every three months, to the Director, Board of Graduate Studies.

Please note that it is the policy of the University that you complete your studies within two years from the date of registration. Do not hesitate to consult this office in case of any difficulties encountered in the course of your studies.

I wish you all the best in your research and hope that your study will yield original contribution for the betterment of humanity.

Yours Sincerely

Dr. Ronald K. Rop

DIRECTOR, BOARD OF GRADUATE STUDIES.


RKR/hk

- cc
1. Dean, SST
 2. HOD, Mathematics, Actuarial & Physical Sciences
 3. Supervisors

Appendix VIII: Research permit




REPUBLIC OF KENYA



NATIONAL COMMISSION FOR SCIENCE, TECHNOLOGY & INNOVATION

Ref No: 761518
Date of Issue: 03/June/2024

RESEARCH LICENSE




This is to Certify that Mr.. WILFRED NYARANGI KIBET of University of Kabianga, has been licensed to conduct research as per the provision of the Science, Technology and Innovation Act, 2013 (Rev.2014) in Kericho on the topic: Design and Evaluation of a Distributed Optical Fiber sensor for Hazard Detection in Mining for the period ending : 03/June/2025.

License No: NACOSTI/P/24/36196

761518


Applicant Identification Number



Director General

NATIONAL COMMISSION FOR SCIENCE, TECHNOLOGY & INNOVATION

Verification QR Code



NOTE: This is a computer generated License. To verify the authenticity of this document, Scan the QR Code using QR scanner application.

See overleaf for conditions